The Geological Society of America
Special Paper 480
2011

# *Tectonic evolution of the Ankara Mélange and associated Eldivan ophiolite near Hançili, central Turkey*

**Anne Dangerfield**
**Ron Harris**
*Department of Geology, Brigham Young University, Provo, Utah 84602, USA*

**Ender Sarıfakıoğlu**
*General Directorate of Mineral Research and Exploration, Department of Geology, TR-06520 Ankara, Turkey*

**Yildirim Dilek**
*Department of Geology, Miami University, Oxford, Ohio 45056, USA*

## ABSTRACT

**Structural field studies and geochemical and age analyses of the Eldivan ophiolite, which is dismembered within the Ankara Mélange, indicates that it developed as a supra-subduction zone basin within the İzmir-Ankara-Erzincan Ocean, which later subducted to form the İzmir-Ankara-Erzincan suture zone through continental block collision. Whole-rock and mineral geochemical evidence show a supra-subduction zone tectonomagmatic affinity for the ophiolitic crust and mantle, revealing that this basin formed in the upper plate of an intra-oceanic subduction zone. Structural restoration of the sheeted dike complex reveals that the supra-subduction zone spreading ridge of the Eldivan ophiolite was nearly parallel to the Sakarya-Pontide continental margin. U/Pb age analyses of detrital zircon in sandstone within the mélange and in the unconformably overlying Karadağ Formation indicate maximum depositional ages for the units of 143.2 ±2 Ma, and 105.2 ±5 Ma, respectively. Thus, thrust imbrication of the ophiolite and the development of serpentinite mélange were mostly complete by 105 Ma, as indicated by an angular unconformity between the ophiolitic units and the overlying Karadağ Formation.**

**These results reveal how and when the Eldivan ophiolite was constructed, destructed, and incorporated into the serpentinite Ankara Mélange and İzmir-Ankara-Erzincan suture zone. The tectonic evolution of the İzmir-Ankara-Erzincan Ocean is similar to that of the Philippine Sea and Banda Sea ocean basins.**

## INTRODUCTION

Suture zones provide some of the most important evidence of how continents form and evolve. Since the discovery of plate tectonics, suture zones have mostly been characterized as remnants of large mid-ocean ridge basalt (MORB)–like ocean basins that were destroyed by subduction and modified by collision of rafted continental blocks of different affinities. The Indus-Tsangpo suture zone of the Himalayan collision provides a type example (Gansser, 1964; Dewey and Bird, 1970). Its interpretation traditionally involves subduction of huge tracts of MORB-like oceanic crust beneath a continental arc system mounted on the southern edge of Asia. The subducting plate rafted India from thousands of kilometers to the south, eventually bringing

Dangerfield, A., Harris, R., Sarifakıoğlu, E., and Dilek, Y., 2011, Tectonic evolution of the Ankara Mélange and associated Eldivan ophiolite near Hançili, central Turkey, *in* Wakabayashi, J., and Dilek, Y., eds., Mélanges: Processes of Formation and Societal Significance: Geological Society of America Special Paper 480, p. 143–169, doi:10.1130/2011.2480(06). 

it northward into continental collision with the Asian continent, which formed the Himalaya and the Tibetan Plateau. New evidence from Himalayan sutures, including the Indus-Tsangpo suture (Yin and Harrison, 2000), and other modern convergent boundaries (Harris, 2003), reveal that this classic model of suture zone development is one end member of diverse types of sutures that involve a variety of tectonic processes that lead to stitching continents together.

This study uses the Ankara Mélange within the İzmir-Ankara-Erzincan suture zone of Turkey to reconstruct tectonic processes and events associated with continental accretion of the eastern Mediterranean region and the origin of its narrow bands of serpentinite mélange. Despite previous studies of the Ankara Mélange, its age, origin, and relations to other tectonic events in the Mediterranean region are still poorly understood. This study uses crustal and mantle geochemistry and petrography of ophiolitic blocks in the Ankara Mélange, U/Pb age analyses of detrital zircon in mélange and overlying sandstone, and structural reconstructions from near Hançili in central Tu key to present a view that differs from the classical or Him layan model of suture zone development. This model not on provides important constraints for the tectonic evolution of th central İzmir-Ankara-Erzincan Ocean, and significance of th Ankara Mélange, but also advances our understanding of sutu zone diversity.

## GEOLOGIC EVOLUTION OF THE İZMIR-ANKARA-ERZINCAN SUTURE ZONE

The İzmir-Ankara-Erzincan suture zone in northern Tu key is a remnant of the İzmir-Ankara-Erzincan Ocean branc of the Neo-Tethys that formed during collision of Gondwana derived micro-continents (Kırşehir block and Tauride-Anatolid platform) with the Sakarya-Pontide terrane of northern Turke (Şengör and Yılmaz, 1981) (Fig. 1). The suture zone is mad up of ophiolitic material and forms the Ankara Mélange, in th

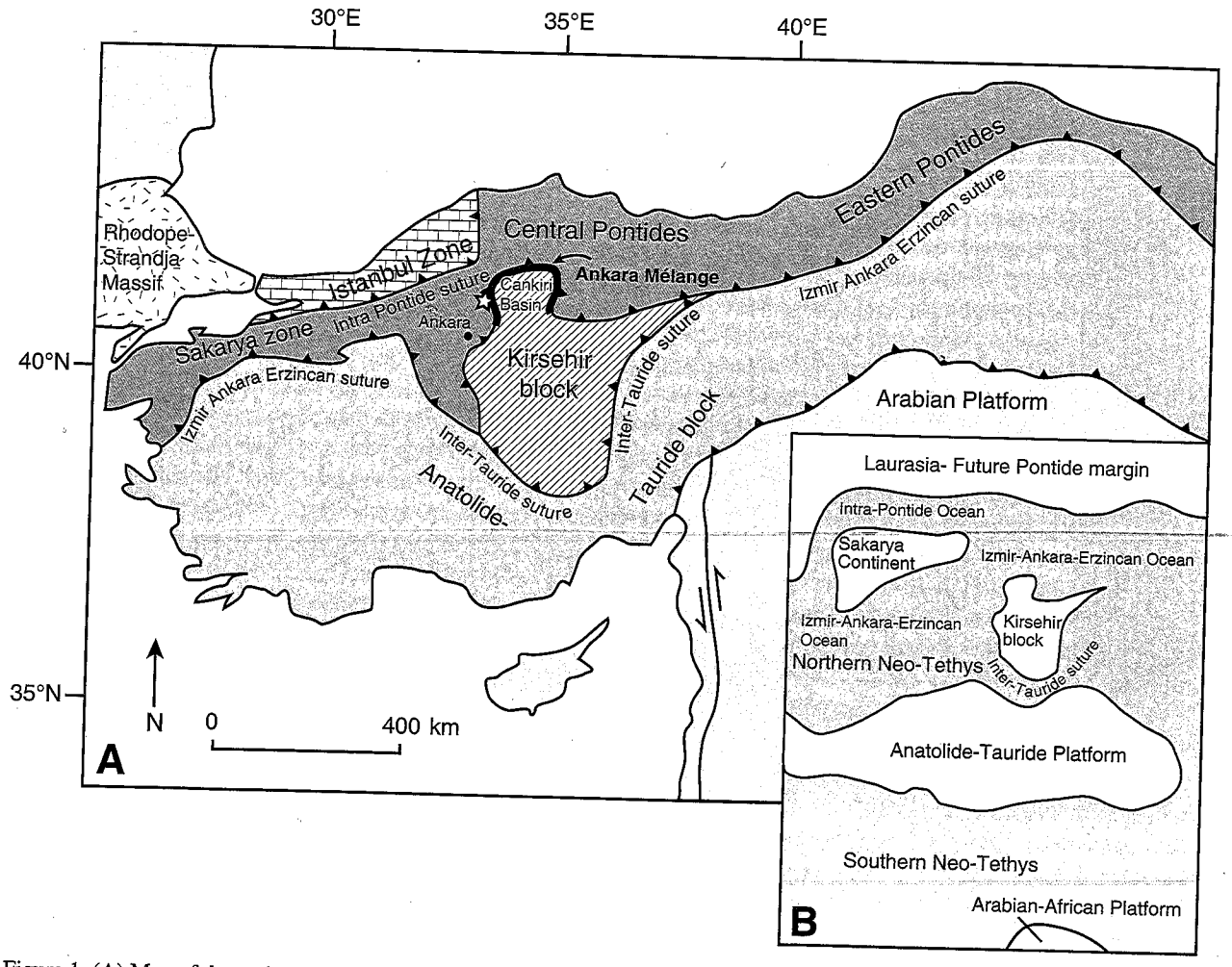


Figure 1. (A) Map of the major tectonic units discussed in this chapter (after Okay and Tüysüz, 1999). The star shows the location of the Eldivan ophiolite and the study area. (B) Reconstruction of the İzmir-Ankara-Erzincan suture zone (after Şengör and Yılmaz, 1981), showing the relationship between ocean branches and continental blocks discussed in this paper.

center of the suture zone between the Kırşehir block and the Sakarya-Pontide terrane.

The Ankara Mélange was first named by Bailey and McCallien (1950) and consists of three major tectonic units. Structurally from top to bottom these units are (1) a metamorphic block mélange, also called the Karakaya Formation (Koçyiğit, 1991) and Karakaya Group (Floyd, 1993); (2) a limestone block mélange; and (3) an ophiolitic mélange (Norman, 1984; Koçyiğit, 1991; Tüysüz et al., 1995; Dilek and Thy, 2006). The tectonically lowest ophiolitic mélange unit consists of blocks of basaltic and rhyolitic volcanic rocks, pillow basalt, serpentinized peridotite and ultramafic rocks, and radiolarian-bearing limestone and chert, with minor shale and sandstone in a serpentinite or tuffaceous matrix (Norman, 1984; Tankut et al., 1998). Dike complexes, where present, are commonly doleritic, cutting sequences of serpentinized peridotite and isotropic gabbro, and including plagiogranite (Dilek and Thy, 2006). During convergence, the İzmir-Ankara-Erzincan Ocean crust was imbricated along northward-dipping thrust faults (Şengör and Yılmaz, 1981) and overlain by flyschoidal (Norman, 1984) and forearc basin (Koçyiğit, 1991) deposits that were subsequently imbricated with the İzmir-Ankara-Erzincan Ocean crust during the collision of the Kırşehir block and the Sakarya-Pontide continent.

The geodynamic history of the İzmir-Ankara-Erzincan Ocean is threefold, beginning with rifting, transitioning to subduction, and finally ending with continental collision. It opened in the Triassic as a MORB-type ocean basin, as determined by geochemical results from basalt and associated Triassic radiolarian limestone found along the İzmir-Ankara-Erzincan suture zone (Tankut, 1984; Tankut et al., 1998; Floyd et al., 2000; Göncüoğlu et al., 2006). Jurassic and Cretaceous alkali basalt is also found in this suture zone and is interpreted as seamount fragments accreted to an accretionary wedge (Tüysüz et al., 1995; Floyd et al., 2000; Rojay et al., 2001; Göncüoğlu et al., 2006), possibly in the form of hot-spot–generated volcanic ridge systems (Floyd, 1993; Tankut et al., 1998). Also documented along the suture are island arc tholeiites (Göncüoğlu et al., 2006; Sarıfakıoğlu, 2006) and calc-alkaline volcanics (Tankut, 1984; Tüysüz et al., 1995; Göncüoğlu et al., 2006), suggesting subduction-related magmatism. The subduction influence is seen in the western and central parts of the suture zone where supra-subduction zone basalt has been documented, indicating intra-oceanic subduction with upper plate extension (Yalınız et al., 1996; Floyd et al., 1998, 2000; Yalınız et al., 2000b; Dilek and Thy, 2006; Sarıfakıoğlu, 2006; Sarıfakıoğlu et al., 2009). This supra-subduction zone signature is similar to other Cretaceous eastern Mediterranean ophiolites (i.e., Pindos, Troodos, Antalya, Hatay (Kızıldağ), Baer-Bassit, and Semail) and has led to correlations of the İzmir-Ankara-Erzincan suture zone with the Vardar suture in Greece (Yalınız et al., 2000b; Göncüoğlu et al., 2006; Sarıfakıoğlu et al., 2009). Granitoids and exhumation in the Kırşehir block and indentation of the Sakarya-Pontide terrane document collisional closure of the basin (Okay et al., 2006; Önen, 2003, Kaymakci et al., 2003).

Although evolutionary phases of the ocean basin are known, their ages, particularly the transition between rifting and subduction leading to closure, are poorly understood. The oldest ages from the basin come from Carnian (Tekin et al., 2002) and Norian (Bragin and Tekin, 1996) radiolarians in limestone and chert blocks that indicate the ocean had rifted open by the Late Triassic Period. Post-collisional granitoid ages in the Kırşehir block suggest that continental collision began in the Late Cretaceous Period (Boztuğ et al., 2007), finally closing the ocean basin. Between these events the transition from rift construction to subduction closure is interpreted to have begun as early as 179 Ma, based on ages of plagiogranite with supra-subduction zone characteristics in the ophiolitic mélange by Dilek and Thy (2006), and as late as ca. 85 Ma by Göncüoğlu et al. (2006), using a compilation of metamorphic sole and radiolarian ages. Thus, although the general range of construction of the İzmir-Ankara-Erzincan Ocean is established as Late Triassic to Late Cretaceous Periods, individual events of its geodynamic history are weakly constrained.

## COMPOSITION AND GEOCHEMISTRY OF THE ELDIVAN OPHIOLITE

The Eldivan ophiolite is part of the ophiolitic mélange of the Ankara Mélange and lies on the mélange's western side, south of the city of Eldivan (Fig. 1). It is mostly dismembered and exists as imbricated fragments of ophiolitic components within a serpentinite mélange matrix (Fig. 2). There is little continental clastic material within the mélange. Ophiolitic units present are serpentinized mantle peridotite, massive gabbro, sheeted dikes, pillow basalt, and sheet flows, and epi-ophiolitic limestone and chert. The units are hydrothermally altered but are otherwise unmetamorphosed. Unconformably overlying this imbricated ophiolitic mélange is the younger Karadağ Formation, composed of radiolarian-bearing limestone and chert. In the mapped area the Karadağ Formation tectonically overlies the ophiolitic mélange, but outside the mapped area an angular unconformity is present between the Karadağ Formation and the underlying mélange, suggesting a multiphase structural history.

Serpentinized peridotite, volcanic rocks, diabase dikes, and gabbro were analyzed for whole rock major, trace, and rare-earth elements (REE) and mineral chemistry. Major and selected trace element X-ray fluorescence (XRF) analysis was conducted at Brigham Young University. Trace and rare earth elements were analyzed by inductively coupled-plasma mass spectrometer (ICP-MS) at ALS Chemex Laboratories, Vancouver, British Columbia (method ME-MS81). Mineral chemistry analysis was conducted using a Cameca SX-50 Electron Microprobe at Brigham Young University. Results of analyses are given in Tables A1 and A2 in the Appendix. Owing to the high degree of alteration indicated by widespread secondary mineralization, most samples are hydrous, resulting in elevated LOI (loss on ignition) values (up to 5% for mafic rocks and 12% for ultramafic rocks). Calcined samples were thus used for analyses,

and only relatively immobile elements (Ti, Zr, Y, Hf, Th, Ta, Cr, Ni, and REE) were used for discrimination of tectonomagmatic setting (Pearce and Cann, 1971, 1973; Pearce and Norry, 1979; Wood, 1980; Pearce et al., 1981 1984a; Pearce, 1982; Shervais, 1982; Mullen, 1983; Meschede and Casey, 1986; Cabanis and Lecolle, 1989; Floyd et al., 1991).

## Mantle Sequence

Serpentinized peridotite forms the matrix of the Eldivan ophiolite. There are small coherent blocks of less altered ultramafic rock, but they are found within a much more massive and indistinct serpentine groundmass that occupies fault zones and separates various crustal fragments of the Eldivan ophiolite. These include blocks of basalt, silicic volcanic rocks, limestone, chert, and gabbro, which range in size from a few meters to hundreds of meters, basalt blocks being the largest found. Much of the serpentinite matrix exhibits a scaly shear fabric with anastomosing slickensides.

Less altered parts of the peridotite consist of (1) 80%–90% serpentinized olivine, (2) up to 5% spinel in the form of primary chromite and secondary magnetite, and (3) 5%–10% pyroxene that is altered to serpentine but still displays low birefringence and mostly parallel extinction.

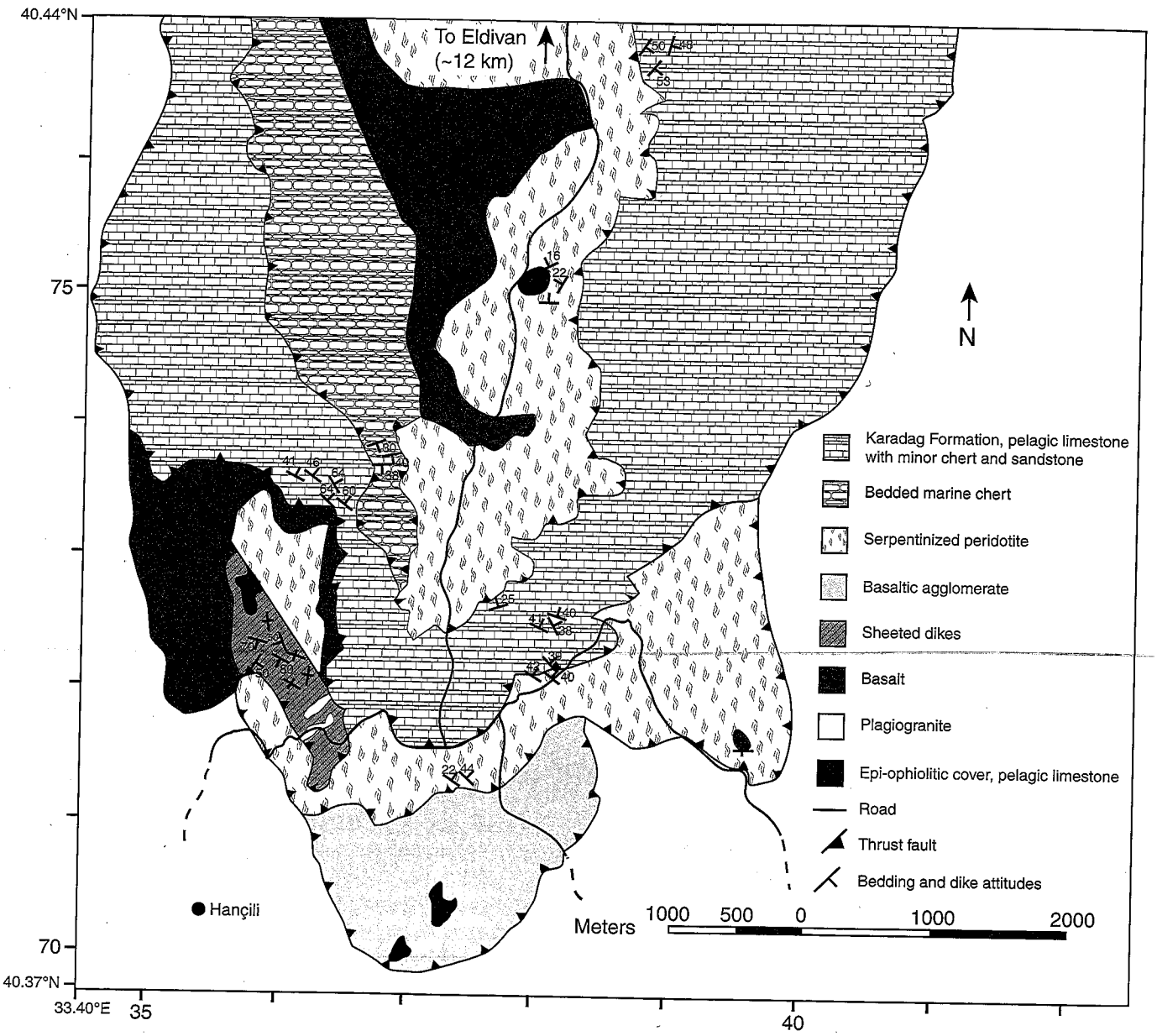


Figure 2. Geologic map of the Çankırı H30-b2 quadrangle (1:25,000 scale), universal transverse Mercator (UTM) zone 36. See star in Figure 1 for location. Latitude, longitude, and UTM coordinates are included. Dashed lines are inferred contacts.

Serpentinized peridotite is characterized by low abundances of Si, Al, Ca, Na, K, and Ti and high abundances of Mg, Cr, and Ni. Light rare-earth element (LREE) concentrations are low, indicating that serpentinization has not affected the original peridotite geochemistry. High degrees of serpentinization, especially where the fluid/rock ratio is large, mobilize LREEs in the serpentinizing fluid, resulting in U-shaped REE patterns that obscure the original igneous chemistry (Paulick et al., 2006). Li and Lee (2006) show that primary $Al_2O_3$ wt% is still preserved in peridotite, with >90% serpentinization and no enrichment in LREE. Peridotites from the Eldivan ophiolite are extensively serpentinized but still show low LREE abundances and are therefore interpreted to have primary $Al_2O_3$ weight percentages. This is important, as these percentages are a proxy for degree of partial melting, as $Al_2O_3$ wt% decreases with high degrees of melt extraction, such as above a subduction zone (Bonatti and Michael, 1989). Eldivan ophiolitic mantle has $Al_2O_3$ weight percentages that range from 0.78% to 2.45%, consistent with values from modern ocean floor and subduction-related mantle (Fisher and Engel, 1969; Ishii, 1985; Shibata and Thompson, 1986; Ishii et al., 1992; Seifert and Brunotte, 1996; Paulick et al., 2006) (Fig. 3).

Chromian spinel accessory minerals are also excellent indicators for degree of mantle extraction (Dick and Bullen, 1984). In Eldivan serpentinized peridotite, Cr numbers (#) (Cr/Cr+Al) of Cr-spinel range from 0.47 to 0.70, which are in the range of type 2 and type 3 peridotites (Dick and Bullen, 1984). Cr#s >0.6 (type 3) are categorized as arc peridotites and show the most depletion, whereas type 2 are transitional between arc and MORB mantle. Eldivan mantle Cr-spinels overlap arc and MORB fields in Dick and Bullen's diagram for Cr-spinel Cr# versus Mg# (Fig. 4A). They also plot in the supra-subduction zone mantle field defined by Kamenetsky et al. (2001) in a $TiO_2$ wt% versus $Al_2O_3$ diagram, with some points in the overlap between supra-subduction zone and MORB mantle fields (Fig. 4B).

## Crustal Sequence

### *Massive-Gabbro-and-Plagiogranite*

Massive gabbro occurs in screens within sheeted dikes and is intruded by plagiogranite. Some bodies of plagiogranite are up to several decimeters in diameter. Plagiogranite dikes mostly lack chilled margins, tentatively suggesting they could be an immiscible liquid phase within a gabbroic magma chamber or intrusions into a non-solidified gabbro.

Gabbro contains 50% mostly albitized plagioclase and 30%–50% clinopyroxene. Rocks show typical hydrothermal metamorphism with actinolite, chlorite, and epidote as common replacement phases of clinopyroxene and plagioclase. Fe-Ti oxides, mostly composed of secondary magnetite, make up ~5% of the rock.

Most gabbro samples are 45–54 wt% $SiO_2$ and are chemically classified as the plutonic equivalents of basalt and basaltic andesite (Fig. 5). A few samples have higher concentrations of alkalis, which could be a reflection of secondary albitization of plagioclase. Gabbro has the lowest abundances of rare earth and trace elements of the crustal sequence, with elemental concentrations 1.5–5 times below normal mid-ocean ridge basalt (N-MORB). REE patterns (Fig. 6A1) show lower LREE relative to heavy rare-earth elements (HREE), similar to N-MORB. Additionally, Th/Ta = 1.25–4.80, La/Nb = 0.54–1.91, and La/Yb = 0.52–1.18 element ratios are generally low, similar to N-MORB. Sample 126a (Fig. 6A1, bold line) is the exception, with higher LREE abundances relative to HREE, perhaps from a subduction source, and high Th/Ta = 9.10, La/Nb = 3.00, and La/Yb = 2.38 ratios. A few samples show flat REE patterns that could be a result of differentiation within the magma chamber.

Trace elements (Fig. 6A2) show scatter in mobile elements, particularly Rb, Ba, K, and Sr, mostly likely due to secondary hydrothermal alteration. Most samples show the similar trace element pattern of large ion lithophile elements (LILE) depleted

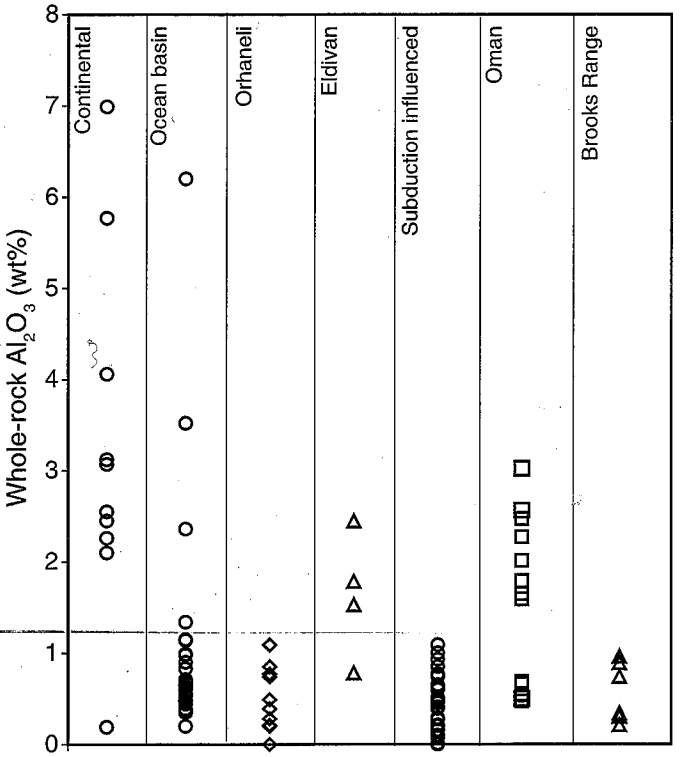


Figure 3. Whole rock $Al_2O_3$ weight percentages for mantle rocks from continental, ocean-floor, and subduction-trench settings compared with the Eldivan ophiolite mantle. The range in $Al_2O_3$ weight percentages in the Eldivan ophiolite spans the range of ocean-floor and subduction-trench mantle. It is also similar to that seen in the Oman ophiolite and somewhat higher than in the Orhaneli ophiolite in the western İzmir-Ankara-Erzincan suture zone and the Brooks Range ophiolite in Alaska, interpreted to have formed in supra-subduction zone settings. Data sources for other mantle compositions are as follows: continental (Carter, 1970; Frey and Prinz, 1978); ocean floor (Shibata and Thompson, 1986; Paulick et al., 2006; Seifert and Brunotte, 1996); subduction trench (Fisher and Engel, 1969; Ishii, 1985; Ishii et al., 1992); Oman (Takazawa et al., 2003); Brooks Range (Harris, 1995); Orhaneli ophiolite (Sarıfakıoğlu et al., 2009).

N-MORB, except for sample 126a (Fig. 6A2, bold line), which has a negative Nb anomaly, again suggesting a subduction influence.

### *Diabase Dikes*

Diabase dikes are found mostly in parallel or sheeted arrays that cut screens of massive gabbro. Many dikes show chilled margins, and some preserve flow fabrics. Shear fractures within the dikes have gouge zones filled with epidote and chlorite, which are common seafloor hydrothermal alteration minerals, indicating that the fractures probably formed during seafloor metamorphism. Dikes show two primary orientations, NNW-SSE and E-W, with dips from 40° to 90°. In one locality, horizontal sheeted dikes feed vertical pillow basalts and sheet flows, indicating a 90° rotation of the units about a horizontal axis.

Dikes are primarily basaltic andesite to andesite with an $SiO_2$ range of ~56–58 wt% (Fig. 5). Element concentrations are most similar to N-MORB (2 times above and below N-MORB concentrations) compared with other units in the Eldivan ophiolite, with REE patterns also similar to N-MORB (Fig. 6B1). Low ratios of Th/Ta = 0.82–4.40, La/Nb = 1.22–1.93, and La/Yb are similar to massive gabbro values and again near N-MORB. One exception is sample 203 (Fig. 6B1, bold line), which shows a slight elevation in LREE with no depletion in the high field strength elements (HFSE), similar to enriched MORB (E-MORB) (Sun and McDonough, 1989). Th/Ta and La/Nb ratios in this sample are similar to those in the other dikes, although La/Yb = 2.42 is higher, reflecting the higher LREE concentrations.

Trace element patterns (Fig. 6B2) show characteristic N-MORB and low LILE abundances compared with the HREE, with hydrothermal alteration reflected in varying concentrations of mobile Rb, Ba, Th, U, K, and Sr. As seen in the REE, sample 203 (Fig. 6B2, bold line), shows higher concentrations of LILE, beginning with Nb and sloping downward to HREE, with a slight increase in Hf and Zr. The absence of a negative Nb-Ta anomaly suggests that higher values of LILE are not due to a subduction component but perhaps to a less depleted mantle source.

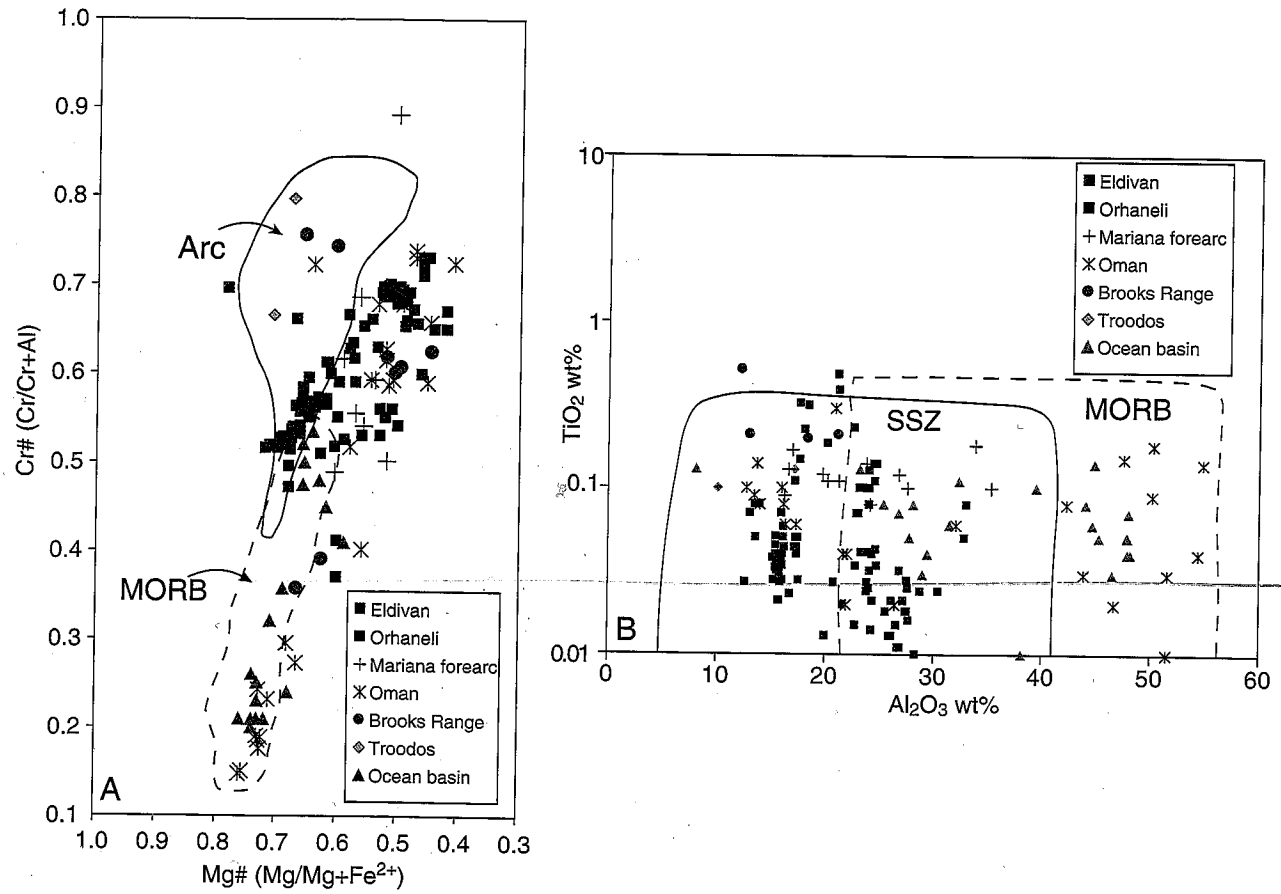


Figure 4. (A) Cr# (Cr/Cr+Al)/Mg# (Mg/Mg+$Fe^{2+}$) of Cr-spinel, the Eldivan serpentinized peridotite. Fields of abyssal (dashed line) and arc peridotites (solid line) are taken from Dick and Bullen (1984). (B) $TiO_2$ wt% vs. $Al_2O_3$ wt% in Cr-spinel of the Eldivan ophiolite. Fields of supra-subduction zone (SSZ; solid line) and MORB (dashed line) are from Kamenetsky et al. (2001). Data are plotted with Cr-spinel data from the Orhaneli ophiolite (Sarıfakıoğlu, 2009), Brooks Range ophiolite (Harris, 1995), ocean basin peridotites (Shibata and Thompson, 1986; Morishita et al., 2007), Troodos and Oman ophiolites (Augé and Johan, 1988; Takazawa et al., 2003; Tamura and Arai, 2006), and Mariana peridotites (Ishii et al., 1992) for comparison. The Eldivan ophiolite plots mostly within the field of arc peridotites (A) and supra-subduction zone peridotites (B), indicating its subduction influenced character.

In tectonic discriminant diagrams, dike rocks plot in fields of supra-subduction zones (Figs. 7A, 7F), island-arc tholeiites (IAT) (Figs. 7B, 7C, 7G) and backarc basin basalts (BABB) (Figs. 7D, 7E), and with some values plotting in the overlap of subduction zone influenced and MORB fields (Figs. 7B, 7D, 7G). Dikes plot consistently in the supra-subduction zone and backarc basin field in diagrams E and F (Fig. 7), which use the most immobile trace elements of La, Nb, and Yb to infer a tectono-magmatic setting. Additional ternary discriminant diagrams (Fig. 8) also plot dikes in subduction related fields. In diagrams B and C, dikes plot almost entirely as island arc basalt and island arc tholeiites, respectively. Diagram D has scatter between the BABB and MORB fields, whereas A and E do not discriminate between subduction and MORB basaltic rocks.

### *Volcanic Rocks*

Volcanic rocks include both basaltic and rhyolitic units as blocks and broken thrust sheets within a serpentinized matrix. Basalt occurs as pillows, sheet flows, and brecciated units up to tens of square meters in area. Large blocks of basalt hundreds of meters in diameter protrude up through serpentinite to form a hummocky landscape typical of eroded mélange units. Silicic volcanic units are found only as small blocks on the meter to decimeter scale.

Major element chemistry reveals a compositional range of volcanic rocks from basalt and andesite to dacite and rhyolite. Basaltic rocks contain 45–53 wt% $SiO_2$ and plot mainly in the basalt field in the total-alkali silica diagram with some overlap into the basaltic andesite field (Fig. 5). Rhyolitic rocks contain 63–74 wt% $SiO_2$ and fall into rhyolite and dacite fields (Fig. 5). Basalts show three distinct geochemical signatures:

1. The most dominant pattern shows LREE depletion characteristic of N-MORB (Fig. 6C1), with low ratios of Th/La = 0.33–2.05, La/Nb = 0.56–2.10, and La/Yb = 0.49–1.29. Element concentrations are equal to and up to 3.5 times more than N-MORB concentrations, giving these basaltic rocks the highest elemental concentrations when compared to the massive gabbros and sheeted dikes. The trace element diagrams for these basaltic volcanics (Fig. 6C2) show a large amount of variation, particularly with mobile elements of Rb, Ba, K, and Sr, which reflect their alteration. However, patterns still show the low LILE abundance (compared with HREE) that is typical of N-MORB. Discriminant diagrams for N-MORB-like basaltic rocks show more scatter than dike rocks but plot in fields of MORB more often than subduction-influenced fields (Figs. 7A–7G). In diagrams B, C, and E, basaltic rocks plot almost entirely within the MORB field, whereas some samples plot close but somewhat outside MORB fields in B, D, and G. In diagrams E and F, which use the

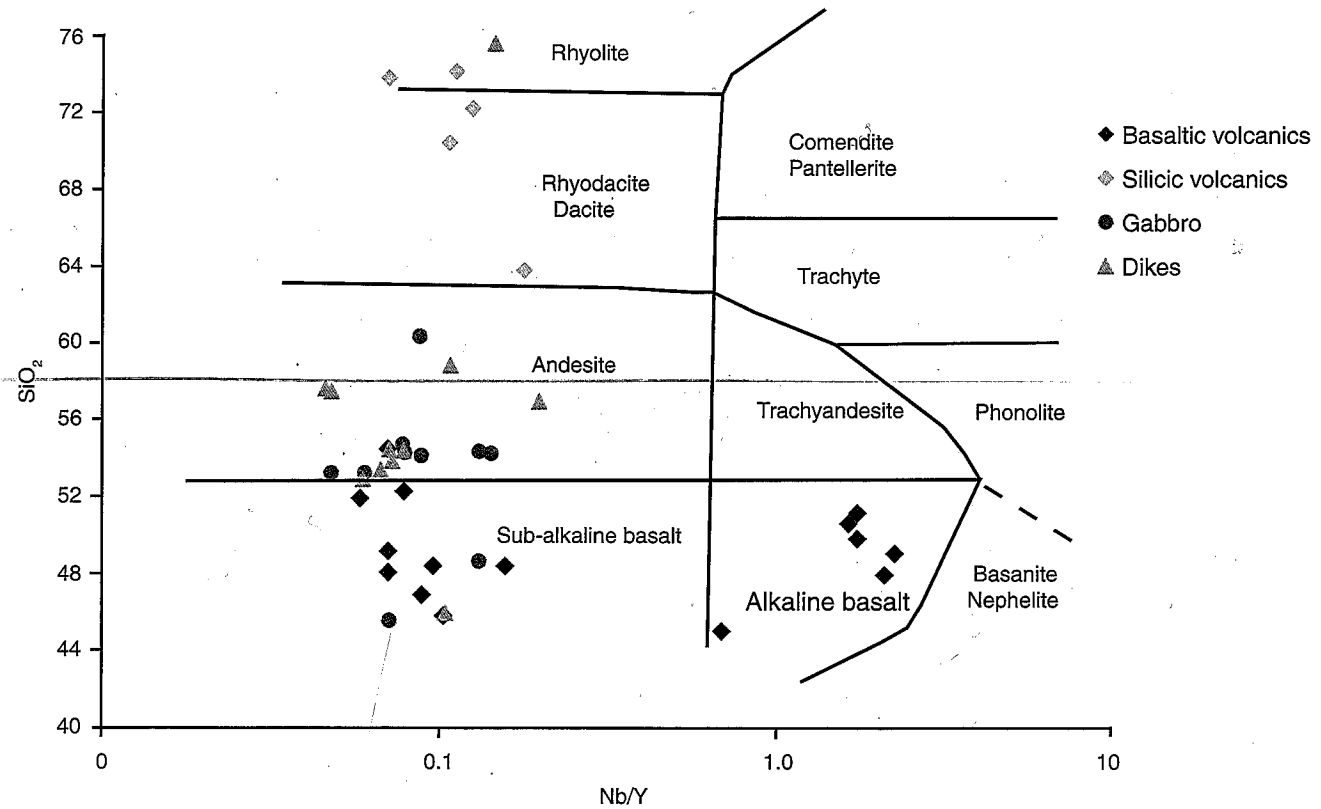


Figure 5. International Union of Geological Sciences (IUGS) total alkali silica classification diagram, illustrating the distribution of rock types in the Eldivan ophiolite. Volcanic rocks are basaltic and rhyolitic, whereas dike rocks plot between the two in the basaltic andesite and andesite fields.

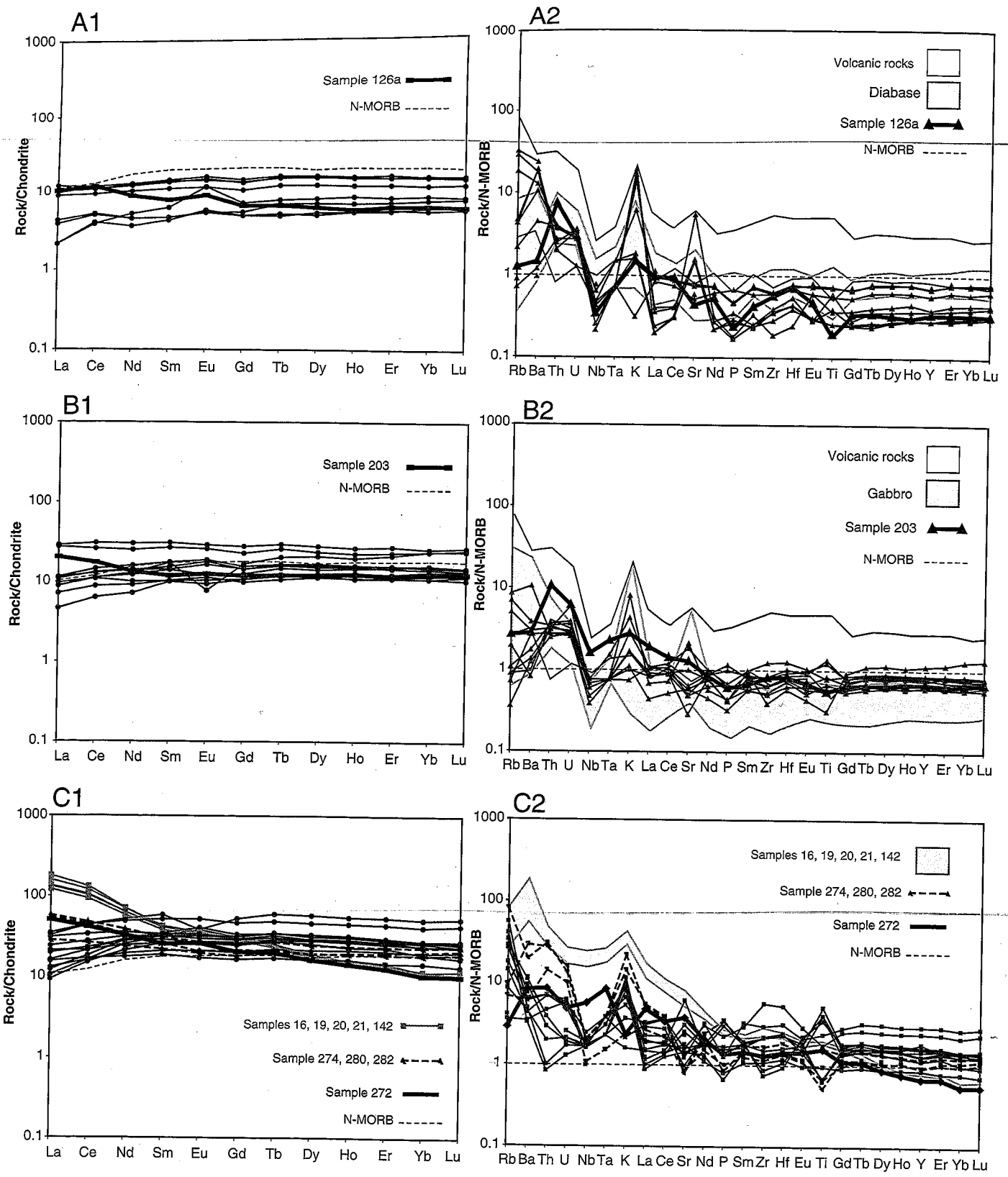


Figure 6. REE (1) and incompatible element (2) diagrams for (A) gabbro, (B) diabase dikes, and (C) volcanic rocks. REE elements were normalized to chondritic meteorite compositions (McDonough and Sun, 1995). Normal mid-oceanic-ridge basalt (N-MORB) reference line (Sun and McDonough, 1989) is marked by a thin dotted line on all diagrams. For comparison of the different rock types within the Eldivan ophiolite, white and gray fields are plotted in each trace element diagram: volcanic rocks in white (A2, B2), gabbro and diabase dikes in gray (A2, B2), and alkaline rocks in gray (C2). Special samples mentioned in the text are distinguished by bold solid or dashed lines.

most immobile elements, most basalt samples plot in the MORB field. Ternary discriminant diagrams have similar results (Fig. 8), with basalts falling clearly into the MORB fields in diagrams B, C, and D. Diagrams A and E do not distinguish between MORB and subduction-related basaltic rocks.

2. Contrastingly, the geochemistry of samples 16, 19, 20, 21, and 142 (Fig. 6C1, light gray lines) shows highly elevated immobile LREE up to 17 times that of N-MORB and HREE below N-MORB concentrations, giving steeply sloping patterns typical of alkaline ocean island basalts (OIB) (Fig. 6C), but reflect alteration in high K abundance. Element ratios of La/Yb are correspondingly high (La/Yb = 16.21–22.47). Sample 272 (Fig. 6C1, bold line) is subparallel to these samples, showing low abundances in HREE but only a moderate LREE elevation. Trace element patterns for samples 16, 19, 20, 21, and 142 (Fig. 6C2, gray field) show the same elevation in the LILE as seen in the LREE, with some variation in mobile elements, most notably Ba and K. Sample 272 (Fig. 6C2, bold line) has LILE abundances more elevated than the N-MORB-type basalts but less than the alkaline samples. The absence of a Nb anomaly, combined with the low HREE concentrations, suggests that this sample source was not modified by subduction but perhaps was derived from a more heterogeneous source transitional between those that produce N-MORB and OIB basalts. These rocks consistently plot in fields for OIB, WPB, and alkaline basalt on discriminant diagrams (Figs. 7A, 7B, 7D, 7F). In diagrams where alkaline fields are not present, these rocks plot outside all fields (G) or overlap both the IAT and MORB fields (C), and cannot be discriminated. In diagram E, these samples plot in the E-MORB field. Similar results are seen with additional ternary discriminant diagrams (Fig. 8). In all diagrams, these rocks plot as within plate alkali (A, B, D), ocean island tholeiite (C), and WPB (E).

3. The third geochemical signature is seen in basaltic sample 274 (Fig. 6C1 and 2, bold dashed line), which shows LILE enrichment and HFSE (Nb, Ta) depletion relative to N-MORB, suggesting a subduction-influenced source (Fig. 6C2). A subduction-influenced source is also reflected in a slight LREE enrichment and high ratios of Th/La (6.48), La/Nb (2.85), and La/Yb (3.66) (Fig. 6C1).

Rhyolitic samples have two separate trace and REE signatures. Most samples are similar to N-MORB in their lower LREE concentrations compared with HREE (Fig. 6C1) but have overall flatter patterns that could reflect higher degrees of differentiation in the magma chamber. This same pattern is also seen in the trace elements (Fig. 6C2), with LILE slightly lower in concentration than HREE, with the exception of Zr and Hf, which show higher abundances. The effects of secondary alteration are seen in the scatter of mobile elements, especially Ba, U, Th, K, and Sr.

Alternatively, rhyolitic samples 280 and 282 (Fig. 6C2, bold dashed line) closely match basaltic sample 274. LREE abundances are elevated, reflected in Th/Ta, La/Nb, and La/Yb ratios similar to sample 274 (Fig. 6C1). LILE (Fig. 6C2) are also more abundant except for negative concentrations of Nb, Ta, and Ti, characteristic of subduction zones. Some scatter is still seen in the mobile elements, particularly Rb, K, and Sr.

Despite the two signatures seen in REE and trace elements, all of the rhyolitic samples plot in fields for volcanic arc granite (Fig. 7, H, I) in discriminant diagrams of Pearce et al. (1984a) that are based on immobile elements of Nb, Ta, and Yb.

## Interpretation of Whole-Rock and Mineral Chemistry

Three different magma affinities are present in the Eldivan ophiolite: N-MORB, alkaline (OIB), and supra-subduction zone. The occurrence of three distinct geochemical signatures in this small area of exposure (~20 km$^2$) implies a high degree of mixing of either (1) upper and lower plate blocks during tectonic emplacement or (2) magma sources during seafloor formation.

Mixing of upper and lower plate units is plausible, considering the current imbricated structure of the ophiolite in the mélange. This has been suggested to account for alkaline rocks within the mélange that are interpreted as seamounts accreted into the serpentine mélange from the downgoing plate (Floyd, 1993; Tüysüz et al., 1995; Tankut et al., 1998). Accretionary mixing of an N-MORB downgoing plate, which included seamounts, with a supra-subduction zone upper plate could explain the geochemical variation in the Eldivan ophiolite, although few modern analogues of this process exist.

Similar chemical variations to those seen in the Eldivan ophiolite are found in modern backarc supra-subduction zone basins due to mixing different magma sources rather than upper and lower plate components. Such supra-subduction zones or backarc ocean basins are extensional upper plate basins that form above subduction zones owing to lower plate movement away from the upper plate through slab rollback. The combination of extension and subduction in supra-subduction zone backarc settings creates conditions of both mantle depletion and enrichment, which result in basalts of different compositions (Sinton and Fryer, 1987; Price et al., 1990; Stern et al., 1990; Eissen et al., 1994; Hawkins and Melchior, 1985; Dril et al., 1997; Fretzdorff et al., 2002; Sinton et al., 2003). Basalts in the North Fiji, Lau, Mariana, Manus, and East Scotia backarc basins show an overprint of LILE enrichment on N-MORB geochemical patterns, which increase with proximity to the subducting slab. Compositional zoning in the Lau basin, with LILE enriched basalt on the west edge near the arc and N-MORB types in the young central spreading center, show that LILE enrichment decreases as rifting continues, owing to decreased subduction influence from slab rollback (Hawkins and Melchior, 1985; Pearce et al., 1984b). Likewise, initial rifts in the Mariana trough erupt basalts similar to those of the Mariana arc, where older rift zones erupt N-MORB (Stern et al., 1990). North Fiji and East Scotia spreading ridges erupt basalt transitional between N-MORB and alkaline basalt owing to influence from hotspot volcanism (Price et al., 1990; Eissen et al., 1994; Fretzdorff et al., 2002). This chemical array is similar to that seen in the Eldivan ophiolite and occurs entirely in the upper plate, caused by mixing of variably depleted

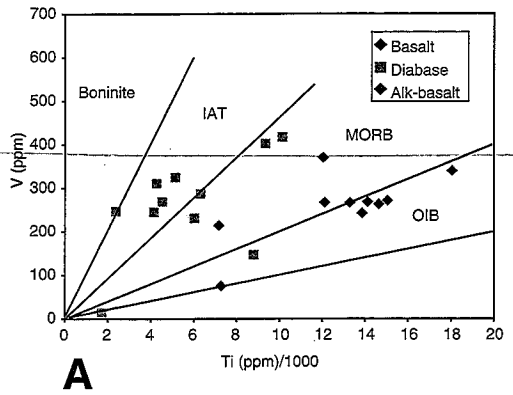
Basalt
Diabase
Alk-basalt
Boninite
IAT
MORB
OIB
V (ppm)
Ti (ppm)/1000

A

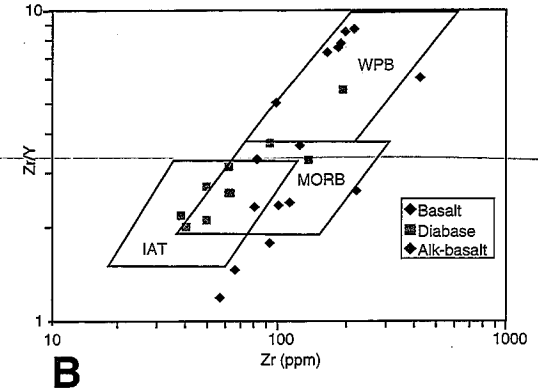
WPB
MORB
IAT
Basalt
Diabase
Alk-basalt
Zr/Y
Zr (ppm)

B

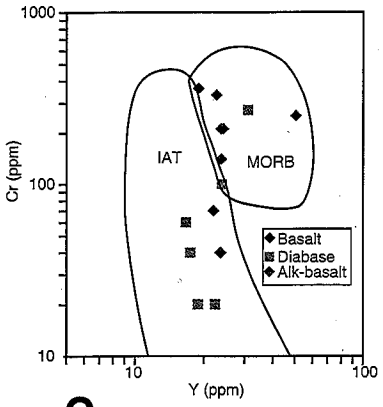
IAT
MORB
Basalt
Diabase
Alk-basalt
Cr (ppm)
Y (ppm)

C

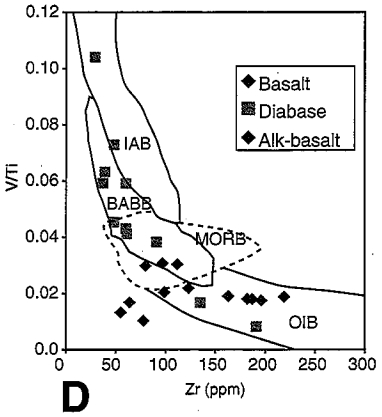
Basalt
Diabase
Alk-basalt
IAB
BABB
MORB
OIB
V/Ti
Zr (ppm)

D

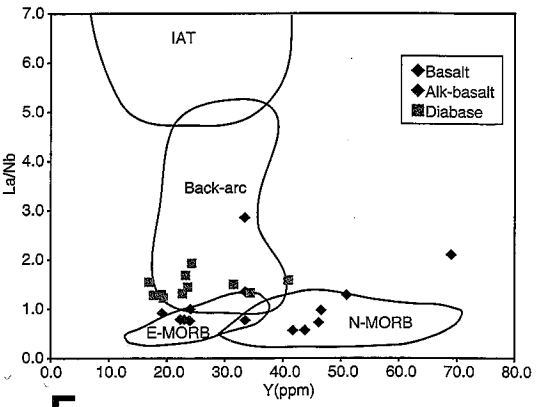
IAT
Basalt
Alk-basalt
Diabase
Back-arc
E-MORB
N-MORB
La/Nb
Y(ppm)

E

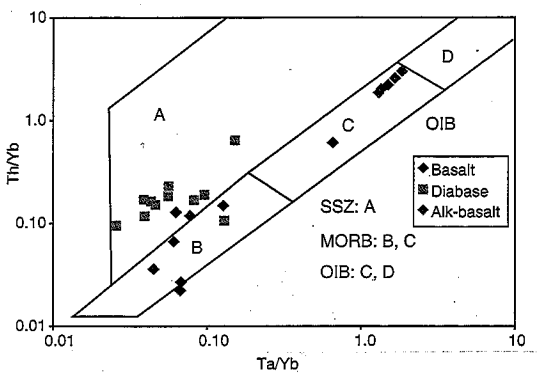
A
B
C
D
OIB
Basalt
Diabase
Alk-basalt
SSZ: A
MORB: B, C
OIB: C, D
Th/Yb
Ta/Yb

F

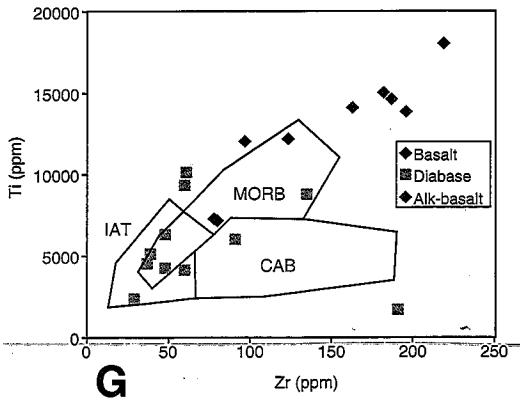
Basalt
Diabase
Alk-basalt
MORB
IAT
CAB
Ti (ppm)
Zr (ppm)

G

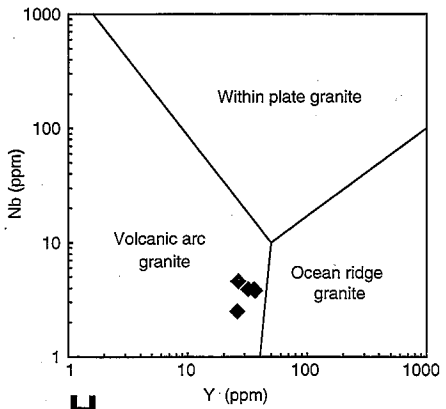
Within plate granite
Volcanic arc granite
Ocean ridge granite
Nb (ppm)
Y (ppm)

H

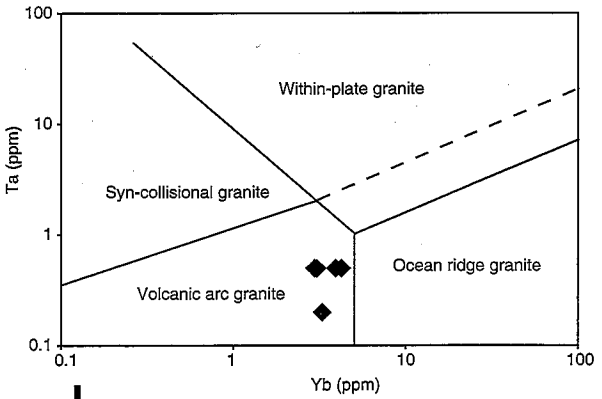
Within-plate granite
Syn-collisional granite
Volcanic arc granite
Ocean ridge granite
Ta (ppm)
Yb (ppm)

I

and enriched mantle sources or melts (Sinton and Fryer, 1987; Price et al., 1990; Stern et al., 1990; Dril et al., 1997).

In this study the backarc basin or supra-subduction zone mixing is favored for the Eldivan ophiolite. Although incompatible and REE diagrams are dominated by N-MORB patterns, there are noticeable subduction and alkaline influences (samples 126a, 203, 280, and 272), as seen in modern backarc and intra-arc settings. Additionally, basalt mostly plots as N-MORB, with some scatter into other fields (Figs. 7 and 8), but dike rocks plot consistently within subduction-influenced fields, including IAT, backarc basin, and supra-subduction zone, with minor overlap into N-MORB fields (Figs. 7 and 8). These dike compositional patterns provide direct evidence that the Eldivan ophiolite was at one time in a supra-subduction setting, as the sheeted dike complex represents ocean floor construction. Additionally, rhyolitic volcanics also plot in volcanic arc fields (Fig. 7), giving more evidence for a significant subduction influence.

Evidence for a supra-subduction zone setting is also found in the mantle sequence of the Eldivan ophiolite. Cr-spinel (Cr#s 0.47–0.70) plots within fields for mantle more depleted than ocean rift mantle and closer to transitional supra-subduction settings (Fig. 4) similar to Oman-type ophiolites as defined by Harris (1992). This is also supported in whole-rock $Al_2O_3$ wt% of the Eldivan ophiolite, which indicates the degree of partial melt extraction, and could be expected for ocean crust in the complex melting regime of a backarc basin. It also closely matches $Al_2O_3$ wt% concentrations from the Oman ophiolite but is slightly higher than the Brooks Range ophiolite and Orhaneli ophiolite (western İzmir-Ankara-Erzincan suture zone), all thought to have formed in supra-subduction zone settings (Fig. 3).

Finally, a supra-subduction zone interpretation is consistent with other studies along the İzmir-Ankara-Erzincan suture zone in the Ankara Mélange, Dağkuplu Mélange, and Kırşehir block ophiolitic massifs. Other areas of the Ankara Mélange contain alkaline basalts (Çapan and Floyd, 1985, 1993; Tankut et al., 1998), N-MORBs (Tankut, 1984; Tankut et al., 1998), and IAT basalts (Tankut, 1984; Tankut et al., 1998; Tüysüz et al., 1995) similar to the Eldivan ophiolite. Our discovery of supra-subduction zone dikes is consistent with the discovery of supra-subduction zone plagiogranite in the Ankara Mélange (Dilek and Thy, 2006). Similarly, the Dağkuplu Mélange in the western İzmir-Ankara-Erzincan suture zone shows the same variety of alkaline, N-MORB, and supra-subduction zone geochemistry (Göncüoğlu et al., 2006; Sarıfakıoğlu, 2006; Sarıfakıoğlu et al., 2009). Supra-subduction geochemistry also characterizes Cretaceous ophiolites from the Kırşehir block (Çiçekdağ and Sarıkarıman massifs) (Yalınız et al., 1996, 2000a; Floyd et al., 2000).

Most of these previous studies use geochemistry of crustal volcanic rocks, cumulate sequences, dike complexes, and massive gabbros for their interpretation without data from associated mantle peridotite. Including analyses of the peridotite provides additional evidence for high degrees of melt extraction inconsistent with a MORB tectonic model for the Eldivan ophiolite. Sarıfakıoğlu et al. (2009) used both mineral and whole-rock geochemistry of crust and mantle rocks to interpret the Orhaneli ophiolite in the western İzmir-Ankara-Erzincan suture zone as a supra-subduction zone ophiolite. Cr-spinel data from lherzolite and harzburgite of the Orhaneli mantle sequence closely match the Eldivan ophiolite (Fig. 4). Whole-rock $Al_2O_3$ from the Orhaneli ophiolite is generally lower but is still within the range of the Eldivan ophiolite (Fig. 3). These results show the same continuity in mantle composition as seen in the crustal-sequence geochemical data that argue for some supra-subduction influence from the western to central İzmir-Ankara-Erzincan Ocean.

## EPI-OPHIOLITIC SEDIMENTARY COVER UNITS

Epi-ophiolitic sediment occurs as blocks, intercalated sediment in pillow lobes, and layered sediments depositionally overlying pillow basalts. Blocks are generally meter to decimeter sized blocks of pelagic, radiolarian-bearing limestone and minor chert within the serpentinized matrix of the mélange but not in direct contact with ophiolitic units. Some radiolarian-bearing red chert is intercalated within pillow basalt lobes. Layered sediments overlying the ophiolite consist of interbedded chert and limestone, and chert interbedded with pillow basalt and volcanic breccia. Individual beds are centimeters thick, but sediment sequences can reach 10 m. In one locality, shale and minor sandstone turbidites were found within the epi-ophiolitic cover.

### Karadağ Formation

The Karadağ Formation overlies the Ankara Mélange along an angular unconformity and, because of multiple deformation phases, also overlies the mélange tectonically as a result of later thrust faulting. It is made up of intercalated volcanic and coarse siliciclastics at its base that grade upward into finer sandstones and mudstones and finally clay-rich limestone (Akyürek et al., 1980; Hakyemez et al., 1986). It is interpreted as flysch deposited in a foredeep setting near a continental margin during the onset of collision. The Kursunluduz Member of the Karadağ Formation contains chert bands alternating with red pelagic limestone (Akyürek et al., 1980; Hakyemez et al., 1986). The presence of

Figure 7. Nine discriminant diagrams for basaltic rocks of the Eldivan ophiolite. In diagrams A–G, basaltic rocks generally plot in MORB fields, although some show too much scatter to be conclusive. Dikes mostly fall into island arc tholeiite (IAT) fields with some overlap in MORB fields. Alkaline basalts plot consistently in ocean island basalt (OIB) or within plate basalt (WPB) fields. Diagrams H and I are for granitic rocks. Samples from the Eldivan ophiolite all plot in volcanic-arc granite fields. These diagrams are from (A) Shervais (1982); (B) Pearce and Norry (1979); (C) Pearce (1982); (D) Woodhead et al. (1993) and Floyd et al. (2000); (E) Floyd et al. (1991); (F) Pearce et al. (1981); (G) Pearce and Cann (1973); (H) Pearce et al. (1984a); (I) Pearce et al. (1984a). BABB—backarc basin basalt; E-MORB—enriched MORB; N-MORB—normal MORB; SSZ—supra-subduction zone; CAB—continental arc basalt.

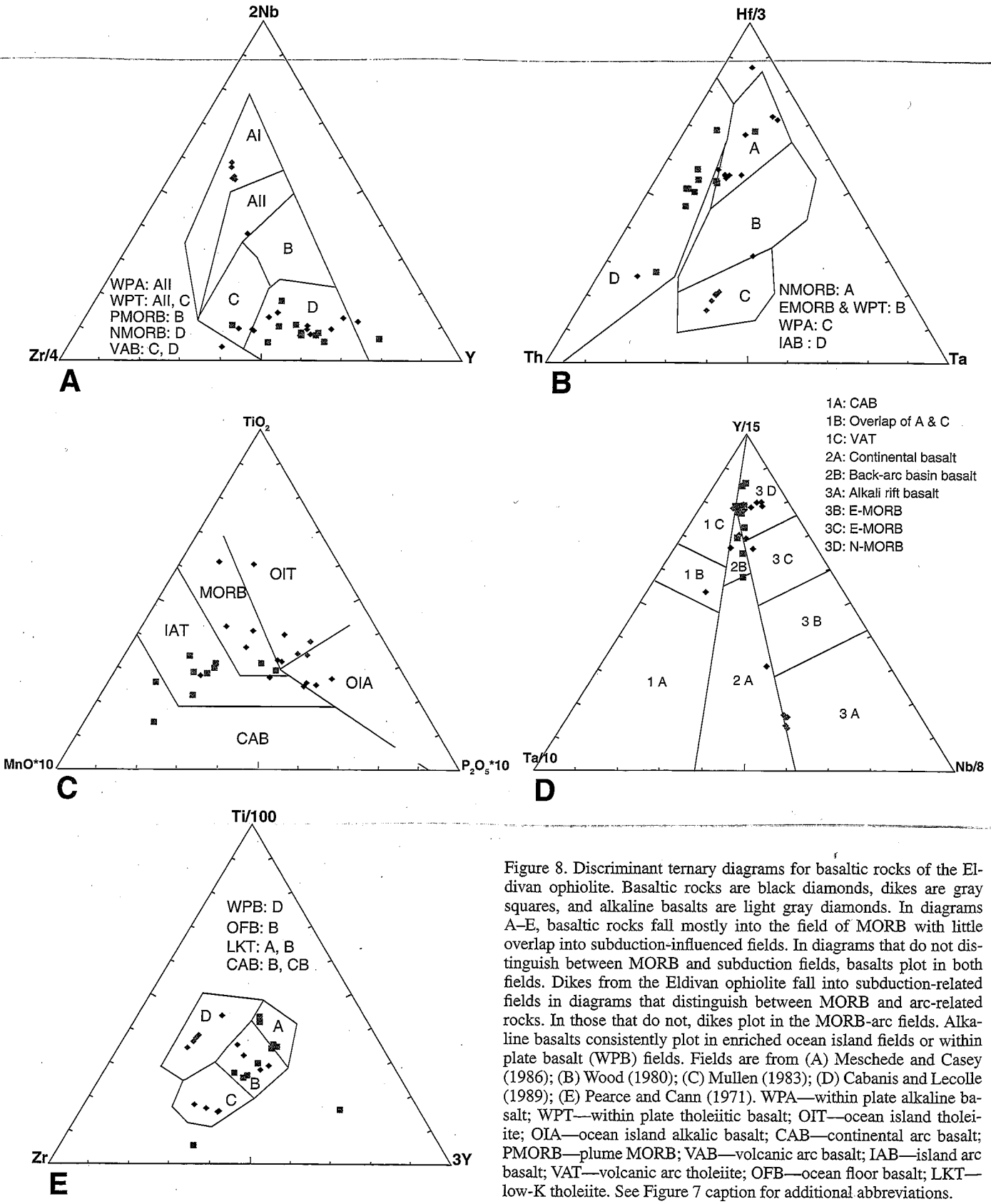


Figure 8. Discriminant ternary diagrams for basaltic rocks of the Eldivan ophiolite. Basaltic rocks are black diamonds, dikes are gray squares, and alkaline basalts are light gray diamonds. In diagrams A–E, basaltic rocks fall mostly into the field of MORB with little overlap into subduction-influenced fields. In diagrams that do not distinguish between MORB and subduction fields, basalts plot in both fields. Dikes from the Eldivan ophiolite fall into subduction-related fields in diagrams that distinguish between MORB and arc-related rocks. In those that do not, dikes plot in the MORB-arc fields. Alkaline basalts consistently plot in enriched ocean island fields or within plate basalt (WPB) fields. Fields are from (A) Meschede and Casey (1986); (B) Wood (1980); (C) Mullen (1983); (D) Cabanis and Lecolle (1989); (E) Pearce and Cann (1971). WPA—within plate alkaline basalt; WPT—within plate tholeiitic basalt; OIT—ocean island tholeiite; OIA—ocean island alkalic basalt; CAB—continental arc basalt; PMORB—plume MORB; VAB—volcanic arc basalt; IAB—island arc basalt; VAT—volcanic arc tholeiite; OFB—ocean floor basalt; LKT—low-K tholeiite. See Figure 7 caption for additional abbreviations.

*Praeglobotruncana stephani*, *Rotaliapora apenninica*, *Hedbergella* sp., *Ticinella* sp., *Globigerina* sp., *Textulariella* sp., *Cuneolina* sp., and *Valvulammina* sp. radiolarians suggests the age of the Karadağ is Cenomanian to Campanian (Akyürek et al., 1980).

Near the Eldivan ophiolite, the Karadağ Formation consists mostly of pelagic limestone and chert, and some clastic material, including sandstone lenses with graded and cross-beds. The angular unconformity between the Karadağ Formation and the underlying imbricated ophiolitic material of the Ankara Mélange suggests that the Karadağ Formation was deposited after or during imbrication of the ophiolite, and is in part correlative with the overlying Maastrichtian flysch of Norman (1984).

## U/Pb Age Analysis of Detrital Zircon in Sandstone Units

Sandstone samples were collected from a block within the Ankara Mélange directly adjacent to basalt and from the Karadağ Formation, which unconformably overlies the mélange. The age and tectonic source region for sandstone samples from the mélange and overlying Karadağ Formation were investigated through detrital zircon and sandstone petrography. Siliciclastic material was scarce, and these two samples represent the only sandstones found within the study area. The entire sample collected was processed for detrital zircons. The error introduced by the limited sample size and small number of zircons found within each sample is recognized, however the results are consistent with age data obtained by other methods throughout the suture zone.

Zircon U-Pb age analyses were conducted by laser-ablation multicollector inductively coupled-plasma mass spectrometry (LA-MC-ICPMS) at the Arizona LaserChron Center. Analytical methods follow those described in Gehrels (2000) and Gehrels et al. (2006). Single point analyses were taken with a 35 μm and a 25 μm diameter beam according to grain size. Common Pb corrections are for $^{204}Pb$, using an initial Pb composition from Stacey and Kramers (1975). Uncertainties are 1.0 for $^{206}Pb/^{204}Pb$, 0.3 for $^{207}Pb/^{204}Pb$, and 2.0 for $^{208}Pb/^{204}Pb$. Detrital zircon age extractor and ISOPLOT 3.00 (Ludwig, 2003) were used to determine and sort reliable age data. This detrital zircon age extractor extracts significant peak ages based on at least three grain analyses and the number of grains constituting each peak age. Results are listed in Table A3.

## Zircon Age Populations

Detrital zircon age populations from sandstone in the mélange and the Karadağ Formation have different minimum, maximum, and peak ages, suggesting that they were sourced from different terranes (Fig. 9). Detailed analysis of the mélange sandstone shows an age distribution from 143.2 ±2 Ma to 164.1 ±1 Ma with a peak age of 153 Ma. The Karadağ sandstone shows an age distribution from 105.2 ±5 Ma to 166 ±3 Ma, with a peak age of 130 Ma. The youngest peak age is used here as a proxy for the maximum age of deposition, which is consistent with the stratigraphic positions of the sandstones. The maximum age of the mélange sandstone, and Eldivan ophiolite, is 143.2 ±2 Ma, whereas the maximum age of the Karadağ sandstone is 105.2 ±5 Ma. Peak ages here are interpreted to represent the average age of the terrane dominantly being eroded at the time of deposition.

An inherited fraction of zircon from the Neoproterozoic to Paleoproterozoic is present in both the mélange and the Karadağ sandstones (Fig. 9). Detrital zircons of similar age from the Tauride block in southwestern Turkey were documented by Kröner and Şengör (1990), who attributed them to the southern Angara

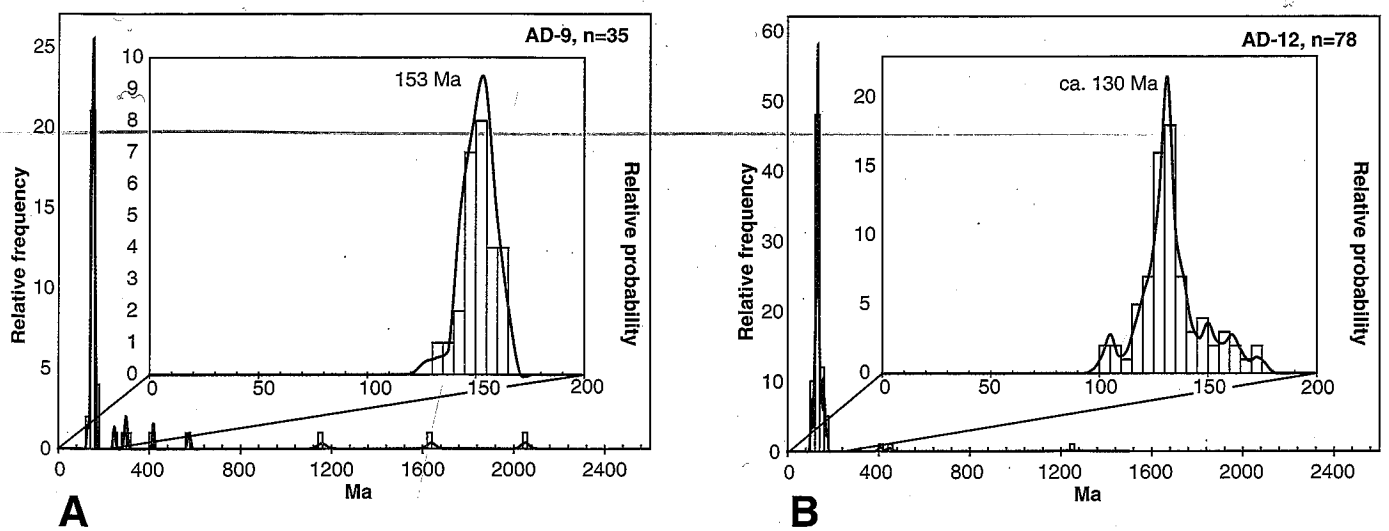


Figure 9. Detrital zircon age populations for sandstones within the mélange (A) and the Karadağ Formation (B), indicating different source terranes for the two units. The larger graphs show the entire zircon population, including those that have Precambrian ages. The inset graph shows the detail of the peak ages. For the ophiolitic sandstone, the distribution of ages is narrow, with a peak age of ca. 153 Ma. The Karadağ sandstone has a larger range in ages, and a peak age of ca. 130 Ma.

craton of Siberia. Dilek and Thy (2006) also found Proterozoic zircon in plagiogranite from the ophiolite near Ankara and interpreted them as a subduction recycled component from the Rhodope-Strandja-Massif in northwestern Turkey and southeastern Bulgaria. These terranes may also have supplied the Paleoproterozoic to Neoproterozoic zircon grains in the mélange and Karadağ sandstones.

### Sandstone Petrography

Sandstone from both formations is compositionally and texturally immature, with low percentages of quartz and angular to subangular clasts. Despite alteration and secondary authigenic growth, the sandstone samples yielded two very different petrographic provenance results. The mélange sandstone is dominated by volcanic lithic fragments (52.33%) and plagioclase (25.33%), with minor quartz (8.66%), K-feldspar (2.00%), and clay minerals (11.66%). In contrast, the overlying Karadağ sandstone is made up of carbonate mud clasts (with some authigenic clay) (45.33%), plagioclase (28.00%), bioclastic grains (15.00%), and quartz (11.33%), with minor volcanic lithic material (0.33%).

The composition of the mélange sandstone with its high percentage of volcanic lithic fragments implies that it was sourced from a nearby volcanic terrane. This idea agrees with the tectonic discriminant diagrams of Dickinson et al. (1983) (not shown). There are a number of sources for lithic fragments in the İzmir-Ankara-Erzincan Ocean, including seamounts, island arcs (Tankut, 1984; Tankut et al., 1998; Tüysüz et al., 1995), and the Pontide continental arc to the north. However, the Pontide arc is younger (Turonian) than detrital zircon grains found in the mélange sandstone, suggesting that it is not the source for volcanic lithics. The other plausible volcanic sources are oceanic, giving more evidence for intra-oceanic subduction away from the continental margin. Sandstone from the Karadağ Formation contains virtually no volcanic lithics, bioclastic grains, carbonate mud, or plagioclase grains. The bioclastic material in this sample is a mix of echinoderm, bryozoan, brachiopod, bivalve, and foraminiferan grains, a compositional variation that suggests a well-developed but relatively shallow carbonate system. No deep water fauna are recorded. These data suggest that the Karadağ sandstone was derived from the carbonate system of a continental margin and was deposited in a nearby marginal basin. This is consistent with the interpretation of the Karadağ Formation as flysch deposited on the imbricated ophiolite, most likely in a foredeep setting near the continental margin, created as continuing subduction brought the Kırşehir and Sakarya-Pontide terranes together.

## STRUCTURE OF THE ELDIVAN OPHIOLITE

The angular unconformity between the Karadağ Formation and the underlying imbricated mélange, and the subsequent shortening of both, imply multiple phases of deformation (Fig. 10). The first phase involved dismemberment of the Eldivan ophiolite and serpentinite mélange development (Fig. 10A). Where paleohorizontal indicators exist, they show predominantly steep dips. Elongated blocks are also commonly vertical, with gaps between them filled with serpentine. If the mélange is associated with an accretionary wedge, it is likely the sections investigated formed near the backstop region, the area where accreted thrust sheets are progressively rotated to steeper dips by accretion of new material beneath them.

Accretionary wedge development commonly produces isoclinally folded units with mostly sub-horizontal fold hinge lines. Although horizontal fold hinge lines are found within the serpentinite matrix and in overlying Karadağ Formation units, no hinge lines were found in the several blocks we investigated. Another way to explain the mostly steep dips in mélange blocks is by strike-slip deformation, which would produce steeply plunging hinge lines. There is no evidence of these in any part of the field area.

The second phase of deformation occurred after the Karadağ Formation was deposited above the Ankara Mélange. During this second phase, the Karadağ Formation and underlying ophiolite and serpentine were thrust along southward-verging thrust faults (Fig. 10B). Some age constraints for these events are provided by detrital zircon populations from the mélange and Karadağ sandstones.

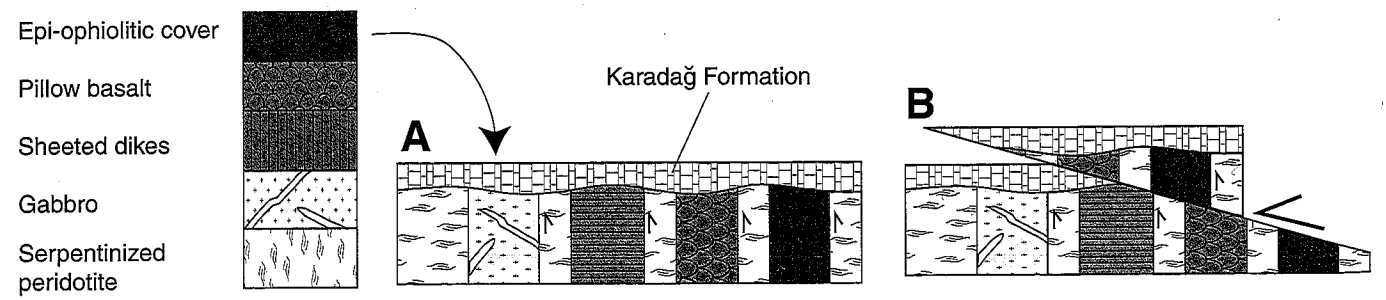


Figure 10. Multiple deformational phases are found in the Ankara Mélange. The first phase imbricated and rotated the oceanic units into mostly vertical units, encased in serpentine mélange (A). Subsequent phases involved shortening of the Ankara Mélange and the unconformably overlying Karadağ Formation (B). Subsequent events included serpentine diapirism and thrusting of mélange over late Miocene deposits of the Hançili Formation.

## Timing of Ophiolite Imbrication

Detrital zircon ages from sandstone within and above the Ankara Mélange provide limits on the timing of mélange formation and dismemberment of the Eldivan ophiolite. Zircon grains as young as 143 ±2 Ma within a sandstone of the mélange indicate that it was incorporated into the mélange after this time and before the youngest age of zircon grains within the unconformably overlying Karadağ sandstone, which yields ages of 105 ±5 Ma. Further imbrication of the ophiolite and the Karadağ Formation occurred after 105 ±5 Ma.

Imbrication of the Eldivan ophiolite between 143 ±2 and 105 ±5 Ma is consistent with data from other parts of the suture zone that suggest collapse of the ocean basin had begun about this time. For example, radiolarians in limestone deposits from the Kirazbaşı foredeep complex are as old as ca. 135 Ma (late Valanginian) (Tüysüz and Tekin, 2007). Intra-oceanic thrusting began prior to 90 Ma near the Kırşehir block (Yalınız et al., 2000b) and 93 ±2 Ma in the western İzmir-Ankara-Erzincan Ocean (Önen, 2003). Granitoids of 94.9 ±3.4 Ma, in the Kırşehir block, interpreted as the result of supra-subduction zone ophiolite obduction, also suggest that subduction must have been active before 95 Ma (Boztuğ et al., 2007).

## Restoration of the Eldivan Ophiolite

The orientation of sheeted dikes in ocean crust is commonly used as a proxy for spreading ridge orientation. For the Eldivan ophiolite, it would represent the orientation of a supra-subduction zone spreading ridge. Commonly, sheeted dikes are perpendicular to overlying basaltic flows that they feed. Most dikes in the Eldivan Ophiolite strike NNW-SSE and are steeply dipping (Fig. 11A). A minor component of E-W dikes is also found, but most are horizontal. In one locality, which represents the largest single mélange block of basaltic rock in the Hançili region, a series of horizontal sheeted dikes is in contact with vertical pillow basalts and sheet flows that strike E-W, indicating that the entire igneous section has rotated 90° about a horizontal axis. Sedimentary blocks are also steeply dipping, indicating a similar amount of rotation about a horizontal E-W axis.

Assuming that other sheeted dikes in the region underwent a similar horizontal axis rotation, applying this rotation to the NNE-SSW dikes provides the original orientation of the supra-subduction zone spreading ridge that produced the Eldivan ophiolite. The rotation maintains the steep dip of the NNW-SSE dikes but changes the average strike to near N-S (Fig. 11B), which is subparallel to the İzmir-Ankara-Erzincan suture zone. However, oroclinal bending of this suture zone from indentation of the Kırşehir block indicates an additional 90° of counterclockwise vertical axis rotation.

Paleomagnetic studies used to test the oroclinal bend hypothesis found that the Ankara Mélange near the Eldivan ophiolite has undergone at least 30° of counterclockwise vertical axis rotation since the Eocene, and that it may have already been rotated counterclockwise by even more before this time (Kaymakci et al., 2003). According to Kaymakci et al. (2003), the Çankırı basin underwent rotation during the Eocene Epoch through the mid-Miocene, and perhaps as early as the Paleocene Epoch. Near the Eldivan ophiolite the Çankırı basin margin rotated 33° counterclockwise during Oligocene time.

A clockwise vertical axis rotation of 33° was applied to correct for these rotations, which moves the average strike direction of most sheeted dikes to 041, which was most likely the orientation in the Eocene (Fig. 11C). To completely restore the İzmir-Ankara-Erzincan suture zone back to its pre-collisional indentation trend, an additional 52° of clockwise rotation is needed. Correcting for the horizontal and vertical axis rotations of the sheeted dikes shows that they are subparallel to the İzmir-Ankara-Erzincan suture zone, which implies mostly orthogonal motion of the spreading ocean with respect to the subduction boundary represented by the suture zone, indicating little strike slip motion in the creation of the suture zone. These results are

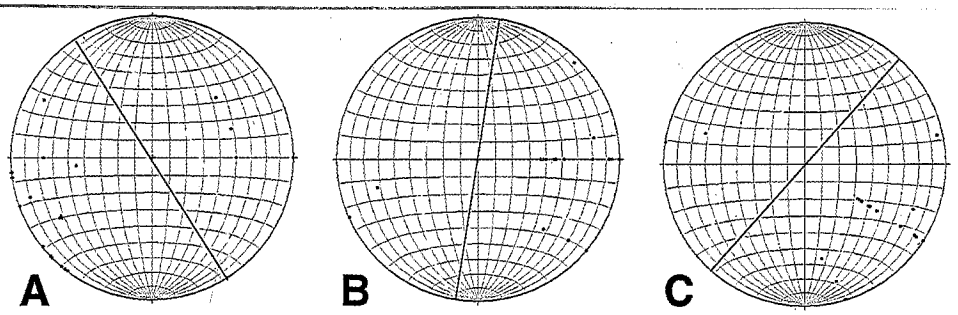


Figure 11. Stereographs of poles to dike attitudes in sheeted dike units of the Eldivan ophiolite. Solid black lines are average strike of sheeted dikes and most likely the spreading ridge: (A) Prior to any restoration. (B) Restored about a horizontal axis according to paleo-horizontal controls. (C) Partially restored to original orientation by 30° of post-Eocene clockwise vertical axis rotation documented from paleomagnetic data. Oroclinal bending of the İzmir-Ankara-Erzincan suture zone indicates that at least another 60° of clockwise rotation is needed to restore the dikes back to their original orientation, which would be near E-W.

consistent with those found by Fayon et al. (2001) and Whitney et al. (2001), who concluded that the northern part of the Kırşehir block was deformed and exhumed by orthogonal collision. However, whereas the İzmir-Ankara-Erzincan suture zone may have formed through orthogonal motion, Fayon et al. (2001) and Whitney et al. (2001) give evidence for a later oblique collision of the Tauride platforms with the southern Kırşehir block, exhuming the southern Kırşehir block through left-lateral wrench faulting.

## TECTONIC EVOLUTION

### Review of the İzmir-Ankara-Erzincan Ocean

Understanding the overall tectonic evolution of this ocean is crucial to reconstructing the role played by the Eldivan ophiolite. Age constraints of various events throughout the İzmir-Ankara-Erzincan suture zone indicate three main phases of İzmir-Ankara-Erzincan Ocean evolution: a constructional phase, a destructional phase, and a suturing phase (Fig. 12A).

The constructional phase began with rifting at least as old as the late Carnian–early Norian Stages (ca. 215 Ma), based on radiolarians associated with MORB in the central and western parts of the suture zone (Bragin and Tekin, 1996; Tekin et al., 2002). Other radiolarians suggest that it developed into an ocean basin by late Bajocian time (Tüysüz and Tekin, 2007), and seamounts formed on the ocean floor during the Jurassic and Cretaceous Periods (Rojay et al., 2001, 2004; Tankut et al., 1998).

Destruction of the ocean basin by intra-oceanic subduction is documented by supra-subduction zone ophiolites, the oldest in the Ankara Mélange, yielding a U/Pb zircon age of 179 ±15 Ma (Dilek and Thy, 2006). Intra-oceanic subduction continued through the Late Cretaceous Period, creating supra-subduction zone ocean crust in the central İzmir-Ankara-Erzincan Ocean, now part of the Kırşehir block (Yalınız et al., 1996; Yalınız et al., 2000b), and the Dağkuplu mélange (Göncüoğlu et al., 2006; Sarıfakıoğlu, 2006; Sarıfakıoğlu et al., 2009). Late Valanginian (ca. 135 Ma) (Tüysüz and Tekin, 2007) to Paleocene (Koyçiğit, 1991) radiolarians are found in foredeep deposits along the Sakarya-Pontide margin, suggesting that active subduction against the continent began in the Early Cretaceous Period.

Other events documenting subduction at this time are the occurrence of accretion complexes along the Pontide margin, which were metamorphosed at ca. 100 Ma (Okay et al., 2006), and Turonian Epoch (ca. 90 Ma) through Paleocene Epoch magmatism in the Ponticles (Yılmaz et al., 1997). It is important to note that the oldest age of supra-subduction zone ophiolites, 179 ± 15 Ma, predate the oldest foredeep deposits (ca. 135 Ma) against the continent, suggesting that intra-oceanic extension occurred prior to subduction against the continental margin. Thrusting and imbrication of the Eldivan supra-subduction zone basin in the central İzmir-Ankara-Erzincan suture zone occurred between 105 and 143 Ma, as shown by detrital zircon ages from this study. In the western İzmir-Ankara-Erzincan Ocean, thrusting began at least by 94 Ma, as recorded by the age of a metamorphic sole (Önen, 2003). This constrains a destructive phase of subduction that began ca. 179 ±15 Ma and ended as early as ca. 60 Ma.

Final closure of the İzmir-Ankara-Erzincan Ocean occurred through continental block collision, collisional indentation, and suturing of the Kırşehir block and the larger Anatolide-Tauride platform with the Sakarya-Pontide terranes during the Late Cretaceous Period to the Miocene Epoch. The first evidence of continental collision comes from post-collisional granitoids of the Kırşehir block, which yielded Rb-Sr whole-rock and $^{207}Pb$-$^{206}Pb$ zircon ages from 110 ±14 Ma (Güleç, 1994) to 74.9 ±3.8 Ma (Boztuğ et al., 2007). Exhumation of the collision zone in the Central Pontides, based on stratigraphic constraints, and granitoids of the Kırşehir block, based on apatite fission-track ages, documents collision between 86 and 93 Ma and 57 and 62 Ma, respectively (Okay et al., 2006; Boztuğ and Jonckheere, 2007). Collisional indentation of the Kırşehir block caused at least 90° of counterclockwise rotation, 33° of which is well constrained since the Eocene. Ages of continental block collision young away from the central part of the suture zone, where the Kırşehir block is present. In the western part of the suture, where the Kırşehir block is absent, and collision of the Sakayra-Pontide terrane occurred only within the Anatolide-Tauride block,

Figure 12. (A) Age constraints for the evolution of the İzmir-Ankara-Erzincan suture zone through time. Three main phases are identified: (1) an initial construction phase in which the ocean basin was forming through ridge spreading with hotspot volcanism creating seamounts on the ocean floor, (2) destruction of the ocean basin through intra-oceanic subduction that resulted in intra-oceanic seafloor spreading above a subduction zone and arc magmatism, and (3) collision and suturing of the Kırşehir and Anatolide-Tauride continental blocks with the Sakarya-Pontide terranes. Numbers in the time line and map correspond with the source of age data (below) and sample locations, respectively. The sample location for detrital zircons of this study is represented with a black star. Sources for data are as follows: (1) Tekin et al. (2002); (2) Bragin and Tekin (1996); (3) Dilek and Thy (2006); (4) Rojay et al. (2004); (5) Rojay et al. (2001); (6) Göncüoğlu et al. (2006); (7) Tüysüz and Tekin (2007); (8) Önen (2003); (9) Yalınız et al. (2000); (10) Koçyiğit (1991); (11) Yalınız et al. (1999); (12) Boztuğ and Jonckheere (2007); (13) Yılmaz et al. (1997); (14) Okay et al. (2006); (15) Kaymakci et al. (2003); (16) Boztuğ et al. (2007) and references therein; (17) Fayon et al. (2001). (B) Schematic cartoon model for the evolution of the Eldivan ophiolite during the Cretaceous, using the Philippine Sea plate and Mariana trough as an analogue. Early Cretaceous time documents the beginning of subduction and upper plate extension, as evidenced by supra-subduction zone (SSZ) basalt, foredeep complexes along the continental margin, and ophiolitic metamorphic soles. In the Late Cretaceous Period supra-subduction zone upper plate subduction began along the Sakarya-Pontide margin, causing active volcanism in the Pontide continental arc. The latest Cretaceous Period through the Oligo-Miocene Epochs was characterized by collision and suturing of the Kırşehir block (KB) and Anatolide-Tauride platform with the Sakarya-Pontide terrane, as evidenced by post-collisional granitoids and fission-track (FT) exhumation ages of the Kırşehir block. Fission-track ages also indicate that wrench faulting exhumed the southern Kırşehir block through left-lateral, strike-slip motion owing to later oblique collision of the Tauride platform with the Kırşehir block. OIB—ocean island basalt.

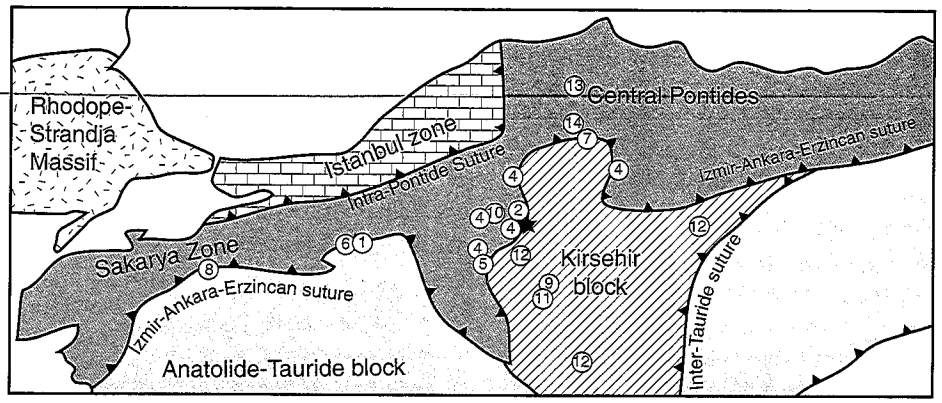
Rhodope-Strandja Massif
Istanbul zone
Intra-Pontide Suture
Central Pontides
Izmir-Ankara-Erzincan suture
Sakarya Zone
Izmir-Ankara-Erzincan suture
Kirsehir block
Inter-Tauride suture
Anatolide-Tauride block

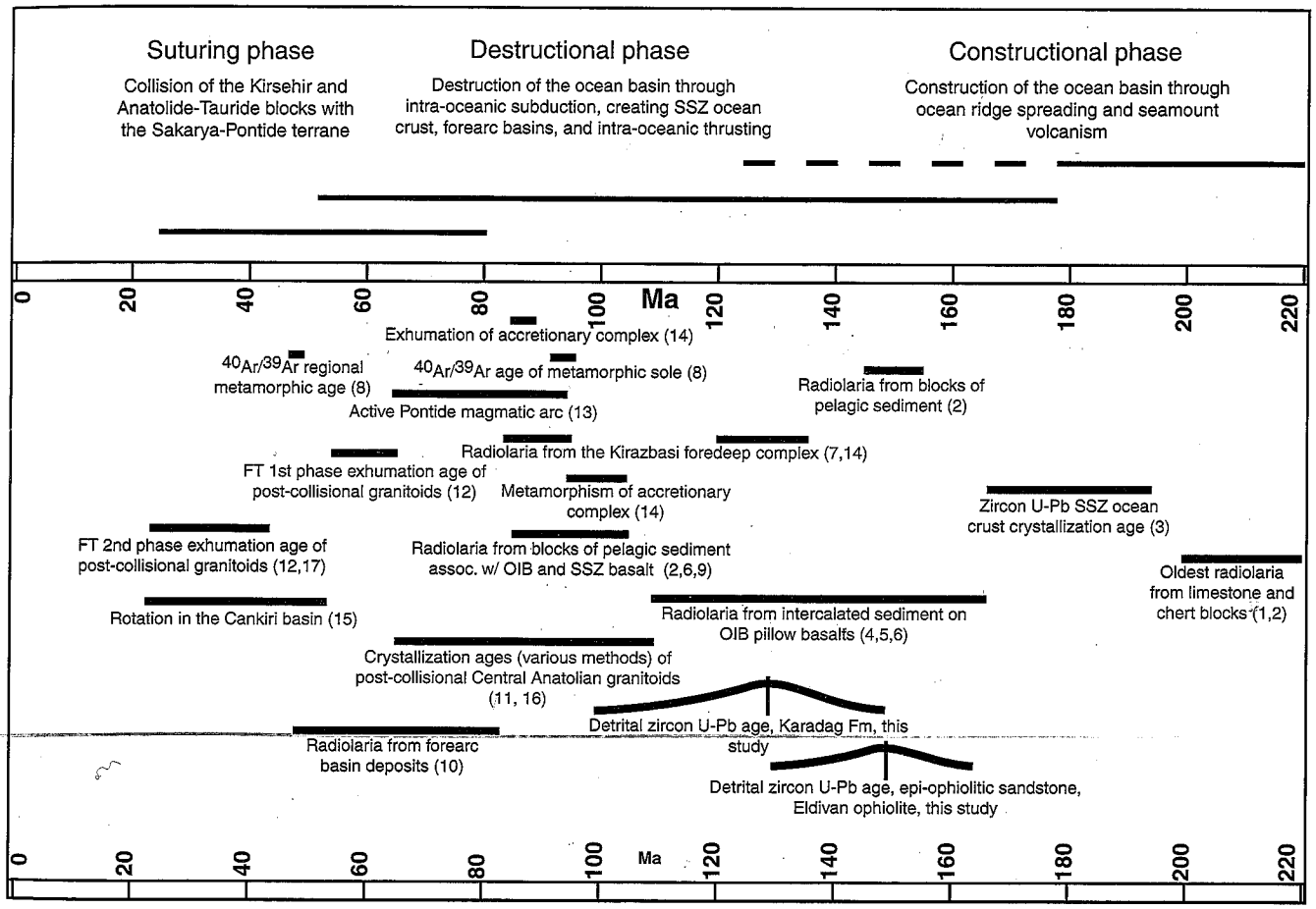
Suturing phase
Collision of the Kirsehir and Anatolide-Tauride blocks with the Sakarya-Pontide terrane
Destructional phase
Destruction of the ocean basin through intra-oceanic subduction, creating SSZ ocean crust, forearc basins, and intra-oceanic thrusting
Constructional phase
Construction of the ocean basin through ocean ridge spreading and seamount volcanism
0 20 40 60 80 100 Ma 120 140 160 180 200 220
Exhumation of accretionary complex (14)
40Ar/39Ar regional metamorphic age (8)
40Ar/39Ar age of metamorphic sole (8)
Active Pontide magmatic arc (13)
Radiolaria from blocks of pelagic sediment (2)
Radiolaria from the Kirazbasi foredeep complex (7,14)
FT 1st phase exhumation age of post-collisional granitoids (12)
Metamorphism of accretionary complex (14)
Zircon U-Pb SSZ ocean crust crystallization age (3)
FT 2nd phase exhumation age of post-collisional granitoids (12,17)
Radiolaria from blocks of pelagic sediment assoc. w/ OIB and SSZ basalt (2,6,9)
Oldest radiolaria from limestone and chert blocks (1,2)
Rotation in the Cankiri basin (15)
Radiolaria from intercalated sediment on OIB pillow basalts (4,5,6)
Crystallization ages (various methods) of post-collisional Central Anatolian granitoids (11, 16)
Detrital zircon U-Pb age, Karadag Fm, this study
Radiolaria from forearc basin deposits (10)
Detrital zircon U-Pb age, epi-ophiolitic sandstone, Eldivan ophiolite, this study
0 20 40 60 80 100 Ma 120 140 160 180 200 220
A

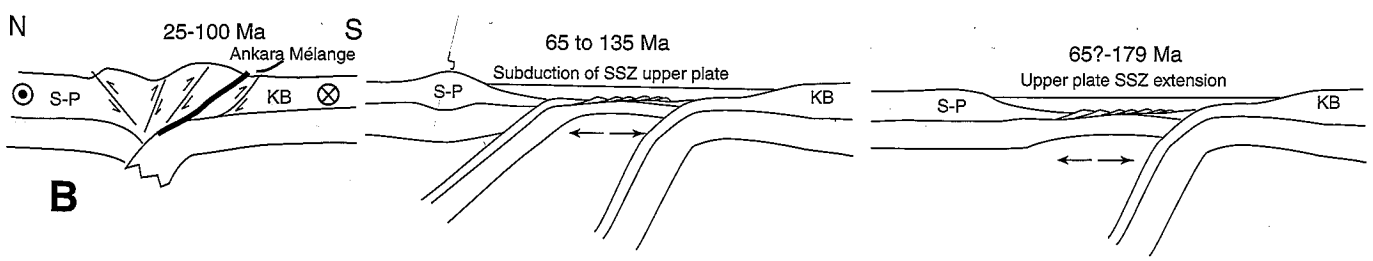
N
25-100 Ma
S
Ankara Mélange
S-P
KB
65 to 135 Ma
Subduction of SSZ upper plate
S-P
KB
65?-179 Ma
Upper plate SSZ extension
S-P
KB
B

exhumation is documented by $^{40}Ar/^{39}Ar$ metamorphic cooling ages of 48 ±12 Ma (Önen, 2003).

These age constraints suggest that the collision of the Kırşehir block with the Central Pontides may have occurred significantly earlier than collision between the Anatolide-Tauride block with the rest of the continental margin. The age of final suturing (no more deformation) between the Kırşehir block and Anatolide-Tauride platform with the Sakarya-Pontide terrane is not constrained. Boztuğ and Jonckheere (2007) attribute a second phase of granitoid exhumation in the Kırşehir block at 28–30 Ma to collision of the Arabian-African platform in the east, where Fayon et al. (2001) interpret exhumation of granitoids at 35 Ma to be from collision of the Anatolide-Tauride platform. Shortening continued into the late Miocene and Pliocene, as indicated by thrusting of the Ankara Mélange over the edge of the Hançili basin.

### Plate Tectonic Setting

The Eldivan ophiolite was created in the upper plate of the İzmir-Ankara-Erzincan Ocean during oblique intra-oceanic subduction as part of a backarc basin. This created a suite of geochemical signatures, as supra-subduction zone melting modified an N-MORB mantle, which was mixed with an enriched OIB mantle that had previously created seamounts on the ocean floor (Fig. 12B). The current Philippine Sea plate and Mariana trough supra-subduction zone basins are suggested as modern analogues for the tectonic setting of the Eldivan ophiolite, İzmir-Ankara-Erzincan Ocean, and Ankara Mélange.

The Philippine Sea plate formed as an upper-plate supra-subduction zone basin caused by intra-oceanic subduction (Harris, 2003). Later, the Philippine Sea supra-subduction zone ocean basin began to subduct to the west, creating the Japan, Ryukyu, and Luzon arcs. In a similar way, formation of the Eldivan intra-oceanic basin began subduction beneath the Pontides, creating the Pontide magmatic arc. Subduction of the Eldivan oceanic basin beneath the Pontides allowed several large fragments of mostly supra-subduction zone oceanic crust and some mantle to accrete to the margin, serpentinize, and produce mélange in the forearc between 105 and 143 Ma (Fig. 12B). Eventually the subduction zone was choked by collision of the Kırşehir block with the Sakarya-Pontide terrane, which further imbricated the ophiolite with the overlying Karadağ Formation. Collision continued to indent the continental margin and rotate the Eldivan ophiolite from its original E-W orientation to its current position on the western edge of the large omega-shaped İzmir-Ankara-Erzincan suture zone.

How far the Kırşehir block has traveled is not yet constrained. However, according to the Philippine Sea plate model, as supra-subduction zone basins open along a continental margin, fragments of the margin are rifted off and travel away as the basin opens (Harris, 2003). Closure of the supra-subduction zone basin eventually brings many of these fragments back into collision with parts of the original continental margin from which they were rifted. These processes are illustrated in many parts of the equatorial Pacific and Indonesian regions (Harris, 2003).

## CONCLUSIONS

1. The dismembered Eldivan ophiolite is a remnant of the İzmir-Ankara-Erzincan Ocean branch of the northern Neo-Tethys that evolved as a supra-subduction zone basin between the Gondwana-derived Kırşehir and Anatolide-Tauride blocks and the Sakarya-Pontide margin.

2. Parts of the İzmir-Ankara-Erzincan Ocean were accreted to the southern Asian margin as it subducted beneath it. These fragments were incorporated into the serpentine-rich Ankara Mélange.

3. During accretion, most of the units scraped from the İzmir-Ankara-Erzincan Ocean were imbricated, steeply inclined, and later broken into blocks surrounded by serpentinite. These include fragments of mostly oceanic crustal material, limestone, chert, and rare sandstone.

4. The ages of some blocks in the Ankara Mélange are younger than 143 ±2 Ma, with imbrication and initial destruction of the ocean basin having occurred between 143 ±2 Ma and 105 ±5 Ma. These ages are older than those of imbrication of the İzmir-Ankara-Erzincan Ocean in the west, which is documented at ca. 94 Ma.

5. Intra-oceanic volcanic arcs or seamounts are likely source terranes for sandstone units associated with the Eldivan ophiolite, suggesting that the ophiolite formed in an intra-oceanic subduction zone away from significant continental influence.

6. Studies of sheeted dike orientations indicate that the spreading ridge of intra-oceanic supra-subduction zone basins was most likely subparallel to the southern margin of Asia before indentation of the Kırşehir block, and has since been rotated nearly 90° counterclockwise.

7. The tectonic setting and evolutionary history of the Eldivan ophiolite can be characterized as a Western Pacific–type suture system in contrast to the more classic Himalayan-type suture that involves subduction of large tracts of MORB-like oceanic lithosphere and juxtaposition far-traveled of continental blocks of different affinities. This interpretation may also apply to many other Cretaceous ophiolite-bearing suture zones of the Eastern Mediterranean.

## ACKNOWLEDGMENTS

Funding for this project was provided by the American Association of Petroleum Geologists and U.S. National Science Foundation grant EAR 0337221. We would especially like to acknowledge the Maden Tetkik ve Arama Genel Müdürlüğü (MTA) in Turkey for supporting the fieldwork for this study, and we thank Mustafa Sevin, Esra Esirtgen, and Serdal Alemdar for their tremendous help in the field. Also, we thank Victor Valencia at the University of Arizona, who dated our detrital zircon samples, and Steve Nelson and Mike Dorais for critical reviews of our manuscript.

TABLE A1A. WHOLE-ROCK CHEMICAL ANALYSES

| Sample | 131 | 265 | 266 | 270 | 103 | 110 | 126a | 250 | 257 | 267 | 292c | 295 | 296a | 297b | 2 | 3 | 4 | 5a | 5b | 10 | 11 | 88 | 220 | 272 | 274 |
|---|---|---|---|---|---|---|---|---|---|---|---|---|---|---|---|---|---|---|---|---|---|---|---|---|---|
| | Peridotite | | | | Massive gabbro | | | | | | | | | | Basalt | | | | | | | | | | |
| $SiO_2$ | 45.01 | 43.42 | 45.52 | 44.78 | 48.97 | 52.65 | 59.70 | 54.57 | 54.24 | 53.59 | 54.45 | 53.26 | 46.22 | 54.67 | 54.62 | 52.91 | 52.17 | 45.45 | 46.64 | 47.72 | 44.59 | 66.10 | 47.53 | 49.51 | 48.21 |
| $TiO_2$ | 0.02 | 0.06 | 0.02 | 0.01 | 0.50 | 0.75 | 0.25 | 0.33 | 0.33 | 0.46 | 0.93 | 0.97 | 0.71 | 0.91 | 3.01 | 1.49 | 2.22 | 5.05 | 4.38 | 5.05 | 6.42 | 1.21 | 1.20 | 2.01 | 2.02 |
| $Al_2O_3$ | 1.79 | 2.45 | 1.53 | 0.78 | 17.92 | 18.00 | 11.67 | 17.47 | 17.63 | 16.62 | 15.48 | 16.08 | 16.49 | 15.84 | 12.23 | 15.87 | 13.99 | 11.50 | 12.66 | 11.22 | 10.84 | 13.41 | 15.60 | 14.02 | 14.82 |
| $Fe_2O_3$ | 8.46 | 9.03 | 8.70 | 8.75 | 11.19 | 10.32 | 6.35 | 8.96 | 8.78 | 9.01 | 11.16 | 11.06 | 10.88 | 11.08 | 12.11 | 12.11 | 12.68 | 19.57 | 18.43 | 16.95 | 20.69 | 7.14 | 10.25 | 13.06 | 11.16 |
| MnO | 0.12 | 0.15 | 0.12 | 0.11 | 0.18 | 0.13 | 0.22 | 0.14 | 0.17 | 0.17 | 0.24 | 0.26 | 0.17 | 0.11 | 0.27 | 0.26 | 0.20 | 0.39 | 0.26 | 0.24 | 0.23 | 0.15 | 0.22 | 0.20 | 0.14 |
| MgO | 42.20 | 42.23 | 42.55 | 43.35 | 9.24 | 5.73 | 8.48 | 5.95 | 5.80 | 7.18 | 6.42 | 6.05 | 6.17 | 6.20 | 4.95 | 4.41 | 5.85 | 4.62 | 4.24 | 5.41 | 4.86 | 2.43 | 14.15 | 7.75 | 5.28 |
| CaO | 0.18 | 0.06 | 0.14 | 0.10 | 9.06 | 5.41 | 6.89 | 10.62 | 10.65 | 8.72 | 5.76 | 5.08 | 19.88 | 5.05 | 7.23 | 7.23 | 8.47 | 8.19 | 7.97 | 7.78 | 7.50 | 2.71 | 6.52 | 10.23 | 11.42 |
| $Na_2O$ | 0.00 | 0.00 | 0.00 | 0.00 | 2.11 | 4.61 | 4.99 | 1.95 | 1.96 | 3.22 | 5.41 | 5.32 | 0.57 | 5.31 | 5.31 | 5.94 | 4.13 | 3.18 | 3.40 | 3.33 | 2.80 | 5.44 | 2.98 | 3.57 | 4.87 |
| $K_2O$ | 0.04 | 0.00 | 0.00 | 0.00 | 1.22 | 1.03 | 0.11 | 0.13 | 0.13 | 1.45 | 0.12 | 0.03 | 0.02 | 0.45 | 0.16 | 0.56 | 0.27 | 0.68 | 0.83 | 0.58 | 0.71 | 0.19 | 0.11 | 0.17 | 1.03 |
| $P_2O_5$ | 0.01 | 0.01 | 0.00 | 0.00 | 0.02 | 0.04 | 0.03 | 0.03 | 0.03 | 0.02 | 0.05 | 0.04 | 0.08 | 0.06 | 0.15 | 0.18 | 0.26 | 0.35 | 0.40 | 0.08 | 0.19 | 0.17 | 0.09 | 0.16 | 0.41 |
| Total | 97.82 | 97.40 | 98.58 | 97.89 | 100.41 | 98.66 | 98.70 | 100.14 | 99.74 | 100.43 | 100.03 | 98.14 | 101.21 | 99.67 | 100.02 | 100.96 | 100.25 | 98.97 | 99.21 | 98.35 | 98.82 | 98.95 | 98.65 | 100.68 | 99.35 |
| (ppm) | | | | | | | | | | | | | | | | | | | | | | | | | |
| Ni | 1960 | 2170 | 2160 | 2210 | 33 | 26 | 41 | 33 | 35 | 127 | 24 | 31 | 24 | 23 | 85 | 63 | 58 | 23 | 18 | 19 | 20 | <5 | 85 | 115 | 34 |
| V | 9.0 | <5 | <5 | <5 | 445 | 659 | 133 | 224 | 226 | 277 | 449 | 419 | 383 | 386 | 339 | 255 | 266 | 510 | 348 | 619 | 1160 | 75 | 214 | 370 | 264 |
| Cr | 2450 | 3230 | 2820 | 3740 | 20 | <10 | 180 | 120 | 120 | 120 | 20 | 80 | 30 | 20 | <10 | 250 | 10 | <10 | <10 | <10 | <10 | <10 | 140 | 360 | 50 |
| Cu | 21 | 8 | 15 | 5 | 43 | <5 | <5 | 20 | 21 | 12 | 84 | <5 | 132 | 65 | 18 | 80 | 35 | 31 | 42 | 64 | 63 | 46 | <5 | 84 | 64 |
| Zn | 47 | 65 | 49 | 45 | 65 | 49 | 44 | 42 | 45 | 62 | 119 | 80 | 77 | 107 | 71 | 125 | 122 | 216 | 193 | 176 | 182 | 100 | 74 | 124 | 128 |
| Rb | 1.1 | 0.2 | 0.2 | 0.4 | 16.0 | 10.2 | 0.7 | 2.4 | 2.6 | 18.2 | 1.2 | 0.5 | 0.4 | 2.4 | 2.0 | 15.8 | 4.8 | 14.8 | 18.9 | 22.5 | 31.1 | 2.3 | 1.6 | 1.6 | 5.2 |
| Sr | 0.7 | 1.4 | 4.2 | 13.1 | 141.5 | 139.5 | 39.8 | 134.5 | 140 | 501 | 67.4 | 52.8 | 46.7 | 71.1 | 110 | 553 | 143 | 230 | 279 | 129.5 | 144 | 210 | 161.5 | 341 | 73.6 |
| Y | 0.5 | 1.6 | 0.6 | <0.5 | 7.8 | 10.3 | 9.4 | 7.8 | 7.9 | 10.8 | 19.5 | 20.9 | 15.9 | 19.8 | 83.4 | 51.0 | 69.0 | 43.8 | 46.2 | 41.7 | 46.6 | 33.5 | 24.1 | 19.2 | 33.4 |
| Zr | 5 | <2 | <2 | <2 | 26 | 29 | 42 | 27 | 21 | 14 | 44 | 47 | 44 | 46 | 219 | 91 | 418 | 64 | 55 | 99 | 112 | 78 | 80 | 97 | 123 |
| Nb | <0.2 | <0.2 | <0.2 | <0.2 | 1.0 | 0.6 | 0.8 | 1.0 | 1.1 | 0.5 | 1.5 | 1.8 | 1.1 | 1.5 | 5.7 | 3.9 | 3.9 | 4.4 | 4.0 | 3.9 | 3.9 | 2.3 | 3.7 | 13.1 | 4.8 |
| Cs | 0.4 | 0.1 | 0.1 | 0.0 | 0.3 | 0.3 | 0.2 | 0.1 | 0.2 | 0.3 | 0.1 | 0.0 | 0.2 | 0.1 | 0.1 | 0.4 | 0.3 | 0.1 | 0.1 | 0.5 | 0.7 | 0.4 | 0.4 | 0.2 | 0.0 |
| Ba | 4.4 | 3.7 | 20.4 | 4.9 | 111.5 | 80.8 | 9.2 | 121.5 | 121.5 | 150 | 28.3 | 6.0 | 7.5 | 66.8 | 21.7 | 68.3 | 28.4 | 39.7 | 46.7 | 20.7 | 30.6 | 72.3 | 58.6 | 52.4 | 183.5 |
| La | <0.5 | <0.5 | <0.5 | <0.5 | 0.9 | 1.0 | 2.4 | 0.5 | 0.6 | 0.5 | 2.5 | 2.8 | 2.1 | 2.4 | 7.7 | 5.0 | 8.2 | 2.5 | 2.9 | 2.2 | 3.8 | 3.1 | 3.7 | 12.0 | 13.7 |
| Ce | <0.5 | <0.5 | <0.5 | <0.5 | 3.0 | 3.1 | 7.0 | 2.4 | 2.3 | 2.3 | 6.5 | 7.0 | 5.6 | 6.5 | 26.9 | 13.2 | 27.2 | 9.9 | 11.2 | 9.3 | 13.1 | 9.9 | 10.4 | 25.5 | 29.3 |
| Pr | <0.03 | <0.03 | <0.03 | <0.03 | 0.4 | 0.4 | 0.9 | 0.3 | 0.3 | 0.4 | 1.0 | 1.1 | 0.9 | 1.1 | 4.4 | 2.1 | 4.3 | 1.9 | 2.1 | 1.6 | 2.3 | 1.7 | 1.6 | 3.4 | 4.0 |
| Nd | <0.1 | 0.1 | 0.1 | 0.1 | 2.0 | 2.0 | 3.9 | 1.6 | 1.6 | 2.3 | 5.3 | 5.6 | 4.5 | 5.4 | 23.7 | 11.3 | 22.4 | 11.6 | 12.9 | 9.7 | 13.3 | 8.9 | 8.1 | 15.0 | 17.7 |
| Sm | <0.03 | 0.1 | 0.0 | 0.0 | 0.7 | 0.7 | 1.1 | 0.6 | 0.6 | 0.9 | 1.9 | 2.0 | 1.5 | 1.9 | 8.7 | 3.8 | 7.7 | 4.7 | 5.1 | 3.9 | 4.7 | 3.1 | 2.8 | 3.8 | 4.6 |
| Eu | <0.03 | 0.1 | <0.03 | <0.03 | 0.3 | 0.3 | 0.5 | 0.3 | 0.3 | 0.6 | 0.8 | 0.8 | 0.6 | 0.8 | 2.2 | 1.5 | 2.9 | 2.2 | 2.3 | 1.5 | 1.8 | 1.2 | 1.0 | 1.5 | 1.5 |
| Gd | <0.05 | 0.1 | 0.1 | <0.05 | 0.9 | 1.0 | 1.3 | 0.9 | 0.9 | 1.4 | 2.5 | 2.7 | 2.0 | 2.5 | 10.5 | 5.4 | 9.3 | 6.2 | 6.7 | 4.9 | 6.3 | 4.0 | 3.3 | 4.1 | 5.2 |
| Tb | <0.01 | 0.0 | <0.01 | <0.01 | 0.2 | 0.2 | 0.2 | 0.2 | 0.2 | 0.3 | 0.5 | 0.5 | 0.4 | 0.5 | 2.2 | 1.1 | 1.8 | 1.3 | 1.2 | 1.0 | 1.2 | 0.8 | 0.6 | 0.7 | 1.0 |
| Dy | 0.1 | 0.3 | 0.1 | 0.1 | 1.2 | 1.7 | 1.5 | 1.3 | 1.2 | 1.9 | 3.6 | 3.7 | 2.8 | 3.5 | 14.3 | 7.2 | 11.5 | 7.8 | 8.2 | 7.0 | 8.2 | 5.3 | 4.0 | 4.0 | 6.1 |
| Ho | 0.0 | 0.1 | 0.0 | 0.0 | 0.3 | 0.4 | 0.3 | 0.3 | 0.3 | 0.5 | 0.8 | 0.8 | 0.6 | 0.8 | 3.0 | 1.6 | 2.5 | 1.7 | 1.7 | 1.5 | 1.8 | 1.2 | 0.9 | 0.8 | 1.3 |
| Er | 0.1 | 0.2 | 0.1 | 0.0 | 0.9 | 1.1 | 1.0 | 0.9 | 0.8 | 1.3 | 2.3 | 2.5 | 1.9 | 2.3 | 8.7 | 4.4 | 7.1 | 4.6 | 4.8 | 4.5 | 4.8 | 3.4 | 2.4 | 2.0 | 3.8 |
| Yb | 0.1 | 0.2 | 0.1 | 0.1 | 0.9 | 1.2 | 1.0 | 1.0 | 0.9 | 1.4 | 2.3 | 2.4 | 1.8 | 2.4 | 8.3 | 3.9 | 6.7 | 4.2 | 4.2 | 4.5 | 4.5 | 3.2 | 2.4 | 1.7 | 3.7 |
| Lu | 0.0 | 0.0 | 0.0 | 0.0 | 0.1 | 0.2 | 0.2 | 0.2 | 0.2 | 0.2 | 0.4 | 0.4 | 0.3 | 0.4 | 1.3 | 0.6 | 1.1 | 0.7 | 0.6 | 0.6 | 0.7 | 0.5 | 0.3 | 0.3 | 0.6 |
| Hf | 0.2 | 0.2 | <0.2 | <0.2 | 0.9 | 1.1 | 1.5 | 0.9 | 0.8 | 0.5 | 1.5 | 1.6 | 1.4 | 1.6 | 6.4 | 2.8 | 10.7 | 2.2 | 1.9 | 3.0 | 3.3 | 2.4 | 2.4 | 2.9 | 3.8 |
| Ta | <0.1 | <0.1 | <0.1 | <0.1 | 0.1 | 0.1 | 0.1 | 0.1 | 0.2 | 0.1 | 0.2 | 0.2 | 0.1 | 0.2 | 0.5 | 0.3 | 0.3 | 0.4 | 0.3 | 0.3 | 0.3 | 0.2 | 0.3 | 1.1 | 0.5 |

TABLE A1B. WHOLE ROCK CHEMICAL ANALYSES

| Sample | 16 | 19 | 20 | 21 | 142 | 114 | 120 | 126b | 127 | 128 | 129 | 203 | 210 | 212 | 215 | 248 | 293 | 293c | 293d | 280 | 282 |
|---|---|---|---|---|---|---|---|---|---|---|---|---|---|---|---|---|---|---|---|---|---|
| | Alkaline Basalt | | | | | Sheeted dykes | | | | | | | | | | | Rhyolitic rocks | | | | |
| $SiO_2$ | 47.77 | 49.47 | 50.32 | 50.05 | 49.54 | 57.37 | 54.75 | 46.65 | 54.54 | 52.99 | 53.21 | 57.00 | 53.77 | 57.97 | 59.02 | 74.90 | 73.57 | 72.68 | 71.79 | 70.55 | 64.40 |
| $TiO_2$ | 2.31 | 2.51 | 2.44 | 2.35 | 2.06 | 0.40 | 1.56 | 0.71 | 1.69 | 1.01 | 0.76 | 0.69 | 1.06 | 0.86 | 1.47 | 0.29 | 0.80 | 0.85 | 0.83 | 0.65 | 0.84 |
| $Al_2O_3$ | 12.65 | 13.67 | 13.57 | 13.38 | 14.69 | 13.27 | 14.58 | 16.80 | 14.72 | 16.14 | 15.94 | 14.85 | 15.87 | 15.48 | 15.59 | 11.97 | 11.28 | 11.07 | 11.55 | 11.91 | 13.96 |
| $Fe_2O_3$ | 11.60 | 11.57 | 10.40 | 11.40 | 10.95 | 9.05 | 13.35 | 8.66 | 14.02 | 10.50 | 9.84 | 8.18 | 11.54 | 10.88 | 11.05 | 4.45 | 5.41 | 5.03 | 6.32 | 5.62 | 8.25 |
| MnO | 0.15 | 0.17 | 0.22 | 0.12 | 0.18 | 0.20 | 0.23 | 0.08 | 0.29 | 0.16 | 0.14 | 0.18 | 0.16 | 0.21 | 0.16 | 0.00 | 0.08 | 0.08 | 0.09 | 0.12 | 0.27 |
| MgO | 11.06 | 7.58 | 6.85 | 6.70 | 5.46 | 7.35 | 4.50 | 5.39 | 4.55 | 6.08 | 7.78 | 5.62 | 7.76 | 5.43 | 2.65 | 0.45 | 1.22 | 1.33 | 1.29 | 1.96 | 3.00 |
| CaO | 9.11 | 8.16 | 7.99 | 8.24 | 11.35 | 5.76 | 6.20 | 22.27 | 5.00 | 8.91 | 6.78 | 6.91 | 4.15 | 3.79 | 5.72 | 0.87 | 1.65 | 1.31 | 1.89 | 4.04 | 4.78 |
| $Na_2O$ | 2.09 | 3.50 | 3.52 | 3.13 | 4.80 | 5.75 | 4.79 | 0.46 | 4.76 | 3.98 | 4.33 | 6.13 | 5.16 | 5.86 | 3.77 | 5.64 | 4.94 | 4.82 | 4.64 | 3.40 | 4.94 |
| $K_2O$ | 2.37 | 2.12 | 2.51 | 3.02 | 1.08 | 0.12 | 0.21 | 0.12 | 0.31 | 0.05 | 0.59 | 0.20 | 0.07 | 0.08 | 0.44 | 0.24 | 0.38 | 0.47 | 0.63 | 1.59 | 0.17 |
| $P_2O_5$ | 0.31 | 0.31 | 0.30 | 0.27 | 0.41 | 0.05 | 0.12 | 0.08 | 0.14 | 0.08 | 0.05 | 0.07 | 0.05 | 0.04 | 0.20 | 0.04 | 0.15 | 0.18 | 0.17 | 0.10 | 0.12 |
| Total | 99.41 | 99.06 | 98.12 | 98.65 | 100.52 | 99.30 | 100.28 | 101.21 | 100.01 | 99.89 | 99.41 | 99.83 | 99.59 | 100.59 | 100.05 | 98.85 | 99.48 | 97.82 | 99.20 | 99.95 | 100.73 |
| (ppm) | | | | | | | | | | | | | | | | | | | | | |
| Ni | 164 | 64 | 57 | 68 | 100 | 88 | <5 | 38 | <5 | 34 | 47 | 29 | 23 | 15 | <5 | <5 | <5 | <5 | <5 | 18 | 18 |
| V | 242 | 271 | 263 | 268 | 221 | 247 | 402 | 311 | 417 | 231 | 269 | 245 | 287 | 325 | 147 | 14 | 20 | 48 | 40 | 183 | 240 |
| Cr | 330 | 40 | 40 | 70 | 210 | 270 | <10 | 40 | <10 | 100 | 60 | 20 | 20 | 10 | <10 | <10 | <10 | <10 | <10 | 30 | 20 |
| Cu | 86 | 107 | 98 | 93 | 66 | <5 | 8 | 343 | 5 | 40 | 51 | 12 | 27 | 10 | 27 | 8 | 5 | <5 | <5 | 48 | 44 |
| Zn | 114 | 130 | 124 | 133 | 134 | 50 | 92 | 42 | 100 | 75 | 85 | 62 | 73 | 36 | 115 | 30 | 101 | 98 | 97 | 84 | 118 |
| Rb | 38.4 | 32.3 | 40.0 | 45.9 | 14.3 | 0.5 | 2.8 | 1.1 | 3.9 | 0.2 | 4.8 | 1.5 | 0.6 | 0.4 | 4.0 | 1.6 | 8.0 | 9.9 | 14.9 | 45.9 | 3.8 |
| Sr | 466 | 715 | 575 | 512 | 502 | 25.9 | 45.3 | 43.7 | 58.1 | 165.5 | 193 | 116.0 | 90.2 | 52.9 | 193 | 77 | 87.3 | 128.5 | 121 | 71.4 | 76.1 |
| Y | 23.0 | 24.0 | 23.9 | 22.3 | 24.6 | 31.5 | 23.2 | 17.7 | 23.6 | 24.3 | 16.9 | 19.1 | 22.7 | 19.4 | 40.9 | 34.4 | 35.7 | 31.9 | 36.5 | 26.3 | 26.0 |
| Zr | 196 | 182 | 187 | 163 | 214 | 29 | 60 | 48 | 61 | 91 | 37 | 60 | 48 | 39 | 135 | 191 | 158 | 164 | 159 | 96 | 84 |
| Nb | 48.1 | 41.6 | 41.4 | 36.4 | 55.2 | 1.4 | 1.6 | 1.8 | 1.8 | 1.4 | 1.1 | 3.7 | 1.6 | 0.9 | 4.3 | 4.9 | 3.9 | 3.9 | 3.8 | 4.6 | 2.5 |
| Cs | 0.1 | 0.8 | 0.1 | 0.1 | 0.5 | 0.0 | 0.1 | 0.2 | 0.1 | 0.0 | 0.2 | 0.1 | 0.1 | 0.0 | 0.2 | 0.1 | 0.2 | 0.5 | 0.7 | 1.9 | 0.3 |
| Ba | 610 | 1105 | 952 | 1130 | 339 | 8.4 | 18.7 | 5.1 | 23.9 | 7.7 | 65.7 | 17.5 | 10.8 | 16.8 | 75.6 | 17.7 | 26.8 | 37.9 | 39.9 | 123 | 37.6 |
| La | 37.7 | 31.5 | 32.0 | 28.7 | 42.7 | 2.1 | 2.7 | 2.3 | 2.6 | 2.7 | 1.7 | 4.8 | 2.1 | 1.1 | 6.8 | 6.5 | 7.3 | 4.7 | 5.7 | 12.9 | 6.7 |
| Ce | 74.2 | 63.2 | 64.9 | 57.4 | 81.4 | 6.8 | 7.9 | 6.7 | 8.0 | 8.9 | 5.4 | 10.7 | 6.9 | 3.9 | 18.7 | 15.9 | 20.7 | 14.1 | 16.9 | 27.5 | 16.3 |
| Pr | 8.2 | 7.3 | 7.2 | 6.6 | 8.5 | 1.1 | 1.2 | 1.0 | 1.2 | 1.4 | 0.8 | 1.3 | 1.0 | 0.6 | 2.7 | 2.3 | 3.3 | 2.4 | 2.8 | 3.6 | 2.3 |
| Nd | 32.3 | 29.0 | 28.9 | 26.5 | 32.6 | 5.9 | 6.4 | 4.6 | 6.5 | 7.3 | 4.2 | 6.1 | 5.6 | 3.3 | 13.8 | 11.5 | 16.3 | 12.8 | 14.4 | 15.4 | 11.0 |
| Sm | 6.3 | 6.2 | 6.1 | 5.7 | 6.3 | 2.6 | 2.3 | 1.5 | 2.1 | 2.6 | 1.5 | 1.8 | 2.1 | 1.5 | 4.6 | 4.0 | 5.0 | 4.3 | 4.8 | 3.9 | 3.3 |
| Eu | 1.9 | 1.9 | 1.9 | 1.8 | 2.0 | 0.4 | 1.0 | 0.6 | 0.9 | 1.1 | 0.6 | 0.7 | 0.7 | 0.5 | 1.6 | 1.5 | 1.9 | 1.5 | 1.7 | 1.2 | 1.1 |
| Gd | 6.3 | 6.1 | 6.0 | 5.6 | 6.3 | 3.4 | 2.9 | 2.2 | 2.9 | 3.1 | 2.0 | 2.4 | 2.5 | 2.2 | 5.6 | 4.6 | 5.9 | 5.2 | 5.7 | 4.3 | 3.6 |
| Tb | 0.9 | 0.9 | 0.9 | 0.8 | 0.9 | 0.7 | 0.6 | 0.4 | 0.6 | 0.6 | 0.4 | 0.4 | 0.5 | 0.5 | 1.1 | 0.9 | 1.2 | 1.0 | 1.1 | 0.8 | 0.7 |
| Dy | 4.4 | 4.7 | 4.7 | 4.3 | 4.6 | 5.2 | 3.8 | 2.9 | 4.0 | 4.1 | 2.8 | 3.0 | 3.5 | 3.1 | 6.9 | 5.8 | 7.1 | 6.3 | 6.9 | 4.8 | 4.7 |
| Ho | 0.9 | 0.9 | 0.9 | 0.8 | 0.9 | 1.1 | 0.8 | 0.6 | 0.9 | 0.9 | 0.6 | 0.7 | 0.8 | 0.7 | 1.5 | 1.2 | 1.5 | 1.3 | 1.5 | 1.1 | 1.1 |
| Er | 2.2 | 2.4 | 2.4 | 2.2 | 2.2 | 3.5 | 2.4 | 1.8 | 2.6 | 2.5 | 1.8 | 1.9 | 2.5 | 2.0 | 4.4 | 3.7 | 4.1 | 3.7 | 4.3 | 3.0 | 3.2 |
| Yb | 1.8 | 1.9 | 1.7 | 1.8 | 1.9 | 3.9 | 2.3 | 1.8 | 2.4 | 2.6 | 1.8 | 2.0 | 2.6 | 2.2 | 4.2 | 3.9 | 3.9 | 3.1 | 4.3 | 3.0 | 3.3 |
| Lu | 0.3 | 0.3 | 0.3 | 0.3 | 0.3 | 0.6 | 0.3 | 0.3 | 0.4 | 0.4 | 0.3 | 0.3 | 0.4 | 0.3 | 0.7 | 0.6 | 0.6 | 0.4 | 0.7 | 0.5 | 0.5 |
| Hf | 5.1 | 4.7 | 4.8 | 4.4 | 5.0 | 1.2 | 1.9 | 1.6 | 2.1 | 2.6 | 1.3 | 1.7 | 1.7 | 1.5 | 4.0 | 5.8 | 4.7 | 5.0 | 4.9 | 3.0 | 2.8 |
| Ta | 3.0 | 2.5 | 2.6 | 2.3 | 3.5 | 0.1 | 0.1 | 0.1 | 0.2 | 0.1 | 0.1 | 0.3 | 0.1 | 0.1 | 0.4 | 0.5 | 0.5 | 0.5 | 0.5 | 0.5 | 0.2 |

TABLE A2A. Cr-SPINEL MINERAL ANALYSES

| Sample | 270 | 270 | 270 | 271 | 271 | 271 | 271 | 271 | 271 | 271 | 271 | 271 | 271 | 271 | 271 | 271 | 271 | 271 | 271 | 271 |
|---|---|---|---|---|---|---|---|---|---|---|---|---|---|---|---|---|---|---|---|---|
| $SiO_2$ | 0.07 | 0.03 | 0.13 | 0.07 | 0.11 | 0.06 | 0.20 | 0.07 | 0.08 | 0.05 | 0.06 | 0.04 | 0.11 | 0.06 | 0.01 | 0.02 | 0.06 | 0.05 | 0.04 | 0.01 |
| $TiO_2$ | 0.01 | 0.01 | 0.02 | 0.31 | 0.48 | 0.39 | 0.19 | 0.22 | 0.14 | 0.13 | 0.32 | 0.23 | 0.15 | 0.00 | 0.03 | 0.00 | 0.00 | 0.02 | 0.01 | 0.03 |
| $Al_2O_3$ | 25.02 | 28.34 | 27.23 | 18.47 | 21.13 | 21.29 | 20.17 | 18.13 | 24.74 | 24.04 | 17.70 | 22.63 | 17.64 | 22.41 | 23.92 | 19.45 | 20.58 | 21.69 | 21.97 | 22.83 |
| $Cr_2O_3$ | 45.64 | 43.88 | 43.49 | 51.73 | 49.77 | 49.86 | 50.97 | 52.63 | 47.41 | 47.86 | 52.49 | 49.28 | 51.27 | 47.93 | 46.06 | 50.34 | 49.47 | 48.46 | 47.20 | 47.62 |
| FeO | 13.96 | 14.60 | 15.28 | 16.64 | 14.77 | 14.99 | 17.02 | 17.14 | 13.15 | 13.97 | 15.86 | 13.90 | 12.65 | 16.24 | 14.79 | 15.91 | 15.96 | 14.79 | 15.29 | 13.22 |
| $Fe_2O_3$ | 1.72 | 0.00 | 0.00 | 0.51 | 0.00 | 0.73 | 0.00 | 0.18 | 0.34 | 0.00 | 1.70 | 0.67 | 4.18 | 0.00 | 1.38 | 1.20 | 0.20 | 0.97 | 1.59 | 0.99 |
| NiO | 0.10 | 0.13 | 0.00 | 0.00 | 0.16 | 0.15 | 0.10 | 0.16 | 0.08 | 0.17 | 0.04 | 0.00 | 0.09 | 0.14 | 0.07 | 0.02 | 0.02 | 0.07 | 0.06 | 0.08 |
| MnO | 0.49 | 0.47 | 0.47 | 0.64 | 0.52 | 0.50 | 0.57 | 0.58 | 0.52 | 0.57 | 0.64 | 0.54 | 0.63 | 0.59 | 0.56 | 0.60 | 0.63 | 0.61 | 0.53 | 0.55 |
| MgO | 14.33 | 13.75 | 13.19 | 11.77 | 13.42 | 13.52 | 10.94 | 11.45 | 14.91 | 13.46 | 12.41 | 14.31 | 14.32 | 12.11 | 13.43 | 12.07 | 12.00 | 13.05 | 12.73 | 14.21 |
| Total | 101.32 | 101.21 | 99.81 | 100.13 | 100.35 | 101.48 | 100.17 | 100.56 | 101.36 | 100.23 | 101.22 | 101.58 | 101.04 | 99.48 | 100.25 | 99.60 | 98.91 | 99.70 | 99.41 | 99.54 |
| FeO* | 13.37 | 12.84 | 12.33 | 11.22 | 12.59 | 12.67 | 10.41 | 10.89 | 13.93 | 12.68 | 11.80 | 13.41 | 13.51 | 11.48 | 12.64 | 11.46 | 11.42 | 12.35 | 11.98 | 13.33 |
| Calculated on 32 oxygens | | | | | | | | | | | | | | | | | | | | |
| Si | 0.02 | 0.01 | 0.03 | 0.02 | 0.03 | 0.01 | 0.05 | 0.02 | 0.02 | 0.01 | 0.02 | 0.01 | 0.03 | 0.01 | 0.00 | 0.01 | 0.02 | 0.01 | 0.01 | 0.00 |
| Ti | 0.00 | 0.00 | 0.00 | 0.06 | 0.09 | 0.07 | 0.04 | 0.04 | 0.03 | 0.02 | 0.06 | 0.04 | 0.03 | 0.00 | 0.01 | 0.00 | 0.00 | 0.00 | 0.00 | 0.01 |
| Al | 7.04 | 7.89 | 7.73 | 5.48 | 6.12 | 6.10 | 5.95 | 5.38 | 6.94 | 6.87 | 5.20 | 6.42 | 5.13 | 6.56 | 6.86 | 5.76 | 6.10 | 6.32 | 6.43 | 6.58 |
| Cr | 8.62 | 8.20 | 8.28 | 10.29 | 9.67 | 9.59 | 10.08 | 10.47 | 8.92 | 9.18 | 10.34 | 9.37 | 10.00 | 9.41 | 8.86 | 10.01 | 9.84 | 9.47 | 9.26 | 9.21 |
| $Fe^{2+}$ | 2.79 | 2.89 | 3.08 | 3.50 | 3.03 | 3.05 | 3.56 | 3.61 | 2.62 | 2.84 | 3.31 | 2.80 | 2.61 | 3.37 | 3.01 | 3.35 | 3.36 | 3.06 | 3.17 | 2.71 |
| $Fe^{3+}$ | 0.31 | 0.00 | 0.00 | 0.10 | 0.00 | 0.13 | 0.00 | 0.03 | 0.06 | 0.00 | 0.32 | 0.12 | 0.78 | 0.00 | 0.25 | 0.23 | 0.04 | 0.18 | 0.30 | 0.18 |
| Ni | 0.02 | 0.03 | 0.00 | 0.00 | 0.03 | 0.03 | 0.02 | 0.03 | 0.02 | 0.03 | 0.01 | 0.00 | 0.02 | 0.03 | 0.01 | 0.00 | 0.00 | 0.01 | 0.01 | 0.02 |
| Mn | 0.10 | 0.09 | 0.10 | 0.14 | 0.11 | 0.10 | 0.12 | 0.12 | 0.10 | 0.12 | 0.13 | 0.11 | 0.13 | 0.12 | 0.12 | 0.13 | 0.13 | 0.13 | 0.11 | 0.11 |
| Mg | 5.10 | 4.85 | 4.74 | 4.41 | 4.92 | 4.90 | 4.08 | 4.30 | 5.29 | 4.87 | 4.61 | 5.13 | 5.27 | 4.49 | 4.87 | 4.52 | 4.50 | 4.81 | 4.71 | 5.18 |
| Cr# [Cr/(Cr+Al)] | 0.55 | 0.51 | 0.52 | 0.65 | 0.61 | 0.61 | 0.63 | 0.66 | 0.56 | 0.57 | 0.67 | 0.59 | 0.66 | 0.59 | 0.56 | 0.63 | 0.62 | 0.60 | 0.59 | 0.58 |
| Mg# [Mg/(Mg/$Fe^{2+}$)] | 0.65 | 0.63 | 0.61 | 0.56 | 0.62 | 0.62 | 0.53 | 0.54 | 0.67 | 0.63 | 0.58 | 0.65 | 0.67 | 0.57 | 0.62 | 0.57 | 0.57 | 0.61 | 0.60 | 0.66 |

| Sample | 271 | 271 | 271 | 271 | 271 | 271 | 271 | 271 | 271 | 271 | 271 | 850 | 850 | 850 | 850 | 850 | 850 | 850 | 850 | 850 |
|---|---|---|---|---|---|---|---|---|---|---|---|---|---|---|---|---|---|---|---|---|
| $SiO_2$ | 1.24 | 0.06 | 0.01 | 0.05 | 0.03 | 0.02 | 0.02 | 0.00 | 0.06 | 0.04 | 0.06 | 0.01 | 0.03 | 0.00 | 0.02 | 0.00 | 0.02 | 0.03 | 0.04 | 0.02 |
| $TiO_2$ | 0.02 | 0.01 | 0.01 | 0.03 | 0.04 | 0.03 | 0.02 | 0.03 | 0.04 | 0.02 | 0.04 | 0.04 | 0.04 | 0.03 | 0.04 | 0.02 | 0.05 | 0.06 | 0.02 | 0.05 |
| $Al_2O_3$ | 22.82 | 20.00 | 24.34 | 24.04 | 23.97 | 24.16 | 24.47 | 24.78 | 23.35 | 23.89 | 24.65 | 17.37 | 17.25 | 17.55 | 16.29 | 15.73 | 15.47 | 16.13 | 16.81 | 16.19 |
| $Cr_2O_3$ | 45.18 | 50.11 | 46.74 | 47.06 | 46.18 | 45.97 | 46.07 | 45.55 | 47.51 | 46.47 | 46.11 | 49.55 | 49.91 | 49.33 | 51.34 | 52.22 | 52.48 | 52.06 | 51.30 | 51.73 |
| FeO | 14.51 | 15.83 | 13.30 | 13.79 | 13.98 | 13.95 | 13.73 | 13.75 | 13.34 | 13.19 | 13.24 | 19.55 | 18.91 | 18.71 | 18.13 | 18.17 | 18.18 | 18.42 | 19.15 | 18.76 |
| $Fe_2O_3$ | 2.30 | 1.08 | 1.14 | 0.55 | 0.49 | 0.17 | 0.70 | 0.25 | 1.06 | 1.17 | 1.08 | 3.64 | 3.45 | 3.35 | 2.86 | 2.80 | 2.90 | 2.40 | 2.14 | 2.77 |
| NiO | 0.05 | 0.08 | 0.06 | 0.15 | 0.12 | 0.10 | 0.09 | 0.14 | 0.11 | 0.05 | 0.12 | 0.10 | 0.06 | 0.02 | 0.10 | 0.03 | 0.08 | 0.03 | 0.02 | 0.02 |
| MnO | 0.55 | 0.57 | 0.52 | 0.55 | 0.60 | 0.57 | 0.52 | 0.00 | 0.53 | 0.51 | 0.52 | 0.63 | 0.64 | 0.61 | 0.61 | 0.65 | 0.68 | 0.66 | 0.68 | 0.68 |
| MgO | 13.14 | 12.27 | 14.55 | 14.10 | 13.70 | 13.67 | 14.09 | 14.26 | 14.35 | 14.40 | 14.57 | 9.65 | 10.00 | 10.05 | 10.31 | 10.23 | 10.23 | 10.14 | 9.69 | 9.96 |
| Total | 99.81 | 100.03 | 100.67 | 100.31 | 99.11 | 98.64 | 99.70 | 98.77 | 100.34 | 99.74 | 100.39 | 100.52 | 100.29 | 99.65 | 99.70 | 99.85 | 100.08 | 99.94 | 99.85 | 100.18 |
| FeO* | 12.38 | 11.62 | 13.62 | 13.24 | 12.93 | 12.87 | 13.19 | 12.83 | 13.44 | 13.46 | 13.63 | 9.31 | 9.64 | 9.65 | 9.88 | 9.86 | 9.88 | 9.78 | 9.39 | 9.64 |
| Calculated on 32 oxygens | | | | | | | | | | | | | | | | | | | | |
| Si | 0.30 | 0.02 | 0.00 | 0.01 | 0.01 | 0.01 | 0.01 | 0.00 | 0.01 | 0.01 | 0.02 | 0.00 | 0.01 | 0.00 | 0.01 | 0.00 | 0.01 | 0.01 | 0.01 | 0.01 |
| Ti | 0.00 | 0.00 | 0.00 | 0.01 | 0.01 | 0.01 | 0.00 | 0.01 | 0.01 | 0.00 | 0.01 | 0.01 | 0.01 | 0.01 | 0.01 | 0.00 | 0.01 | 0.01 | 0.01 | 0.01 |
| Al | 6.56 | 5.88 | 6.90 | 6.86 | 6.93 | 7.00 | 7.00 | 7.13 | 6.67 | 6.84 | 6.99 | 5.24 | 5.20 | 5.32 | 4.95 | 4.79 | 4.70 | 4.90 | 5.11 | 4.91 |
| Cr | 8.71 | 9.89 | 8.89 | 9.01 | 8.95 | 8.94 | 8.85 | 8.80 | 9.10 | 8.92 | 8.77 | 10.03 | 10.10 | 10.02 | 10.46 | 10.66 | 10.70 | 10.60 | 10.46 | 10.53 |
| $Fe^{2+}$ | 2.96 | 3.30 | 2.68 | 2.79 | 2.87 | 2.87 | 2.79 | 2.81 | 2.70 | 2.68 | 2.66 | 4.19 | 4.05 | 4.02 | 3.91 | 3.92 | 3.92 | 3.97 | 4.13 | 4.04 |
| $Fe^{3+}$ | 0.42 | 0.20 | 0.21 | 0.10 | 0.09 | 0.03 | 0.13 | 0.05 | 0.19 | 0.21 | 0.20 | 0.70 | 0.66 | 0.65 | 0.56 | 0.54 | 0.56 | 0.47 | 0.42 | 0.54 |
| Ni | 0.01 | 0.02 | 0.01 | 0.03 | 0.02 | 0.02 | 0.02 | 0.03 | 0.02 | 0.01 | 0.02 | 0.02 | 0.01 | 0.00 | 0.02 | 0.01 | 0.02 | 0.01 | 0.00 | 0.00 |
| Mn | 0.11 | 0.12 | 0.11 | 0.11 | 0.13 | 0.12 | 0.11 | 0.00 | 0.11 | 0.10 | 0.11 | 0.14 | 0.14 | 0.13 | 0.13 | 0.14 | 0.15 | 0.14 | 0.15 | 0.15 |
| Mg | 4.78 | 4.57 | 5.22 | 5.09 | 5.01 | 5.01 | 5.10 | 5.19 | 5.18 | 5.21 | 5.23 | 3.68 | 3.82 | 3.85 | 3.96 | 3.94 | 3.93 | 3.90 | 3.72 | 3.82 |
| Cr# [Cr/(Cr+Al)] | 0.57 | 0.63 | 0.56 | 0.57 | 0.56 | 0.56 | 0.56 | 0.55 | 0.58 | 0.57 | 0.56 | 0.66 | 0.66 | 0.65 | 0.68 | 0.69 | 0.69 | 0.68 | 0.67 | 0.68 |
| Mg# [Mg/(Mg/$Fe^{2+}$)] | 0.62 | 0.58 | 0.66 | 0.65 | 0.64 | 0.64 | 0.65 | 0.65 | 0.66 | 0.66 | 0.66 | 0.47 | 0.49 | 0.49 | 0.50 | 0.50 | 0.50 | 0.50 | 0.47 | 0.49 |

TABLE A2B. Cr-SPINEL ANALYSES

| Sample | 270 | 270 | 270 | 271 | 271 | 271 | 271 | 271 | 271 | 271 | 271 | 271 | 271 | 271 | 271 | 271 | 271 | 271 | 271 | 271 |
|---|---|---|---|---|---|---|---|---|---|---|---|---|---|---|---|---|---|---|---|---|
| $SiO_2$ | 0.07 | 0.03 | 0.13 | 0.07 | 0.11 | 0.06 | 0.20 | 0.07 | 0.08 | 0.05 | 0.06 | 0.04 | 0.11 | 0.06 | 0.01 | 0.02 | 0.06 | 0.05 | 0.04 | 0.01 |
| $TiO_2$ | 0.01 | 0.01 | 0.02 | 0.31 | 0.48 | 0.39 | 0.19 | 0.22 | 0.14 | 0.13 | 0.32 | 0.23 | 0.15 | 0.00 | 0.03 | 0.00 | 0.00 | 0.02 | 0.01 | 0.03 |
| $Al_2O_3$ | 25.02 | 28.34 | 27.23 | 18.47 | 21.13 | 21.29 | 20.17 | 18.13 | 24.74 | 24.04 | 17.70 | 22.63 | 17.64 | 22.41 | 23.92 | 19.45 | 20.58 | 21.69 | 21.97 | 22.83 |
| $Cr_2O_3$ | 45.64 | 43.88 | 43.49 | 51.73 | 49.77 | 49.86 | 50.97 | 52.63 | 47.41 | 47.86 | 52.49 | 49.28 | 51.27 | 47.93 | 46.06 | 50.34 | 49.47 | 48.46 | 47.20 | 47.62 |
| FeO | 13.96 | 14.60 | 15.28 | 16.64 | 14.77 | 14.99 | 17.02 | 17.14 | 13.15 | 13.97 | 15.86 | 13.90 | 12.65 | 16.24 | 14.79 | 15.91 | 15.96 | 14.79 | 15.29 | 13.22 |
| $Fe_2O_3$ | 1.72 | 0.00 | 0.00 | 0.51 | 0.00 | 0.73 | 0.00 | 0.18 | 0.34 | 0.00 | 1.70 | 0.67 | 4.18 | 0.00 | 1.38 | 1.20 | 0.20 | 0.97 | 1.59 | 0.99 |
| NiO | 0.10 | 0.13 | 0.00 | 0.00 | 0.16 | 0.15 | 0.10 | 0.16 | 0.08 | 0.17 | 0.04 | 0.00 | 0.09 | 0.14 | 0.07 | 0.02 | 0.02 | 0.07 | 0.06 | 0.08 |
| MnO | 0.49 | 0.47 | 0.47 | 0.64 | 0.52 | 0.50 | 0.57 | 0.58 | 0.52 | 0.57 | 0.64 | 0.54 | 0.63 | 0.59 | 0.56 | 0.60 | 0.63 | 0.61 | 0.53 | 0.55 |
| MgO | 14.33 | 13.75 | 13.19 | 11.77 | 13.42 | 13.52 | 10.94 | 11.45 | 14.91 | 13.46 | 12.41 | 14.31 | 14.32 | 12.11 | 13.43 | 12.07 | 12.00 | 13.05 | 12.73 | 14.21 |
| Total | 101.32 | 101.21 | 99.81 | 100.13 | 100.35 | 101.48 | 100.17 | 100.56 | 101.36 | 100.23 | 101.22 | 101.58 | 101.04 | 99.48 | 100.25 | 99.60 | 98.91 | 99.70 | 99.41 | 99.54 |
| FeO* | 13.37 | 12.84 | 12.33 | 11.22 | 12.59 | 12.67 | 10.41 | 10.89 | 13.93 | 12.68 | 11.80 | 13.41 | 13.51 | 11.48 | 12.64 | 11.46 | 11.42 | 12.35 | 11.98 | 13.33 |
| Calculated on 32 oxygens | | | | | | | | | | | | | | | | | | | | |
| Si | 0.02 | 0.01 | 0.03 | 0.02 | 0.03 | 0.01 | 0.05 | 0.02 | 0.02 | 0.01 | 0.02 | 0.01 | 0.03 | 0.01 | 0.00 | 0.01 | 0.02 | 0.01 | 0.01 | 0.00 |
| Ti | 0.00 | 0.00 | 0.00 | 0.06 | 0.09 | 0.07 | 0.04 | 0.04 | 0.03 | 0.02 | 0.06 | 0.04 | 0.03 | 0.00 | 0.01 | 0.00 | 0.00 | 0.00 | 0.00 | 0.01 |
| Al | 7.04 | 7.89 | 7.73 | 5.48 | 6.12 | 6.10 | 5.95 | 5.38 | 6.94 | 6.87 | 5.20 | 6.42 | 5.13 | 6.56 | 6.86 | 5.76 | 6.10 | 6.32 | 6.43 | 6.58 |
| Cr | 8.62 | 8.20 | 8.28 | 10.29 | 9.67 | 9.59 | 10.08 | 10.47 | 8.92 | 9.18 | 10.34 | 9.37 | 10.00 | 9.41 | 8.86 | 10.01 | 9.84 | 9.47 | 9.26 | 9.21 |
| $Fe^{2+}$ | 2.79 | 2.89 | 3.08 | 3.50 | 3.03 | 3.05 | 3.56 | 3.61 | 2.62 | 2.84 | 3.31 | 2.80 | 2.61 | 3.37 | 3.01 | 3.35 | 3.36 | 3.06 | 3.17 | 2.71 |
| $Fe^{3+}$ | 0.31 | 0.00 | 0.00 | 0.10 | 0.00 | 0.13 | 0.00 | 0.03 | 0.06 | 0.00 | 0.32 | 0.12 | 0.78 | 0.00 | 0.25 | 0.23 | 0.04 | 0.18 | 0.30 | 0.18 |
| Ni | 0.02 | 0.03 | 0.00 | 0.00 | 0.03 | 0.03 | 0.02 | 0.03 | 0.02 | 0.03 | 0.01 | 0.00 | 0.02 | 0.03 | 0.01 | 0.00 | 0.00 | 0.01 | 0.01 | 0.02 |
| Mn | 0.10 | 0.09 | 0.10 | 0.14 | 0.11 | 0.10 | 0.12 | 0.12 | 0.10 | 0.12 | 0.13 | 0.11 | 0.13 | 0.12 | 0.12 | 0.13 | 0.13 | 0.13 | 0.11 | 0.11 |
| Mg | 5.10 | 4.85 | 4.74 | 4.41 | 4.92 | 4.90 | 4.08 | 4.30 | 5.29 | 4.87 | 4.61 | 5.13 | 5.27 | 4.49 | 4.87 | 4.52 | 4.50 | 4.81 | 4.71 | 5.18 |
| Cr# [Cr/(Cr+Al)] | 0.55 | 0.51 | 0.52 | 0.65 | 0.61 | 0.61 | 0.63 | 0.66 | 0.56 | 0.57 | 0.67 | 0.59 | 0.66 | 0.59 | 0.56 | 0.63 | 0.62 | 0.60 | 0.59 | 0.58 |
| Mg# [Mg/(Mg/$Fe^{2+}$)] | 0.65 | 0.63 | 0.61 | 0.56 | 0.62 | 0.62 | 0.53 | 0.54 | 0.67 | 0.63 | 0.58 | 0.65 | 0.67 | 0.57 | 0.62 | 0.57 | 0.57 | 0.61 | 0.60 | 0.66 |

| Sample | 271 | 271 | 271 | 271 | 271 | 271 | 271 | 271 | 271 | 271 | 271 | 850 | 850 | 850 | 850 | 850 | 850 | 850 | 850 | 850 |
|---|---|---|---|---|---|---|---|---|---|---|---|---|---|---|---|---|---|---|---|---|
| $SiO_2$ | 1.24 | 0.06 | 0.01 | 0.05 | 0.03 | 0.02 | 0.02 | 0.00 | 0.06 | 0.04 | 0.06 | 0.01 | 0.03 | 0.00 | 0.02 | 0.00 | 0.02 | 0.03 | 0.04 | 0.02 |
| $TiO_2$ | 0.02 | 0.01 | 0.01 | 0.03 | 0.04 | 0.03 | 0.02 | 0.03 | 0.04 | 0.02 | 0.04 | 0.04 | 0.04 | 0.03 | 0.04 | 0.02 | 0.05 | 0.06 | 0.02 | 0.05 |
| $Al_2O_3$ | 22.82 | 20.00 | 24.34 | 24.04 | 23.97 | 24.16 | 24.47 | 24.78 | 23.35 | 23.89 | 24.65 | 17.37 | 17.25 | 17.55 | 16.29 | 15.73 | 15.47 | 16.13 | 16.81 | 16.19 |
| $Cr_2O_3$ | 45.18 | 50.11 | 46.74 | 47.06 | 46.18 | 45.97 | 46.07 | 45.55 | 47.51 | 46.47 | 46.11 | 49.55 | 49.91 | 49.33 | 51.34 | 52.22 | 52.48 | 52.06 | 51.30 | 51.73 |
| FeO | 14.51 | 15.83 | 13.30 | 13.79 | 13.98 | 13.95 | 13.73 | 13.75 | 13.34 | 13.19 | 13.24 | 19.55 | 18.91 | 18.71 | 18.13 | 18.17 | 18.18 | 18.42 | 19.15 | 18.76 |
| $Fe_2O_3$ | 2.30 | 1.08 | 1.14 | 0.55 | 0.49 | 0.17 | 0.70 | 0.25 | 1.06 | 1.17 | 1.08 | 3.64 | 3.45 | 3.35 | 2.86 | 2.80 | 2.90 | 2.40 | 2.14 | 2.77 |
| NiO | 0.05 | 0.08 | 0.06 | 0.15 | 0.12 | 0.10 | 0.09 | 0.14 | 0.11 | 0.05 | 0.12 | 0.10 | 0.06 | 0.02 | 0.10 | 0.03 | 0.08 | 0.03 | 0.02 | 0.02 |
| MnO | 0.55 | 0.57 | 0.52 | 0.55 | 0.60 | 0.57 | 0.52 | 0.00 | 0.53 | 0.51 | 0.52 | 0.63 | 0.64 | 0.61 | 0.61 | 0.65 | 0.68 | 0.66 | 0.68 | 0.68 |
| MgO | 13.14 | 12.27 | 14.55 | 14.10 | 13.70 | 13.67 | 14.09 | 14.26 | 14.35 | 14.40 | 14.57 | 9.65 | 10.00 | 10.05 | 10.31 | 10.23 | 10.23 | 10.14 | 9.69 | 9.96 |
| Total | 99.81 | 100.03 | 100.67 | 100.31 | 99.11 | 98.64 | 99.70 | 98.77 | 100.34 | 99.74 | 100.39 | 100.52 | 100.29 | 99.65 | 99.70 | 99.85 | 100.08 | 99.94 | 99.85 | 100.18 |
| FeO* | 12.38 | 11.62 | 13.62 | 13.24 | 12.93 | 12.87 | 13.19 | 12.83 | 13.44 | 13.46 | 13.63 | 9.31 | 9.64 | 9.65 | 9.88 | 9.86 | 9.88 | 9.78 | 9.39 | 9.64 |
| Calculated on 32 oxygens | | | | | | | | | | | | | | | | | | | | |
| Si | 0.30 | 0.02 | 0.00 | 0.01 | 0.01 | 0.01 | 0.01 | 0.00 | 0.01 | 0.01 | 0.02 | 0.00 | 0.01 | 0.00 | 0.01 | 0.00 | 0.01 | 0.01 | 0.01 | 0.01 |
| Ti | 0.00 | 0.00 | 0.00 | 0.01 | 0.01 | 0.01 | 0.00 | 0.01 | 0.01 | 0.00 | 0.01 | 0.01 | 0.01 | 0.01 | 0.01 | 0.00 | 0.01 | 0.01 | 0.01 | 0.01 |
| Al | 6.56 | 5.88 | 6.90 | 6.86 | 6.93 | 7.00 | 7.00 | 7.13 | 6.67 | 6.84 | 6.99 | 5.24 | 5.20 | 5.32 | 4.95 | 4.79 | 4.70 | 4.90 | 5.11 | 4.91 |
| Cr | 8.71 | 9.89 | 8.89 | 9.01 | 8.95 | 8.94 | 8.85 | 8.80 | 9.10 | 8.92 | 8.77 | 10.03 | 10.10 | 10.02 | 10.46 | 10.66 | 10.70 | 10.60 | 10.46 | 10.53 |
| $Fe^{2+}$ | 2.96 | 3.30 | 2.68 | 2.79 | 2.87 | 2.87 | 2.79 | 2.81 | 2.70 | 2.68 | 2.66 | 4.19 | 4.05 | 4.02 | 3.91 | 3.92 | 3.92 | 3.97 | 4.13 | 4.04 |
| $Fe^{3+}$ | 0.42 | 0.20 | 0.21 | 0.10 | 0.09 | 0.03 | 0.13 | 0.05 | 0.19 | 0.21 | 0.20 | 0.70 | 0.66 | 0.65 | 0.56 | 0.54 | 0.56 | 0.47 | 0.42 | 0.54 |
| Ni | 0.01 | 0.02 | 0.01 | 0.03 | 0.02 | 0.02 | 0.02 | 0.03 | 0.02 | 0.01 | 0.02 | 0.02 | 0.01 | 0.00 | 0.02 | 0.01 | 0.02 | 0.01 | 0.00 | 0.00 |
| Mn | 0.11 | 0.12 | 0.11 | 0.11 | 0.13 | 0.12 | 0.11 | 0.00 | 0.11 | 0.10 | 0.11 | 0.14 | 0.14 | 0.13 | 0.13 | 0.14 | 0.15 | 0.14 | 0.15 | 0.15 |
| Mg | 4.78 | 4.57 | 5.22 | 5.09 | 5.01 | 5.01 | 5.10 | 5.19 | 5.18 | 5.21 | 5.23 | 3.68 | 3.82 | 3.85 | 3.96 | 3.94 | 3.93 | 3.90 | 3.72 | 3.82 |
| Cr# [Cr/(Cr+Al)] | 0.57 | 0.63 | 0.56 | 0.57 | 0.56 | 0.56 | 0.56 | 0.55 | 0.58 | 0.57 | 0.56 | 0.66 | 0.66 | 0.65 | 0.68 | 0.69 | 0.69 | 0.68 | 0.67 | 0.68 |
| Mg# [Mg/(Mg/$Fe^{2+}$)] | 0.62 | 0.58 | 0.66 | 0.65 | 0.64 | 0.64 | 0.65 | 0.65 | 0.66 | 0.66 | 0.66 | 0.47 | 0.49 | 0.49 | 0.50 | 0.50 | 0.50 | 0.50 | 0.47 | 0.49 |

TABLE A3A. GEOCHRONOLOGICAL ZIRCON ANALYSES

| | | | | Isotope ratios | | | | | | | Apparent ages (Ma) | | | | | |
|---|---|---|---|---|---|---|---|---|---|---|---|---|---|---|---|---|
| # | U | $^{206}Pb$ | U/Th | $^{206}Pb^*$ | ± | $^{207}Pb^*$ | ± | $^{206}Pb^*$ | ± | error | $^{206}Pb^*$ | ± | $^{207}Pb^*$ | ± | $^{206}Pb^*$ | ± |
| | (ppm) | $^{204}Pb$ | | $^{207}Pb^*$ | (%) | $^{235}U^*$ | (%) | $^{238}U$ | (%) | corr. | $^{238}U^*$ | (Ma) | $^{235}U$ | (Ma) | $^{207}Pb^*$ | (Ma) |
| **Sample AD012 Karadag Fm** | | | | | | | | | | | | | | | | |
| 2 | 66 | 1136 | 1.0 | 17.2828 | 30.1 | 0.1573 | 30.2 | 0.0197 | 2.5 | 0.08 | 125.8 | 3.1 | 148.3 | 41.7 | 524.5 | 673.3 |
| 3 | 52 | 828 | 1.0 | 16.1761 | 36.6 | 0.1598 | 36.8 | 0.0188 | 3.5 | 0.10 | 119.8 | 4.2 | 150.6 | 51.5 | 667.8 | 809.1 |
| 4 | 51 | 804 | 1.0 | 24.4570 | 22.2 | 0.1155 | 22.2 | 0.0205 | 1.0 | 0.05 | 130.7 | 1.3 | 111.0 | 23.3 | −294.6 | 571.8 |
| 5 | 95 | 1228 | 0.7 | 25.1848 | 21.4 | 0.1122 | 21.5 | 0.0205 | 1.7 | 0.08 | 130.8 | 2.2 | 108.0 | 22.0 | −370.0 | 560.3 |
| 6 | 79 | 980 | 1.0 | 22.6647 | 17.4 | 0.1246 | 17.5 | 0.0205 | 1.9 | 0.11 | 130.7 | 2.5 | 119.3 | 19.7 | −103.9 | 430.8 |
| 7 | 472 | 10,136 | 1.5 | 17.6135 | 6.7 | 0.5104 | 7.1 | 0.0652 | 2.4 | 0.33 | 407.2 | 9.3 | 418.7 | 24.5 | 482.8 | 148.9 |
| 8 | 552 | 10,496 | 1.2 | 20.5296 | 1.8 | 0.1557 | 2.4 | 0.0232 | 1.7 | 0.69 | 147.8 | 2.4 | 147.0 | 3.3 | 133.9 | 41.5 |
| 9 | 128 | 7416 | 1.8 | 18.3564 | 3.8 | 0.5382 | 4.7 | 0.0717 | 2.8 | 0.60 | 446.1 | 12.2 | 437.2 | 16.8 | 390.8 | 84.9 |
| 10 | 83 | 2284 | 2.1 | 20.4875 | 10.5 | 0.1664 | 10.7 | 0.0247 | 1.7 | 0.16 | 157.4 | 2.6 | 156.3 | 15.5 | 138.7 | 248.2 |
| 11 | 67 | 1092 | 1.0 | 22.7613 | 10.4 | 0.1223 | 11.4 | 0.0202 | 4.5 | 0.40 | 128.8 | 5.7 | 117.1 | 12.6 | −114.4 | 257.4 |
| 12 | 55 | 876 | 1.2 | 22.6311 | 28.1 | 0.1225 | 28.3 | 0.0201 | 2.9 | 0.10 | 128.3 | 3.7 | 117.3 | 31.3 | −100.3 | 702.3 |
| 13 | 97 | 1596 | 0.8 | 21.3839 | 12.3 | 0.1303 | 12.4 | 0.0202 | 1.8 | 0.14 | 129.0 | 2.3 | 124.4 | 14.5 | 37.2 | 294.7 |
| 14 | 1159 | 15,476 | 1.7 | 20.1553 | 1.7 | 0.1603 | 3.0 | 0.0234 | 2.5 | 0.82 | 149.3 | 3.6 | 151.0 | 4.2 | 177.0 | 40.1 |
| 15 | 67 | 872 | 1.1 | 17.1830 | 45.8 | 0.1496 | 45.9 | 0.0186 | 3.6 | 0.08 | 119.1 | 4.2 | 141.6 | 60.8 | 537.2 | 1055.6 |
| 17 | 42 | 1064 | 1.5 | 20.7232 | 40.4 | 0.1425 | 40.4 | 0.0214 | 2.3 | 0.06 | 136.6 | 3.1 | 135.3 | 51.3 | 111.8 | 989.3 |
| 18 | 221 | 2936 | 0.5 | 21.0379 | 4.7 | 0.1327 | 4.9 | 0.0203 | 1.4 | 0.29 | 129.3 | 1.8 | 126.5 | 5.8 | 76.1 | 110.7 |
| 19 | 56 | 876 | 1.0 | 25.6751 | 23.3 | 0.1106 | 23.4 | 0.0206 | 1.2 | 0.05 | 131.4 | 1.6 | 106.5 | 23.6 | −420.2 | 617.7 |
| 20 | 51 | 660 | 1.2 | 20.4148 | 27.5 | 0.1441 | 27.6 | 0.0213 | 2.2 | 0.08 | 136.1 | 2.9 | 136.7 | 35.3 | 147.0 | 655.9 |
| 21 | 124 | 1524 | 0.4 | 22.4847 | 18.8 | 0.1197 | 19.0 | 0.0195 | 3.0 | 0.16 | 124.6 | 3.7 | 114.8 | 20.7 | −84.3 | 463.7 |
| 22 | 120 | 1456 | 0.6 | 20.0308 | 13.7 | 0.1416 | 13.8 | 0.0206 | 1.4 | 0.10 | 131.3 | 1.8 | 134.5 | 17.4 | 191.4 | 321.1 |
| 23 | 70 | 1404 | 1.1 | 18.7970 | 17.6 | 0.1400 | 18.1 | 0.0191 | 4.1 | 0.23 | 121.9 | 4.9 | 133.0 | 22.6 | 337.3 | 402.1 |
| 24 | 63 | 408 | 0.9 | 18.9393 | 11.9 | 0.1494 | 12.3 | 0.0205 | 3.2 | 0.26 | 130.9 | 4.1 | 141.3 | 16.2 | 320.2 | 270.2 |
| 25 | 57 | 760 | 0.8 | 19.0061 | 11.8 | 0.1500 | 11.9 | 0.0207 | 1.8 | 0.15 | 131.9 | 2.4 | 141.9 | 15.8 | 312.2 | 269.3 |
| 27 | 237 | 2708 | 0.6 | 18.5119 | 10.9 | 0.1533 | 11.1 | 0.0206 | 1.6 | 0.14 | 131.3 | 2.0 | 144.8 | 14.9 | 371.8 | 247.1 |
| 28 | 162 | 2108 | 0.7 | 23.0425 | 12.1 | 0.1309 | 12.2 | 0.0219 | 1.3 | 0.11 | 139.5 | 1.8 | 124.9 | 14.3 | −144.8 | 300.4 |
| 29 | 89 | 712 | 0.7 | 15.2699 | 23.2 | 0.1991 | 23.2 | 0.0220 | 1.3 | 0.06 | 140.6 | 1.8 | 184.3 | 39.1 | 790.0 | 492.1 |
| 31 | 64 | 772 | 1.0 | 30.8811 | 36.0 | 0.0913 | 36.2 | 0.0205 | 3.3 | 0.09 | 130.5 | 4.2 | 88.7 | 30.7 | −930.1 | 1078.9 |
| 32 | 141 | 2804 | 0.9 | 21.8494 | 8.2 | 0.1559 | 8.6 | 0.0247 | 2.6 | 0.30 | 157.3 | 4.0 | 147.1 | 11.8 | −14.6 | 199.6 |
| 33 | 323 | 2560 | 0.4 | 17.1379 | 18.9 | 0.1636 | 18.9 | 0.0203 | 1.0 | 0.05 | 129.8 | 1.3 | 153.9 | 27.0 | 542.9 | 416.0 |
| 35 | 98 | 680 | 0.7 | 14.9228 | 17.9 | 0.2048 | 18.0 | 0.0222 | 1.5 | 0.08 | 141.3 | 2.1 | 189.2 | 31.0 | 838.1 | 375.3 |
| 36 | 155 | 1856 | 0.8 | 21.1470 | 7.9 | 0.1265 | 8.3 | 0.0194 | 2.5 | 0.30 | 123.9 | 3.1 | 121.0 | 9.4 | 63.8 | 188.1 |
| 37 | 246 | 2292 | 0.6 | 20.9586 | 5.7 | 0.1339 | 6.2 | 0.0204 | 2.5 | 0.40 | 129.9 | 3.2 | 127.6 | 7.4 | 85.0 | 134.5 |
| 38 | 174 | 3116 | 1.2 | 21.3721 | 8.7 | 0.1361 | 8.8 | 0.0211 | 1.4 | 0.16 | 134.5 | 1.9 | 129.5 | 10.7 | 38.5 | 208.5 |
| 39 | 65 | 996 | 0.9 | 20.3217 | 15.7 | 0.1338 | 16.7 | 0.0197 | 5.9 | 0.35 | 125.9 | 7.4 | 127.5 | 20.1 | 157.7 | 368.2 |
| 40 | 57 | 932 | 0.9 | 21.4935 | 31.1 | 0.1322 | 31.2 | 0.0206 | 1.4 | 0.04 | 131.5 | 1.8 | 126.0 | 36.9 | 24.9 | 762.7 |
| 41 | 82 | 1256 | 0.9 | 20.8703 | 16.7 | 0.1351 | 16.8 | 0.0204 | 1.4 | 0.08 | 130.5 | 1.8 | 128.7 | 20.3 | 95.1 | 397.9 |
| 42 | 52 | 756 | 0.8 | 23.2365 | 27.7 | 0.1196 | 28.2 | 0.0201 | 4.8 | 0.17 | 128.6 | 6.1 | 114.7 | 30.5 | −165.5 | 701.8 |
| 43 | 70 | 1028 | 0.8 | 27.4376 | 27.9 | 0.0992 | 28.2 | 0.0197 | 4.1 | 0.15 | 126.0 | 5.1 | 96.0 | 25.8 | −597.3 | 769.6 |
| 44 | 67 | 1048 | 0.8 | 19.8264 | 32.6 | 0.1408 | 32.7 | 0.0202 | 2.4 | 0.07 | 129.2 | 3.0 | 133.7 | 41.0 | 215.2 | 774.2 |
| 45 | 128 | 1864 | 0.8 | 22.9935 | 12.2 | 0.1206 | 12.5 | 0.0201 | 2.8 | 0.23 | 128.3 | 3.6 | 115.6 | 13.6 | −139.4 | 301.9 |
| 46 | 186 | 3592 | 1.1 | 20.2601 | 8.8 | 0.1743 | 9.0 | 0.0256 | 1.8 | 0.19 | 163.0 | 2.8 | 163.2 | 13.6 | 164.8 | 206.7 |
| 47 | 43 | 484 | 1.4 | 20.3063 | 35.6 | 0.1121 | 35.6 | 0.0165 | 1.2 | 0.03 | 105.6 | 1.3 | 107.9 | 36.5 | 159.5 | 857.1 |
| 48 | 499 | 4048 | 0.4 | 20.9745 | 3.5 | 0.1383 | 3.8 | 0.0210 | 1.6 | 0.41 | 134.2 | 2.1 | 131.5 | 4.7 | 83.2 | 83.0 |
| 49 | 93 | 1448 | 0.6 | 26.8236 | 29.7 | 0.1141 | 29.7 | 0.0222 | 1.1 | 0.04 | 141.5 | 1.6 | 109.7 | 30.9 | −536.2 | 809.9 |
| 50 | 79 | 784 | 1.0 | 17.9530 | 21.1 | 0.1537 | 21.2 | 0.0200 | 2.5 | 0.12 | 127.7 | 3.2 | 145.2 | 28.7 | 440.4 | 474.0 |
| 51 | 49 | 712 | 1.0 | 23.9027 | 16.6 | 0.1237 | 16.7 | 0.0214 | 1.6 | 0.10 | 136.7 | 2.2 | 118.4 | 18.6 | −236.4 | 420.9 |
| 52 | 268 | 3716 | 0.5 | 20.8364 | 4.4 | 0.1540 | 4.7 | 0.0233 | 1.7 | 0.36 | 148.3 | 2.4 | 145.4 | 6.3 | 98.9 | 103.1 |

TABLE A3B. GEOCHRONOLOGICAL ZIRCON ANALYSES

| | | | | Isotope ratios | | | | | | | Apparent ages (Ma) | | | | | |
|---|---|---|---|---|---|---|---|---|---|---|---|---|---|---|---|---|
| # | U | $^{206}$Pb | U/Th | $^{206}$Pb* | ± | $^{207}$Pb* | ± | $^{206}$Pb* | ± | error | $^{206}$Pb* | ± | $^{207}$Pb* | ± | $^{206}$Pb* | ± |
| | (ppm) | $^{204}$Pb | | $^{207}$Pb* | (%) | $^{235}$U* | (%) | $^{238}$U | (%) | corr. | $^{238}$U* | (Ma) | $^{235}$U | (Ma) | $^{207}$Pb* | (Ma) |
| **Sample AD012 Karadag Fm** | | | | | | | | | | | | | | | | |
| 53 | 588 | 4528 | 0.3 | 19.2872 | 12.3 | 0.1343 | 13.1 | 0.0188 | 4.6 | 0.35 | 119.9 | 5.5 | 127.9 | 15.8 | 278.7 | 282.4 |
| 54 | 76 | 508 | 1.2 | 19.6078 | 63.0 | 0.1493 | 63.4 | 0.0212 | 7.6 | 0.12 | 135.5 | 10.2 | 141.3 | 83.9 | 240.8 | 1615.1 |
| 55 | 200 | 4080 | 1.1 | 20.6207 | 7.3 | 0.1746 | 7.3 | 0.0261 | 1.0 | 0.14 | 166.1 | 1.6 | 163.4 | 11.1 | 123.5 | 171.6 |
| 57 | 377 | 2436 | 1.2 | 21.1660 | 5.0 | 0.1760 | 5.4 | 0.0270 | 2.1 | 0.38 | 171.9 | 3.5 | 164.6 | 8.2 | 61.6 | 119.3 |
| 59 | 113 | 984 | 1.0 | 21.0459 | 13.6 | 0.1414 | 13.7 | 0.0216 | 1.2 | 0.09 | 137.6 | 1.6 | 134.3 | 17.2 | 75.2 | 324.9 |
| 60 | 75 | 1040 | 0.9 | 25.9392 | 22.6 | 0.1039 | 23.2 | 0.0195 | 5.2 | 0.22 | 124.8 | 6.4 | 100.4 | 22.2 | –447.1 | 602.5 |
| 61 | 66 | 1084 | 1.0 | 25.4259 | 21.7 | 0.1038 | 21.9 | 0.0191 | 2.8 | 0.13 | 122.3 | 3.4 | 100.3 | 20.9 | –394.8 | 571.6 |
| 62 | 77 | 1060 | 0.9 | 22.5195 | 11.8 | 0.1284 | 12.3 | 0.0210 | 3.4 | 0.28 | 133.8 | 4.5 | 122.6 | 14.2 | –88.1 | 290.1 |
| 63 | 1509 | 12,208 | 1.4 | 20.2377 | 5.4 | 0.1627 | 5.5 | 0.0239 | 1.0 | 0.19 | 152.1 | 1.5 | 153.1 | 7.9 | 167.4 | 127.0 |
| 64 | 1789 | 3204 | 1.5 | 16.8013 | 16.3 | 0.1951 | 16.4 | 0.0238 | 1.4 | 0.08 | 151.5 | 2.0 | 181.0 | 27.1 | 586.1 | 355.9 |
| 65 | 68 | 472 | 0.8 | 22.6108 | 28.7 | 0.1226 | 28.8 | 0.0201 | 2.3 | 0.08 | 128.3 | 2.9 | 117.4 | 32.0 | –98.1 | 718.3 |
| **25-1** | **75** | **330** | **0.7** | **22.9893** | **35.5** | **0.1131** | **35.7** | **0.0189** | **3.4** | **0.10** | **120.5** | **4.1** | **108.8** | **36.8** | **–139.0** | **903.7** |
| **25-2** | **58** | **549** | **1.0** | **18.0383** | **16.8** | **0.1617** | **16.9** | **0.0212** | **2.3** | **0.13** | **135.0** | **3.0** | **152.2** | **24.0** | **429.9** | **376.6** |
| **25-3** | **59** | **735** | **0.7** | **15.7366** | **37.7** | **0.1880** | **37.8** | **0.0215** | **2.2** | **0.06** | **136.9** | **3.0** | **174.9** | **60.7** | **726.5** | **827.5** |
| **25-4** | **131** | **960** | **1.1** | **17.4696** | **24.2** | **0.1472** | **24.5** | **0.0186** | **3.6** | **0.15** | **119.1** | **4.2** | **139.4** | **31.9** | **500.9** | **540.6** |
| **25-5** | **1731** | **4161** | **0.5** | **20.3773** | **3.4** | **0.1685** | **3.8** | **0.0249** | **1.7** | **0.44** | **158.5** | **2.7** | **158.1** | **5.6** | **151.4** | **80.8** |
| **25-6** | **188** | **2292** | **1.1** | **22.6023** | **10.0** | **0.1276** | **10.2** | **0.0209** | **1.6** | **0.16** | **133.5** | **2.1** | **121.9** | **11.7** | **–97.2** | **246.8** |
| **25-7** | **279** | **2790** | **0.9** | **20.1748** | **8.4** | **0.1428** | **8.8** | **0.0209** | **2.6** | **0.30** | **133.3** | **3.5** | **135.5** | **11.1** | **174.7** | **195.2** |
| **25-8** | **699** | **6546** | **2.0** | **20.7225** | **8.1** | **0.1063** | **8.8** | **0.0160** | **3.5** | **0.39** | **102.2** | **3.5** | **102.6** | **8.6** | **111.8** | **192.3** |
| **25-9** | **929** | **8340** | **1.4** | **20.7391** | **1.8** | **0.1115** | **2.9** | **0.0168** | **2.3** | **0.78** | **107.2** | **2.4** | **107.4** | **2.9** | **110.0** | **42.9** |
| **25-10** | **731** | **6039** | **1.6** | **18.2844** | **24.8** | **0.1207** | **24.9** | **0.0160** | **2.5** | **0.10** | **102.3** | **2.5** | **115.7** | **27.3** | **399.6** | **563.6** |
| **25-11** | **485** | **4314** | **2.2** | **19.7491** | **4.3** | **0.1910** | **4.5** | **0.0274** | **1.5** | **0.33** | **174.0** | **2.6** | **177.5** | **7.3** | **224.2** | **98.4** |
| **25-12** | **132** | **963** | **0.5** | **18.4186** | **11.5** | **0.1344** | **12.0** | **0.0180** | **3.3** | **0.27** | **114.7** | **3.7** | **128.1** | **14.4** | **383.2** | **260.1** |
| **25-13** | **133** | **6114** | **1.5** | **12.1793** | **3.2** | **1.9907** | **4.0** | **0.1758** | **2.5** | **0.62** | **1044.2** | **23.8** | **1112.4** | **27.1** | **1248.0** | **61.9** |
| **25-14** | **1066** | **10,971** | **1.6** | **14.0484** | **12.5** | **0.2483** | **12.5** | **0.0253** | **1.0** | **0.08** | **161.0** | **1.6** | **225.2** | **25.3** | **962.6** | **256.0** |
| **25-15** | **105** | **912** | **0.7** | **15.4967** | **15.3** | **0.1683** | **16.5** | **0.0189** | **6.3** | **0.38** | **120.8** | **7.6** | **157.9** | **24.2** | **759.0** | **324.1** |
| **25-15a** | **63** | **747** | **1.1** | **21.8308** | **19.7** | **0.1467** | **19.8** | **0.0232** | **1.3** | **0.06** | **148.0** | **1.9** | **139.0** | **25.7** | **–12.5** | **480.2** |
| **25-16** | **202** | **2004** | **0.8** | **13.8938** | **8.2** | **0.2047** | **8.3** | **0.0206** | **1.0** | **0.12** | **131.6** | **1.3** | **189.1** | **14.2** | **985.2** | **167.0** |
| **25-17** | **111** | **486** | **0.5** | **21.0250** | **25.6** | **0.1306** | **25.8** | **0.0199** | **3.3** | **0.13** | **127.1** | **4.1** | **124.7** | **30.3** | **77.5** | **617.9** |
| **25-18** | **148** | **1488** | **1.0** | **18.5027** | **7.9** | **0.1503** | **8.0** | **0.0202** | **1.6** | **0.20** | **128.7** | **2.1** | **142.2** | **10.6** | **373.0** | **177.2** |
| **25-20** | **68** | **1149** | **0.9** | **16.7655** | **24.4** | **0.1545** | **24.8** | **0.0188** | **4.3** | **0.17** | **120.0** | **5.1** | **145.9** | **33.7** | **590.7** | **536.8** |
| **Sample AD009 Ophiolitic Mélange** | | | | | | | | | | | | | | | | |
| 1 | 112 | 42,955 | 4.0 | 12.7606 | 1.0 | 2.0815 | 1.7 | 0.1926 | 1.4 | 0.81 | 1135.7 | 14.5 | 1142.7 | 11.7 | 1156.2 | 19.8 |
| 2 | 505 | 20,945 | 1.2 | 20.0645 | 1.0 | 0.1680 | 2.0 | 0.0244 | 1.8 | 0.87 | 155.7 | 2.7 | 157.7 | 3.0 | 187.5 | 23.3 |
| 3 | 233 | 24,905 | 2.7 | 19.6550 | 2.9 | 0.3295 | 3.6 | 0.0470 | 2.1 | 0.59 | 295.9 | 6.1 | 289.2 | 9.1 | 235.3 | 67.2 |
| 4 | 97 | 5005 | 1.3 | 20.8711 | 8.3 | 0.1529 | 8.4 | 0.0231 | 1.7 | 0.20 | 147.5 | 2.5 | 144.5 | 11.4 | 95.0 | 196.2 |
| 5 | 344 | 23,360 | 2.1 | 19.6607 | 4.7 | 0.2734 | 5.1 | 0.0390 | 2.0 | 0.39 | 246.5 | 4.7 | 245.4 | 11.1 | 234.6 | 108.3 |
| 6 | 201 | 9185 | 1.5 | 19.4428 | 6.2 | 0.1716 | 6.3 | 0.0242 | 1.0 | 0.16 | 154.2 | 1.5 | 160.8 | 9.4 | 260.3 | 143.6 |
| 7 | 272 | 9275 | 0.9 | 21.0865 | 3.9 | 0.1508 | 5.0 | 0.0231 | 3.0 | 0.61 | 147.0 | 4.4 | 142.6 | 6.6 | 70.6 | 93.1 |
| 8 | 711 | 28,700 | 1.0 | 20.5243 | 3.2 | 0.1704 | 3.4 | 0.0254 | 1.0 | 0.30 | 161.4 | 1.6 | 159.7 | 5.0 | 134.5 | 76.0 |
| 9 | 113 | 5540 | 2.2 | 21.5410 | 9.4 | 0.1518 | 9.5 | 0.0237 | 1.3 | 0.13 | 151.1 | 1.9 | 143.5 | 12.7 | 19.6 | 226.5 |
| 10 | 175 | 12,395 | 1.3 | 21.3972 | 6.8 | 0.1548 | 6.9 | 0.0240 | 1.2 | 0.17 | 153.0 | 1.8 | 146.2 | 9.4 | 35.7 | 162.3 |
| 11 | 110 | 5920 | 1.3 | 21.0325 | 11.5 | 0.1570 | 11.9 | 0.0239 | 2.9 | 0.24 | 152.6 | 4.4 | 148.1 | 16.4 | 76.7 | 274.7 |
| 12 | 525 | 10,380 | 1.1 | 21.0241 | 4.1 | 0.1533 | 4.4 | 0.0234 | 1.7 | 0.38 | 149.0 | 2.5 | 144.8 | 6.0 | 77.6 | 97.5 |
| 13 | 109 | 5445 | 1.5 | 19.7789 | 7.8 | 0.1802 | 7.8 | 0.0258 | 1.0 | 0.13 | 164.5 | 1.6 | 168.2 | 12.2 | 220.7 | 180.2 |
| 15 | 177 | 72,730 | 3.0 | 9.9249 | 1.0 | 3.9799 | 1.4 | 0.2865 | 1.0 | 0.71 | 1623.9 | 14.4 | 1630.1 | 11.5 | 1638.1 | 18.6 |
| 16 | 481 | 8750 | 1.6 | 18.0945 | 6.3 | 0.1744 | 6.5 | 0.0229 | 1.6 | 0.24 | 145.8 | 2.2 | 163.2 | 9.8 | 423.0 | 140.5 |

TABLE A3C. GEOCHRONOLOGICAL ZIRCON ANALYSES

| # | U | $^{206}Pb$ | U/Th | Isotope ratios | | | | | | | Apparent ages (Ma) | | | | | |
|---|---|---|---|---|---|---|---|---|---|---|---|---|---|---|---|---|
| | (ppm) | $^{204}Pb$ | | $^{206}Pb^*$ | ± | $^{207}Pb^*$ | ± | $^{206}Pb^*$ | ± | error | $^{206}Pb^*$ | ± | $^{207}Pb^*$ | ± | $^{206}Pb^*$ | ± |
| | | | | $^{207}Pb^*$ | (%) | $^{235}U^*$ | (%) | $^{238}U$ | (%) | corr. | $^{238}U^*$ | (Ma) | $^{235}U$ | (Ma) | $^{207}Pb^*$ | (Ma) |
| **Sample AD009 Ophiolitic Mélange** | | | | | | | | | | | | | | | | |
| 17 | 432 | 13,730 | 1.5 | 20.6133 | 4.6 | 0.1558 | 4.9 | 0.0233 | 1.7 | 0.34 | 148.4 | 2.4 | 147.0 | 6.6 | 124.3 | 107.6 |
| 18 | 124 | 47,620 | 1.5 | 7.9033 | 1.0 | 6.2503 | 1.5 | 0.3583 | 1.1 | 0.75 | 1974.0 | 19.4 | 2011.5 | 13.3 | 2050.3 | 17.7 |
| 13 | 212 | 6110 | 0.9 | 21.2261 | 5.8 | 0.1461 | 5.9 | 0.0225 | 1.0 | 0.17 | 143.4 | 1.4 | 138.5 | 7.7 | 54.9 | 139.6 |
| 20 | 544 | 8540 | 1.4 | 18.5369 | 13.0 | 0.1632 | 13.1 | 0.0219 | 1.5 | 0.12 | 139.9 | 2.1 | 153.5 | 18.6 | 368.8 | 293.6 |
| 22 | 379 | 13,920 | 1.5 | 20.3626 | 4.5 | 0.1583 | 4.8 | 0.0234 | 1.8 | 0.37 | 149.0 | 2.6 | 149.2 | 6.7 | 153.0 | 105.0 |
| 23 | 116 | 2320 | 1.3 | 14.3073 | 10.1 | 0.2300 | 10.2 | 0.0239 | 1.6 | 0.15 | 152.1 | 2.4 | 210.2 | 19.4 | 925.2 | 207.9 |
| 24 | 222 | 10,605 | 2.1 | 18.0167 | 2.4 | 0.3652 | 3.1 | 0.0477 | 2.0 | 0.64 | 300.5 | 5.8 | 316.1 | 8.4 | 432.6 | 52.9 |
| 25 | 127 | 4445 | 1.3 | 19.0159 | 10.3 | 0.1742 | 10.5 | 0.0240 | 2.0 | 0.19 | 153.0 | 3.0 | 163.1 | 15.8 | 311.0 | 234.5 |
| **25-1** | **256** | **636** | **2.6** | **18.8858** | **15.8** | **0.1766** | **16.1** | **0.0242** | **3.2** | **0.20** | **154.1** | **4.8** | **165.1** | **24.6** | **326.6** | **361.4** |
| **25-2** | **636** | **17,583** | **2.2** | **16.0144** | **1.9** | **0.8031** | **2.3** | **0.0933** | **1.2** | **0.54** | **574.9** | **6.7** | **598.6** | **10.2** | **689.3** | **40.5** |
| **25-3** | **179** | **4185** | **1.4** | **17.0760** | **14.9** | **0.2052** | **14.9** | **0.0254** | **1.0** | **0.07** | **161.8** | **1.6** | **189.5** | **25.8** | **550.8** | **326.6** |
| **25-4** | **222** | **6018** | **1.9** | **20.6592** | **11.3** | **0.1639** | **11.4** | **0.0246** | **1.6** | **0.14** | **156.4** | **2.5** | **154.1** | **16.3** | **119.1** | **267.5** |
| **25-5** | **540** | **10,473** | **1.1** | **20.4560** | **3.2** | **0.1686** | **3.4** | **0.0250** | **1.3** | **0.38** | **159.3** | **2.0** | **158.2** | **5.0** | **142.3** | **74.2** |
| **25-6** | **268** | **8841** | **1.3** | **21.2937** | **7.4** | **0.1603** | **7.9** | **0.0248** | **2.8** | **0.35** | **157.7** | **4.3** | **151.0** | **11.0** | **47.3** | **176.2** |
| **25-7** | **898** | **50,112** | **1.7** | **18.2908** | **1.0** | **0.5066** | **1.4** | **0.0672** | **1.0** | **0.69** | **419.3** | **4.1** | **416.1** | **4.9** | **398.8** | **23.3** |
| **25-8** | **987** | **6642** | **1.0** | **18.5354** | **8.5** | **0.1745** | **8.7** | **0.0235** | **1.8** | **0.20** | **149.5** | **2.6** | **163.3** | **13.2** | **369.0** | **192.9** |
| **25-9** | **1067** | **1734** | **1.6** | **15.4770** | **31.7** | **0.1999** | **31.7** | **0.0224** | **1.0** | **0.03** | **143.1** | **1.4** | **185.0** | **53.7** | **761.7** | **684.9** |
| **25-10** | **168** | **630** | **0.8** | **15.4446** | **37.0** | **0.1821** | **37.2** | **0.0204** | **3.3** | **0.09** | **130.2** | **4.2** | **169.9** | **58.2** | **766.1** | **806.8** |
| **25-11** | **254** | **5991** | **1.1** | **20.6852** | **10.9** | **0.1689** | **11.0** | **0.0253** | **1.1** | **0.10** | **161.3** | **1.7** | **158.5** | **16.1** | **116.1** | **258.7** |
| **25-11a** | **239** | **8184** | **1.3** | **19.2827** | **6.8** | **0.1720** | **6.9** | **0.0241** | **1.5** | **0.22** | **153.2** | **2.3** | **161.2** | **10.3** | **279.2** | **155.2** |

## REFERENCES CITED


Akyürek, B., Bilginer, E., Catal, E., Dager, Z., Soysal, Y., and Sunu, O., 1980, Eldivan-Sabanozu (Çankırı) ve Hasayaz- Çandır (Kalecik-Ankara) dolayinin jeolojisi [the geology of Eldivan-Sabanozu (Çankırı) and Hasayaz-Candir (Kalecik-Ankara) surroundings]: MTA report no. 6741 (unpublished, in Turkish).

Augé, T., and Johan, Z., 1988, Comparative study of chromite deposits from Troodos, Vourinos, and North Oman and New Caledonia ophiolites, *in* Boissonas, J., and Omenetto, P., eds., Mineral Deposits within the European Community: Berlin, Heidelberg, Springer-Verlag, p. 267–288.

Bailey, E.B., and McCallien, W.J., 1950, The Ankara Mélange and the Anatolian Thrust: Bulletin of Mineral Research and Exploration, Turkey, v. 40, p. 17–22.

Bonatti, E., and Michael, P.J., 1989, Mantle peridotites from continental rift zones to ocean basins to subduction zones: Earth and Planetary Science Letters, v. 91, p. 297–311, doi:10.1016/0012-821X(89)90005-8.

Boztuğ, D., and Jonckheere, R.C., 2007, Apatite fission track data from central Anatolian granitoids (Turkey): Constraints on Neo-Tethyan closure: Tectonics, v. 26, TC3011, doi:10.1029/2006TC001988.

Boztuğ, D., Tichomirowa, M., and Bombach, K., 2007, $^{207}Pb$–$^{206}Pb$ single-zircon evaporation ages of some granitoids rocks reveal continent–oceanic island arc collision during the Cretaceous geodynamic evolution of the central Anatolian crust, Turkey: Journal of Asian Earth Sciences, v. 31, p. 71–86, doi:10.1016/j.jseaes.2007.04.004.

Bragin, N.Y., and Tekin, U.K., 1996, Age of radiolarian-chert blocks from the Senonian Ophiolitic Mélange (Ankara, Turkey): Island Arc, v. 5, p. 114–122, doi:10.1111/j.1440-1738.1996.tb00018.x.

Cabanis, B., and Lecolle, M., 1989, Le diagramme La/10-Y/15-Nb/8: Un outil pour la discrimination des séries volcaniques et la mise en évidence des processus de mélange et/ou de contamination crustale [The La/10-Y/15-Nb/8 diagram: A tool for distinguishing volcanic series and discovering crustal mixing and/or contamination]: Comptes Rendus de l'Académie des Sciences, sér. 2, v. 309, p. 2023–2029.

Çapan, U.Z., and Floyd, P.A., 1985, Geochemical and petrographic features of metabasalts within units of the Ankara Mélange, Turkey: Ofioliti, v. 10, p. 3–18.

Carter, J.L., 1970, Mineralogy and chemistry of the Earth's upper mantle based on the partial fusion–partial crystallization model: Geological Society of America Bulletin, v, 81, p. 2021–2034.

Dewey, J.F., and Bird, J.M., 1970, Mountain belts and the new global tectonics: Journal of Geophysical Research, v. 75, p. 2625–2647, doi:10.1029/JB075i014p02625.

Dick, H.J.B., and Bullen, T., 1984, Chromian spinel as a petrogenetic indicator in abyssal and alpine-type peridotites and spatially associated lavas: Contributions to Mineralogy and Petrology, v. 86, p. 54–76, doi:10.1007/BF00373711.

Dickinson, W.R., Beard, L.S., Brakenridge, G.R., Erjavec, J.L., Ferguson, R.C., Inman, K.F., Knepp, R.A., Lindber, F.A., and Byberg, P.T., 1983, Provenance of North American Phanerozoic sandstones in relation to tectonic setting: Geological Society of America Bulletin, v. 94, p. 222–235, doi:10.1130/0016-7606(1983)94<222:PONAPS>2.0.CO;2.

Dilek, Y., and Thy, P., 2006, Age and petrogenesis of plagiogranite intrusions in the Ankara mélange, central Turkey: Island Arc, v. 15, p. 44–57, doi:10.1111/j.1440-1738.2006.00522.x.

Dril, S.I., Kuzmin, M.I., Tsipukova, S.S., and Zonenshain, L.P., 1997, Geochemistry of basalts from Woodlark, Lau and Manus basins: Implications for their petrogenesis and source rock compositions: Marine Geology, v. 142, p. 57–83, doi:10.1016/S0025-3227(97)00041-8.

Eissen, J.-P., Nohara, M., Cotten, J., and Hirose, K., 1994, North Fiji basin basalts and their magma source: Part I, Incompatible element constraints: Marine Geology, v. 116, p. 153–178, doi:10.1016/0025-3227(94)90174-0.

Fayon, A.K., Whitney, D.L., Teyssier, C., Garver, J.I., and Dilek, Y., 2001, Effects of plate convergence obliquity on timing and mechanisms of exhumation of a mid-crustal terrain, the Central Anatolian Crystalline Complex: Earth and Planetary Science Letters, v. 192, p. 191–205, doi:10.1016/S0012-821X(01)00440-X.

Fisher, R.L., and Engel, C.G., 1969, Ultramafic and basaltic rocks dredged from the nearshore flank of the Tonga trench: Geological Society of America Bulletin, v. 80, p. 1373–1378, doi:10.1130/0016-7606(1969)80[1373:UABRDF]2.0.CO;2.

Floyd, P.A., 1993, Geochemical discrimination and petrogenesis of alkalic basalt sequences in part of the Ankara mélange, central Turkey: Journal

of the Geological Society [London], v. 150, p. 541–550, doi:10.1144/gsjgs.150.3.0541.

Floyd, P.A., Kelling, G., Gökçen, S.L., and Gökçen, N., 1991, Geochemistry and tectonic environment of basaltic rocks from the Misis ophiolitic mélange, south Turkey: Chemical Geology, v. 89, p. 263–280, doi:10.1016/0009-2541(91)90020-R.

Floyd, P.A., Yalınız, M.K., and Göncüoğlu, M.C., 1998, Geochemistry and petrogenesis of intrusive and extrusive ophiolitic plagiogranites, Central Anatolian Crystalline Complex, Turkey: Lithos, v. 42, p. 225–241, doi:10.1016/S0024-4937(97)00044-3.

Floyd, P.A., Göncüoğlu, M.C., Winchester, J.A., and Yalınız, M.K., 2000, Geochemical character and tectonic environment of Neotethyan ophiolitic fragments and metabasites in the Central Anatolian Crystalline Complex, Turkey, *in* Bozkurt, E., Winchester, J.A., and Piper, J.D.A., eds., Tectonics and Magmatism in Turkey and the Surrounding Area: Geological Society [London] Special Publication 173, p. 183–202.

Fretzdorff, S., Livermore, R.A., Devey, C.W., Leat, P.T., and Stoffers, P., 2002, Petrogenesis of the back-arc East Scotia ridge, South Atlantic Ocean: Journal of Petrology, v. 43, p. 1435–1467, doi:10.1093/petrology/43.8.1435.

Frey, F., and Prinz, M., 1978, Ultramafic inclusions from San Carlos, Arizona: Petrologic and geochemical data bearing on their petrogenesis: Earth and Planetary Science Letters, v. 38, p. 129–176, doi:10.1016/0012-821X(78)90130-9.

Gansser, A., 1964, Geology of the Himalayas: London, Wiley Interscience, 289 p.

Gehrels, G.E., 2000, Introduction to detrital zircon studies of Paleozoic and Triassic strata in western Nevada and northern California, *in* Soreghan, M.J., and Gehrels, G.E., eds., Paleozoic and Triassic Paleography and Tectonics of Western Nevada and Northern California: Geological Society of America Special Paper 347, p. 1–17.

Gehrels, G., Valencia, V., and Pullen, A., 2006, Detrital zircon geochronology by laser-ablation multicollector ICPMS at the Arizona LaserChron Center: Paleontological Society Papers, v. 12, p. 67–76.

Göncüoğlu, M.C., Yalınız, M.K., and Tekin, U.K., 2006, Geochemistry, tectono-magmatic discrimination and radiolarian ages of basic extrusives within the İzmir-Ankara suture belt (NW Turkey): Time constraints for the Neotethyan evolution: Ofioliti, v. 31, p. 25–38.

Güleç, N., 1994, Rb–Sr isotope data from the Ağaçören granitoid (east of Tuz Gölü): Geochronological and genetical implications: Turkish Journal of Earth Science, v. 3, p. 39–43.

Hakyemez, Y., Barkurt, M.Y., Bilginer, E., Pehlivan, S., Can, B., Dager, Z., and Sozeri, B., 1986, Yapraklı-Ilgaz-Çankırı-Çandır dolayinin jeolojisi: MTA report no. 7966 (unpublished, in Turkish).

Harris, R.A., 1992, Peri-collisional extension and the formation of Oman-type ophiolites in the Banda Arc and Brooks Range *in* Parson, L.M., Murton, B.J., and Browning P., eds., Ophiolites and Their Modern Ocean Analogues: Geological Society [London] Special Publication 60, p. 301–325, doi:10.1144/GSL.SP.1992.060.01.19.

Harris, R.A., 1995, Geochemistry and tectonomagmatic affinity of the Misheguk massif, Brooks Range ophiolite, Alaska: Lithos, v. 35, p. 1–25, doi:10.1016/0024-4937(94)00048-7.

Harris, R.A., 2003, Geodynamic patterns of ophiolites and marginal basins of the Indonesian and New Guinea regions, *in* Dilek, Y., and Robinson, P.T., eds., Ophiolites in Earth History: Geological Society [London] Special Publication 218, p. 481–505.

Hawkins, J.W., and Melchior, J.T., 1985, Petrology of Mariana trough and Lau basin basalts: Journal of Geophysical Research, v. 90, p. 11,431–11,468, doi:10.1029/JB090iB13p11431.

Ishii, T., 1985, Dredged samples from the Ogasawara fore-arc seamount or "Ogasawara Paleoland"–"fore-arc ophiolite," *in* Nasu, N., ed., Formation of Active Ocean Margins: Tokyo, Terra Scientific Publishing, p. 3307–3342.

Ishii, T., Robinson, P.T., Maekawa, H., and Fiske, R., 1992, Petrological studies of peridotites from diapiric serpentinite seamounts in the Izu-Ogasawara-Mariana forearc, Leg 125: College Station, Texas, Proceedings of the Ocean Drilling Program, Scientific Results, v. 125, p. 445–485.

Kamenetsky, V.S., Crawford, A.J., and Meffre, S., 2001, Factors controlling chemistry of magmatic spinel: And empirical study of associated olivine, Cr-spinel, and melt inclusions from primitive rocks: Journal of Petrology, v. 42, p. 655–671, doi:10.1093/petrology/42.4.655.

Kaymakci, N., Duermeijer, C.E., Langereis, C., White, S.H., and Van Dijk, P.M., 2003, Paleomagnetic evolution of the Çankırı basin (central Anatolia, Turkey): Implications for oroclinal bending due to indentation: Geological Magazine, v. 140, p. 343–355, doi:10.1017/S001675680300757X.

Koçyiğit, A., 1991, An example of an accretionary forearc basin from northern Central Anatolia and its implications for the history of Neo-Tethys in Turkey: Geological Society of America Bulletin, v. 103, p. 22–36, doi:10.1130/0016-7606(1991)103<0022:AEOAAF>2.3.CO;2.

Kröner, A., and Şengör, A.M.C., 1990, Archean and Proterozoic ancestry in late Precambrian to early Paleozoic crustal elements of southern Turkey as revealed by single zircon dating: Geology, v. 18, p. 1186–1190, doi:10.1130/0091-7613(1990)018<1186:AAPAIL>2.3.CO;2.

Li, Z.-X.A., and Lee, C.-Y.A., 2006, Geochemical investigation of serpentinized ocean lithospheric mantle in the Feather River Ophiolite, California: Implications for the recycling rate of water by subduction: Chemical Geology, v. 235, p. 161–185, doi:10.1016/j.chemgeo.2006.06.011.

Ludwig, K.J., 2003, Isoplot 3.00: Berkeley, California, Geochronology Center Special Publication 4, 70 p.

McDonough, W.F., and Sun, S.-s., 1995, The composition of the Earth: Chemical Geology, v. 120, p. 223–253, doi:10.1016/0009-2541(94)00140-4.

Meschede, J.N., and Casey, J.F., 1986, A method of discriminating between different types of mid-ocean-ridge basalts and continental tholeiites with the Nb-Zr-Y diagram: Chemical Geology, v. 56, p. 207–218, doi:10.1016/0009-2541(86)90004-5.

Morishita, T., Maeda, J., Miyashita, S., Kumagai, H., Matsumoto, T., and Dick, H.J.B., 2007, Petrology of local concentration of chromian spinel in dunite from the slow-spreading Southwest Indian Ridge: European Journal of Mineralogy, v. 19, p. 871–882, doi:10.1127/0935-1221/2007/0019-1773.

Mullen, E.D., 1983, $MnO/TiO_2/P_2O_5$: A major element discriminant for basaltic rocks of oceanic environments and its implications for petrogenesis: Earth and Planetary Science Letters, v. 62, p. 53–62, doi:10.1016/0012-821X(83)90070-5.

Norman, T.N., 1984, The role of the Ankara mélange in the development of Anatolia (Turkey), *in* Dixon, J.E., and Robertson, A.H.F., eds., The Geological Evolution of the Eastern Mediterranean: Geological Society [London] Special Publication 17, p. 441–447.

Okay, A.I., and Tüysüz, O., 1999, Tethyan sutures of northern Turkey, *in* Durand, B., Jolivet, L., Horvath, F., and Seranne, M., eds., The Mediterranean Basins: Tertiary Extension within the Alpine Orogen: Geological Society [London] Special Publication 156, p. 475–515.

Okay, A.I., Tüysüz, O., Satır, M., Ozkan-Altıner, S., Altıner, D., Sherlock, S., and Eren, R.H., 2006, Cretaceous and Triassic subduction-accretion, high-pressure–low-temperature metamorphism, and continental growth in the Central Pontides, Turkey: Geological Society of America Bulletin, v. 118, p. 1247–1269, doi:10.1130/B25938.1.

Önen, A.P., 2003, Neotethyan ophiolitic rocks of the Anatolides of NW Turkey and comparison with Tauride ophiolites: Journal of the Geological Society [London], v. 160, p. 947–962, doi:10.1144/0016-764902-125.

Paulick, H., Bach, W., Godard, M., De Hoog, J.C.M., Suhr, G., and Harvey, J., 2006, Geochemistry of abyssal peridotites (Mid-Atlantic Ridge, 15°20′N, ODP Leg 209): Implications for fluid/rock interaction in slow spreading environments: Chemical Geology, v. 234, p. 179–210, doi:10.1016/j.chemgeo.2006.04.011.

Pearce, J.A., 1982, Trace element characteristics of lavas from destructive plate boundaries, *in* Thorpe, R.S., ed., Andesites: Orogenic Andesites and Related Rocks: Chichester, UK, Wiley and Sons, p. 525–548.

Pearce, J.A., and Cann, J.R., 1971, Ophiolitic origin investigated by discriminant analysis using Ti, Zr, and Y: Earth and Planetary Science Letters, v. 12, p. 339–349, doi:10.1016/0012-821X(71)90220-2.

Pearce, J.A., and Cann, J.R., 1973, Tectonic setting of basic volcanic rocks determined using trace element analyses: Earth and Planetary Science Letters, v. 19, p. 290–300, doi:10.1016/0012-821X(73)90129-5.

Pearce, J.A., and Norry, M.J., 1979, Petrogenetic implications of Ti, Zr, Y, and Nb variations in volcanic rocks: Contributions to Mineralogy and Petrology, v. 69, p. 33–47, doi:10.1007/BF00375192.

Pearce, J.A., Alabaster, T., Shelton, A.W., and Searle, M.P., 1981, The Oman ophiolite as a Cretaceous arc-basin complex: Evidence and implications: Philosophical Transactions of the Royal Society of London, ser. A, v. 300, p. 299–317.

Pearce, J.A., Harris, N.B.W., and Tindle, A.G., 1984a, Trace element discrimination diagrams for the tectonic interpretation of granitic rocks: Journal of Petrology, v. 25, p. 956–983.

Pearce, J.A., Lippard, S.J., and Roberts, S., 1984b, Characteristics and tectonic significance of supra-subduction zone ophiolites, *in* Kokellar, B.P., and Howells, M.F., eds., Marginal Basin Geology: Volcanic and Associated Sedimentary and Tectonic Processes in Modern and Ancient Marginal Basins: Geological Society [London] Special Publication 16, p. 77–94.

Price, R.C., Johnson, L.E., and Crawford, A.J., 1990, Basalts of the North Fiji basin: The generation of back-arc basin magmas by mixing of depleted and enriched mantle sources: Contributions to Mineralogy and Petrology, v. 105, p. 106–121, doi:10.1007/BF00320970.

Rojay, B., Yalınız, K.M., and Altıner, D., 2001, Tectonic implications of some Cretaceous pillow basalts from the North Anatolian ophiolitic mélange (Central Anatolia–Turkey) to the evolution of Neotethys: Turkish Journal of Earth Sciences, v. 10, p. 93–102.

Rojay, B., Altıner, D., Altıner, S.O., Önen, A.P., James, S., and Thirlwall, M.F., 2004, Geodynamic significance of the Cretaceous pillow basalts from the North Anatolian Ophiolitic Mélange Belt (Central Anatolia, Turkey): Geochemical and paleontological constraints: Geodinamica Acta, v. 17, p. 349–361, doi:10.3166/ga.17.349-361.

Sarıfakıoğlu, E., 2006, Petrology and origin of plagiogranites from the Daşkuplu (Eskişehir) ophiolite along the Izmir-Ankara-Erzincan suture zone, Turkey: Ofioliti, v. 32, p. 39–51.

Sarıfakıoğlu, E., Özen, H., and Winchester, J.A., 2009, Whole rock and mineral chemistry of ultramafic-mafic cumulates from the Orhaneli (Bursa) ophiolite: NW Anatolia: Turkish Journal of Earth Sciences, v. 18, p. 55–83, doi:10.3906/yer-0806-8.

Seifert, K., and Brunotte, D., 1996, Geochemistry of serpentinized mantle peridotite from Site 897 in the Iberia abyssal plain: College Station, Texas, Proceedings of the Ocean Drilling Program, Scientific Results, v. 149, p. 413–424.

Şengör, A., and Yılmaz, Y., 1981, Tethyan evolution of Turkey: A plate tectonic approach: Tectonophysics, v. 75, p. 181–241.

Shervais, J.W., 1982, Ti-V plots and the petrogenesis of modern and ophiolitic lavas: Earth and Planetary Science Letters, v. 59, p. 101–118, doi:10.1016/0012-821X(82)90120-0.

Shibata, T., and Thompson, G., 1986, Peridotites from the Mid-Atlantic Ridge at 43°N and their petrogenetic relation to abyssal tholeiites: Contributions to Mineralogy and Petrology, v. 93, p. 144–159, doi:10.1007/BF00371316.

Sinton, J.M., and Fryer, P., 1987, Mariana lavas from 18°N: Implications for the origin of back-arc basin basalts: Journal of Geophysical Research, v. 92, p. 12,782–12,802, doi:10.1029/JB092iB12p12782.

Sinton, J.M., Ford, L.L., Chappell, B., and McCulloch, M.T., 2003, Magma genesis and mantle heterogeneity in the Manus back-arc basin, Papua New Guinea: Journal of Petrology, v. 44, p. 159–195, doi:10.1093/petrology/44.1.159.

Stacey, J.S., and Kramers, J.D., 1975, Approximation of terrestrial lead isotope evolution by a two-stage model: Earth and Planetary Science Letters, v. 26, p. 207–221, doi:10.1016/0012-821X(75)90088-6.

Stern, R.J., Lin, P.-N., Morris, J.D., Jackson, M.C., Fryer, P., Bloomer, S.H., and Ito, E., 1990, Enriched back-arc basin basalts from the northern Mariana Trough: Implications for the evolution of back-arc basins: Earth and Planetary Science Letters, v. 100, p. 210–225, doi:10.1016/0012-821X(90)90186-2.

Sun, S.-s., and McDonough, W.F., 1989, Chemical and isotopic systematics of oceanic basalts: Implications for mantle composition and processes, *in* Saunders, A.D., and Norry, M.J., eds., Magmatism in the Ocean Basins: Geological Society [London] Special Publication 42, p. 313–345.

Takazawa, E., Okayasu, T., and Satoh, K., 2003, Geochemistry and origin of the basal lherzolites from the northern Oman ophiolite (northern Fizh block): Geochemistry Geophysics Geosystems, v. 4, 8605, 31 p., doi:10.1029/2001GC000232.

Tamura, A., and Arai, S., 2006, Harzburgite-dunite-orthopyroxenite suite as a record of supra-subduction zone setting for the Oman ophiolite mantle: Lithos, v. 90, p. 43–56, doi:10.1016/j.lithos.2005.12.012.

Tankut, A., 1984, Basic and ultrabasic rocks from the Ankara mélange, Turkey, *in* Dixon, J.E., and Robertson, A.H.F., eds., The Geological Evolution of the Eastern Mediterranean: Geological Society [London] Special Publication 17, p. 449–454.

Tankut, A., Dilek, Y., and Önen, P., 1998, Petrology and geochemistry of the Neo-Tethyan volcanism as revealed in the Ankara mélange, Turkey: Journal of Volcanology and Geothermal Research, v. 85, p. 265–284, doi:10.1016/S0377-0273(98)00059-6.

Tekin, U.K., Göncüoğlu, M.C., and Turhan, N., 2002, First evidence of Late Carnian radiolarians from the İzmir–Ankara suture complex, central Sakarya, Turkey: Implications for the opening age of the İzmir–Ankara branch of Neo-Tethys: Geobios, v. 35, p. 127–135, doi:10.1016/S0016-6995(02)00015-3.

Tüysüz, O., and Tekin, U.K., 2007, Timing of imbrication of an active continental margin facing the northern branch of Neotethys, Kargı Massif, northern Turkey: Cretaceous Research, v. 28, p. 754–764, doi:10.1016/j.cretres.2006.11.006.

Tüysüz, O., Dellaloğu, A., and Terzioğlu, N., 1995, A magmatic belt within the Neo-Tethyan suture zone and its role in the tectonic evolution of northern Turkey: Tectonophysics, v. 243, p. 173–191, doi:10.1016/0040-1951(94)00197-H.

Whitney, D.L., Teyssier, C., Dilek, Y., and Fayon, A.K., 2001, Metamorphism of the Central Anatolian Crystalline Complex, Turkey: Influence of orogen-normal collision vs. wrench dominated tectonics on P-T-t paths: Journal of Metamorphic Geology, v. 19, p. 411–432, doi:10.1046/j.0263-4929.2001.00319.x.

Winchester, J.A., and Floyd, P.A., 1977, Geochemical discrimination of different magma series and their differentiation products using immobile elements: Chemical Geology, v. 20, p. 325–343, doi:10.1016/0009-2541(77)90057-2.

Wood, D.A., 1980, The application of a Th-Hf-Ta diagram to problems of tectonomagmatic classification and to establishing the nature of crustal contamination of basaltic lavas of the British Tertiary volcanic province: Earth and Planetary Science Letters, v. 50, p. 11–30, doi:10.1016/0012-821X(80)90116-8.

Woodhead, J., Eggins, S., and Gamble, J., 1993, High field strength and transitional element systematics in island arc and back-arc basin basalts: Evidence for multi-phase melt extraction and a depleted mantle wedge: Earth and Planetary Science Letters, v. 114, p. 491–504, doi:10.1016/0012-821X(93)90078-N.

Yalınız, K.M., Floyd, P.A., and Göncüoğlu, M.C., 1996, Supra-subduction zone ophiolites of Central Anatolia: Geochemical evidence from the Sarıkarıman Ophiolite, Aksarya, Turkey: Mineralogical Magazine, v. 60, p. 697–710, doi:10.1180/minmag.1996.060.402.01.

Yalınız, K.M., Aydin, N.S., Göncüoğlu, M.C., and Parlak, O., 1999, Terlemez quartz monzonite of Central Anatolia (Arksaray-Sarıkarıman): Age, petrogenesis and geotectonic implications for ophiolite emplacement: Geological Journal, v. 34, p. 233–242, doi:10.1002/(SICI)1099-1034(199907/09)34:3<233::AID-GJ824>3.0.CO;2-5.

Yalınız, K.M., Floyd, P.A., and Göncüoğlu, C., 2000a, Geochemistry of volcanic rocks from the Çiçekdağ Ophiolite, Central Anatolia, Turkey, and their inferred tectonic setting within the northern branch of the Neotethyan Ocean, *in* Bozkurt, E., Winchester, J.A., and Piper, J.D.A., eds., Tectonics and Magmatism in Turkey and the Surrounding Area: Geological Society [London] Special Publication 173, p. 203–218.

Yalınız, K.M., Göncüoğlu, M.C., and Ozkan-Altıner, S., 2000b, Formation and emplacement ages of the SSZ-type Neotethyan ophiolites in Central Anatolia, Turkey: Palaeotectonic implications: Geological Journal, v. 35, p. 53–68.

Yılmaz, Y., Tüysüz, O., Yiğitbaş, E., Genç, S.C., and Şengör, A.M.C., 1997, Geology and tectonic evolution of the Pontides, *in* Robinson, A.G., ed., Regional and Petroleum Geology of the Black Sea and the Surrounding Region: American Association of Petroleum Geologists Memoir 68, p. 183–226.

Yin, A., and Harrison, T.M., 2000, Geologic evolution of the Himalayan-Tibetan orogen: Annual Review of Earth and Planetary Sciences Letters, v. 28, p. 211–280.

Manuscript Accepted by the Society 21 December 2010

Printed in the USA